UNIVERSITÀ DEGLI STUDI
DI MODENA E REGGIO EMILIA

Dottorato di ricerca in INGEGNERIA INDUSTRIALE E DEL TERRITORIO

Ciclo XXXIV

Development of a numerical methodology for the structure-borne-noise reduction in the acoustic cavity of high-performance vehicles

Candidato Andrea Vettorello

Relatore (Tutor): Prof. Ing. Sara Mantovani

Eventuale Correlatore (Co-Tutor): Prof. Ing. Matteo Giacopini

Coordinatore del Corso di Dottorato: Prof. Ing. Alberto Muscio

Preface

In the recent years, the description and reduction of noise in the passenger compartment have become an increasingly central aspect in the automotive field, especially for the spread of vehicles equipped with electric power units. The description of this dynamic phenomenon requires the identification of the source of the noise, as well as its propagation paths to the ears of the occupants of the vehicle.

Generally, noise propagates either via air, or through the vibration of the vehicle's structural subsystems, which represent the transfer function between source and receiver. All the components that determine the modal behaviour of the system must be included in the simulation model to obtain the acoustic characteristics of the vehicle. Besides these systems, the acoustic cavity is defined as the air volume within the passenger compartment, in the Trimmed body (TB) configuration of the vehicle.

The study of noise in the passenger compartment takes place experimentally and through simulation on a TB. Finite Element (FE) analyses consent to reconstruct the Noise Transfer Functions (NTF) through fluid-structure frequency response analysis. From these analyses, it might also be evaluated the participation of the vibrating components, with their relative modes, to the noise inside the cavity. The results allow the appropriate measures to be devised to solve any noise problem.

In the development of a new vehicle, the noise performance is evaluated at the final stages of the project, in which many components are already approved, and thus no longer adjustable. If noise levels do not meet the desired targets, restricted modifications to the project must be adopted to solve the issues. Furthermore, the identification of the causes of the noise could be a costly process due to the great complexity of the system.

This thesis aims to define a CAE methodology to predict problems related to in-borne noise since the earliest stages of development of a new vehicle, i.e., during the definition of the so-called Body-in-White (BIW) layout.

The proposed study is based on the analysis of the Equivalent Radiated Power (ERP) of vibrating components as a tool to discriminate the components likely to cause most of the noise in the passenger compartment. The link between the vibration of structural components and the perturbation of the pressure field of the fluid, that wets these components, allows to free oneself from the modelling of the acoustic cavity. Thus, approximate NTF may be calculated directly in BiW models, identifying possible noise problems.

Once the problematic components are identified, numerical optimization techniques are proposed to meet the performance targets, reducing the number of calculations required by conventional methods (e.g. trial and error loops). The main tool of these analyses is Finite Element simulation.

This methodology offers the possibility of developing a Trimmed-Body model with an improved level of acoustic comfort by reducing the development time of a new vehicle.

Summary

In the recent years, the description and the reduction of noise in the passenger compartment have become an increasingly central aspect in the automotive field, especially for the spread of vehicles equipped with electric power units. The description of this dynamic phenomenon requires the identification of the source of the noise and its propagation paths to the receiver, which is usually the ears of the driver and of the occupants of the vehicle. Generally, noise propagates either via air, or through the vibration of the vehicle's structural subsystems, which represent the transfer function between the source and the receiver. All the components, that determine the modal behaviour of the system, must be included in the simulation model to obtain the acoustic characteristics of the vehicle. Therefore, the study of these phenomena takes place experimentally and through simulation models on a Trimmed-Body (TB). The acoustic cavity may be defined as the air volume within the passenger compartment, in TB configuration of the vehicle, as shown in Figure 1.

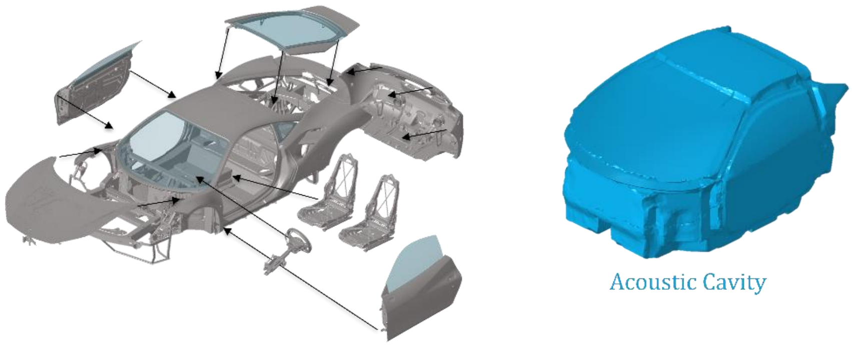

Figure 1: The panels included in TB configuration define the acoustic cavity

Finite Element analyses consent to reconstruct the trend of the Noise Transfer Functions (NTF) through fluid-structure frequency response analysis. From these analyses, it might also be evaluated the participation factors of the vibrating components, with the relative modes, to the noise at the ear inside the cavity. The results allow the appropriate measures to be devised to solve any noise problem.

Thus, in the development of a new vehicle, the noise performance is only evaluated at the final stage of the vehicle project, in which many components are already established and no longer adjustable. If noise levels do not meet the desired targets, restricted modifications to the project can be adopted to solve the issues. Furthermore, the identification of the causes of the noise could be a costly process due to the great complexity of the system.

This thesis aims to define a CAE methodology that aims to predict problems related to in-borne noise since the earliest stages of development of a new vehicle, i.e., in the definition phase of the so-called Body-in-White (BiW) layout. The proposed methodology is based on the analyses of the ERP that stands for Equivalent Radiated Power. This parameter combines the normal velocity of vibrating structural panel to the material properties of the fluid. This relation is reported in Equation 1:

$$ERP = \rho_F c_F \int_A \left|\hat{v}_{S,n}\right|^2 dA \qquad 1$$

where ρ_F indicates the fluid density, c_F is the velocity of sound in the fluid and $\hat{v}_{S,n}$ represents the normal velocity of a node of the structural vibrating panel. This equation is founded on the assumption that the velocity of a fluid particle equals the corresponding node of the structural domain. Several analyses on simplified models were conducted to calibrate the FE model to seize properly the dynamic behaviour of the BiW systems and its components. The simplified approaches suggest the possibility to obtain information about the acoustical behaviour of the panels that surround a fluid volume without considering fluid elements. Figure 2 (a) shows the simplified model of a simply supported plate and a rectangular fluid cavity. Figure 2 (b) presents the results of a frequency response analysis characterized by an external excitation that loads the aluminium plate normally and it is applied at the centre of gravity of the plate.

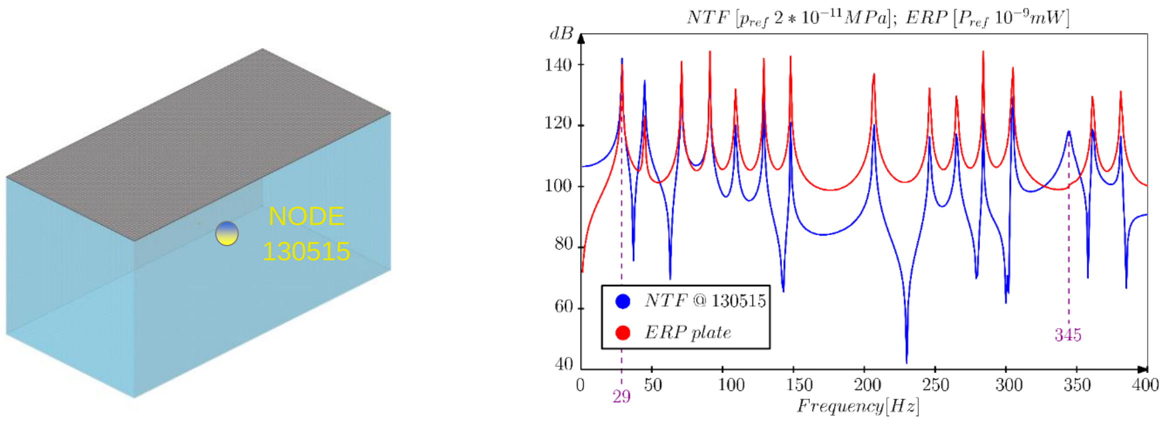

(a) (b)

Figure 2: (a) *FE model of simply supported plate coupled to the rectangular acoustic cavity.* (b) *box type cavity sensitivity analysis: comparison between NTF @ 130515 and ERP of the plate.*

An aspect of primary importance for this research activity is the good correspondence between the trends of the ERP of the plate and of the pressure field. This is only a qualitative aspect, which may give an overall consistent indication of the natural frequency of the plate normal modes generating the noise resonance peaks. The ERP can seize properly the dynamic behaviour of the structural component which perturbs the pressure field in the fluid domain.

The methodology proposes to describe the acoustical behaviour of the panels that surround the vehicle cabin in the BiW configurations in terms of ERP. For this purpose, a new participation factor was defined to discriminate the most influent panels that contribute to radiate the power inside the vehicle cabin. The Equivalent Panel Participation Factor (EPPF) is defined in the following equations:

$$EPPF = \frac{ERP_i}{ERP_{tot}} \cdot R_{Lin,ave} \qquad 2$$

The first term is the ratio between the radiated power of the i-th panel to the Total ERP evaluated at a specific frequency. The Total ERP is the sum of the ERP of all the panels, as shown in the following equation:

$$ERP_{TOT} = \sum_{i=1}^{N=\#\,panels} ERP_i \qquad 3$$

The $R_{Lin,ave}$ factor is the average linear correlation index between two linear correlation indexes. The former concerns a left around interval of frequencies to the specific frequency under investigation, and the latter considers an equal right interval of frequencies:

$$R_{Lin,ave} = \frac{1}{2}\left|\frac{cov(ERP_i, ERP_{tot})_{lh}}{\sqrt{D(ERP_i)_{lh}} \cdot \sqrt{D(ERP_{tot})_{lh}}} + \frac{cov(ERP_i, ERP_{tot})_{rh}}{\sqrt{D(ERP_i)_{rh}} \cdot \sqrt{D(ERP_{tot})_{rh}}}\right| \qquad 4$$

The linear correlation index formulation considers the ratio between the covariance of the ERP of the i-th panel related to the Total ERP in the interval of frequencies and the product of the root mean square of the two ERPs considered (Eq. 5-6-7).

$$cov(ERP_i, ERP_{tot}) = \sum_{lx=i\pm eps=1}^{lx=eps=15} (ERPi_{lx} - \overline{ERPi_{lx}}) \cdot (ERP_{tot} - \overline{ERP_{tot,\ lx}}) \tag{5}$$

$$D(ERP_i) = \sum_{lx=i\pm\varepsilon=1}^{lx=\varepsilon=15} (ERPi_{lx} - \overline{ERPi_{lx}})^2 \tag{6}$$

$$D(ERP_{tot}) = \sum_{lx=i\pm\varepsilon=1}^{lx=\varepsilon=15} (ERP_{tot,\ lx} - \overline{ERP_{tot,lx}})^2 \tag{7}$$

For the sake of simplicity in Figure 3, an example of the comparison between the Total ERP and the ERP of the roof of the vehicle is reported. The peak of Total ERP at 82 Hz was studied, and an around interval ε = 15 Hz was considered.

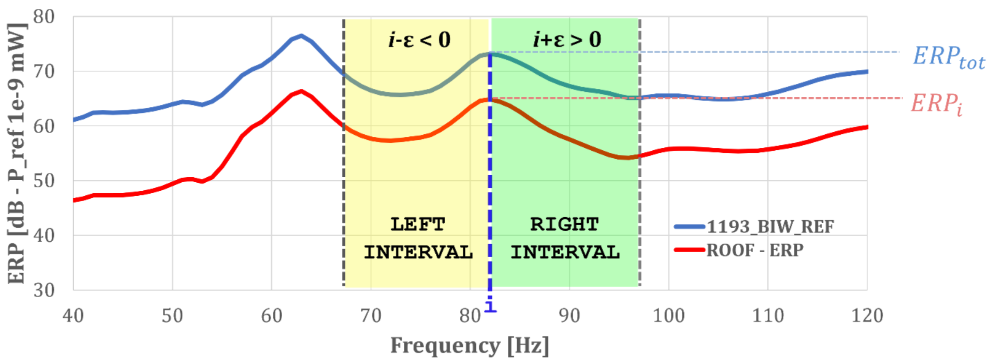

Figure 3: Comparison between the ERP of the roof to the Total ERP.

The linear correlation index gives information about how the i-th panels (red curve) influence the shapes of the Total ERP (blue curve) in the around interval considered. This coefficient describes the relationship of the two curves on the hypothesis of linearity. The two different short intervals of frequency around the peak under investigation could better approximate the linearity condition. The extrapolation of the dominant panels of the BiW was obtained considering the average of the all the peaks of the load-cases. The dominant panels extrapolated are reported in the following histogram:

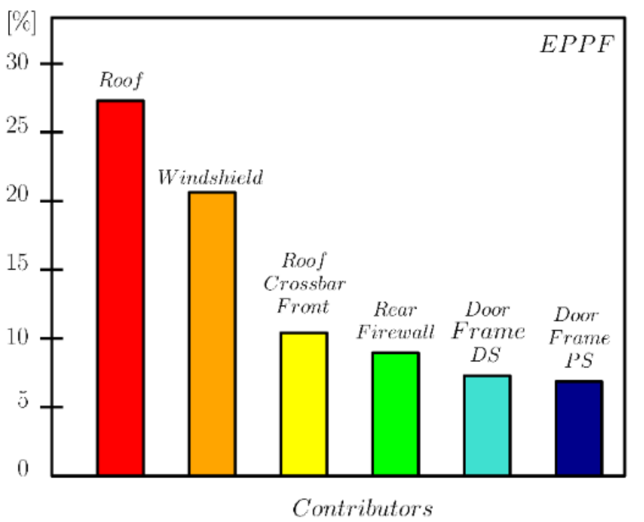

Figure 4: Panels that mainly contribute to generating the peaks of Total ERP for the considered load-cases.

The next steps of the methodology consist in the structural modification of the discriminated panels and in some cases of their frameworks. The first design modification concerns a shape optimisation of different zones of the bench. These zones define the design space of the first step of optimisation. The objective is to move at higher frequencies the first mode of the system by the variation of the plate's shape. During each iteration, the optimisation algorithm moves the nodes of the design space in the normal direction of the shell. In this way, ribs along the surface of the design space with both free and constraint geometry are identified. The advantage of this peculiar optimisation technique is obtaining stiff plate-shaped structures avoiding the increase of the thickness and the mass of the part. Figure 5 reports the optimised result.

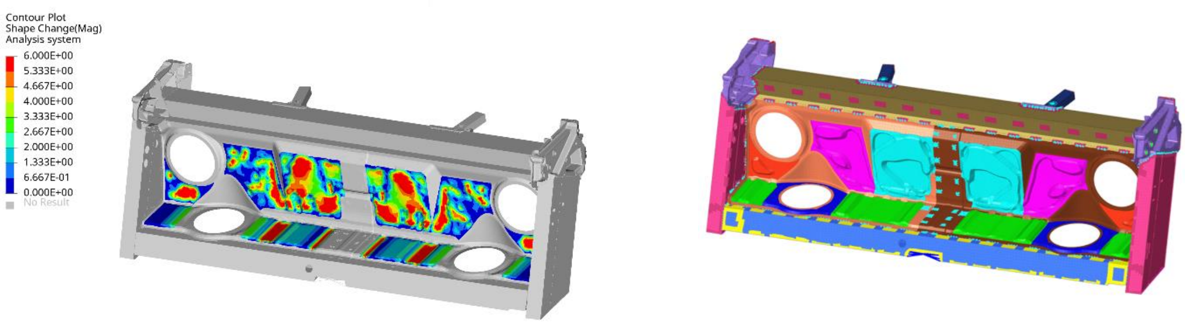

(a) (b)

Figure 5: (a) Topography Optimisation results; (b) FE model of the new optimised layout.

Other optimization analyses were performed to obtain a new BiW configuration, this analysis tries to improve the acoustical behaviour of the more influent panels minimising the increment of weight. The design modifications are listed in the following Table T1:

T 1: Summary of the modification applied to the new BiW configuration

COMPONENTS	REFERENCE [kg]	NEW CONFIGURATION [kg]
ROOF	5.04	7.18
ROOF DAMPING LAYER	0.99	1.29
BENCH	3.81	3.87
REAR FIREWALL	1.87	1.90
FRONT ROOF CROSSBAR	2.17	2.44
COWL	1.98	2.34
REAR ROOF CROSSBAR	2.02	2.39
UPPER DOOR FRAMES	3.39	3.60
TOTAL	**21.26**	**25.01**

For simplicity, the components listed in the table are reported also in Figure 6, where the components modified by a specific numerical optimisation are highlighted in red and the further are shown in light blue.

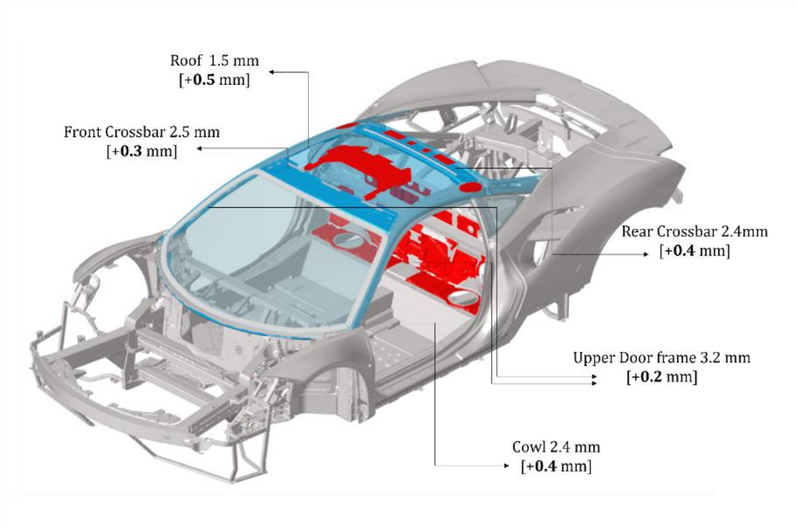

Figure 6: New configuration of BiW: optimised components in red and in light blue the components with augmented thickness.

The new configuration of the BiW is finally evaluated in the TB configuration. Thus, the acoustical frequency analyses were performed to extrapolate the NTF of each suspensions' attachments points, as shown in Figure 7.

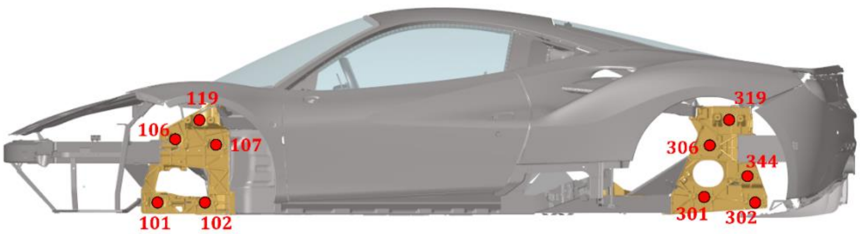

Figure 7: Attachments nodes at front and rear shock towers.

The results are reported in Figure 8. The new TB configuration is compared to the reference model.

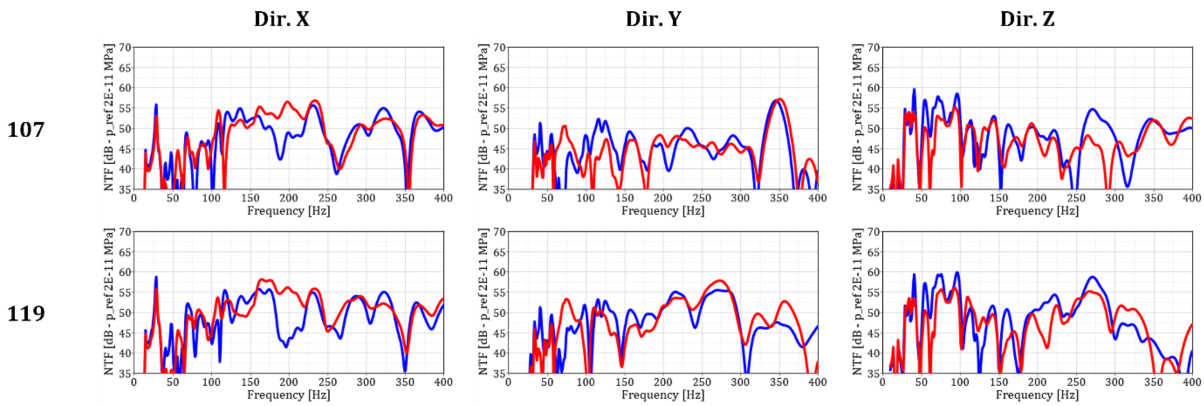

Figure 7.4: Noise Transfer Function of front shock towers. The blue curves represent the reference TB model acoustical behaviour. The red curves are referred to the new configuration of the TB model.

The results along the X-direction highlight a coherent behaviour of the new TB configuration to the reference model. Two main trends could be observed from these curves. The former ranges from 10 Hz to 100 Hz, in which the new configuration is globally at lower levels of sound pressure than the reference. This behaviour is coherent to the observations extrapolated from the study of the Total ERP of the BiW configuration. The range between 150 Hz and 250 Hz shows the opposite trends, but the overall level of the pressure is close to the acoustic target. The behaviour of the acoustic response by loads from Y-direction and Z-direction is better than the reference model. The highest peaks of the pressure of the reference model are reduced, moving the performance at the target levels. This result confirms the forecasts hypothesis made in the BiW configuration analyses at the early phase of the methodology. There is no evidence to associate the reduction of a specific quantity of the total ERP of the BiW configuration with a corresponding reduction of noise levels in the vehicle cabin in the TB configuration, but it remains a robust qualitative indicator. The methodology offers a helpful tool for the designer to orient the design closer to the acoustic targets without considering all the necessary subsystems that characterise the TB dynamics and define the acoustic cavity.

Riassunto

Negli ultimi anni, la descrizione e l'abbattimento del rumore nell'abitacolo sono diventati un aspetto sempre più centrale nel campo automobilistico, soprattutto per la diffusione dei veicoli dotati di propulsori elettrici. La descrizione di questo fenomeno dinamico richiede l'identificazione della fonte del rumore e dei suoi percorsi di propagazione al ricevitore, che è solitamente l'orecchio del conducente e degli occupanti del veicolo. In genere, il rumore si propaga sia per via aerea, sia attraverso la vibrazione dei sottosistemi strutturali del veicolo, che rappresentano la funzione di trasferimento tra sorgente e ricevitore. Tutti i componenti che determinano il comportamento modale del sistema devono essere inclusi nel modello di simulazione per ottenere le caratteristiche acustiche del veicolo. Pertanto, lo studio di questi fenomeni avviene sperimentalmente e attraverso modelli di simulazione su un Trimmed-Body (TB). La cavità acustica può essere definita come il volume d'aria all'interno dell'abitacolo, in configurazione TB del veicolo, come mostrato in Figura 1.

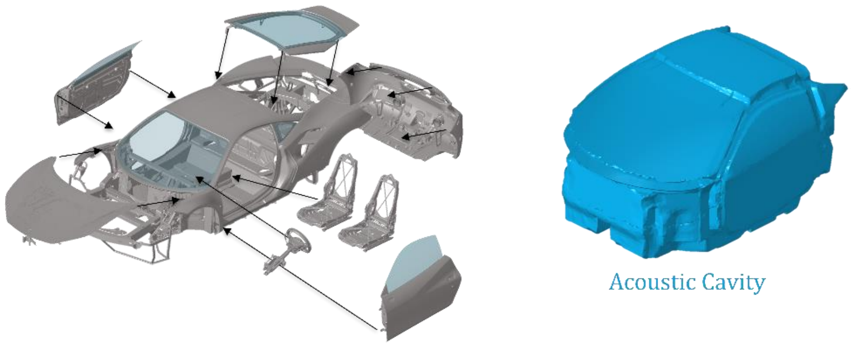

Figure 1: Pannelli che circondano la cavità acustica in configurazione TB

All'atto pratico, le analisi agli elementi finiti consentono di razionalizzare l'andamento delle funzioni di trasferimento del rumore (NTF) attraverso l'analisi della risposta in frequenza a struttura fluido. Da queste analisi si potrebbero anche valutare i fattori di partecipazione delle componenti vibranti con modalità relative al rumore all'orecchio all'interno della cavità. I risultati consentono di escogitare le misure appropriate per risolvere qualsiasi problema di rumore.

Pertanto, nello sviluppo di un nuovo veicolo, le prestazioni acustiche vengono valutate solo nelle fasi finali del progetto, in cui molti componenti sono già stabiliti e non più regolabili. Se i livelli di rumore non soddisfano gli obiettivi desiderati, è possibile adottare modifiche limitate al progetto per risolvere i problemi. Inoltre, l'identificazione delle cause del rumore potrebbe essere un processo costoso a causa della grande complessità del sistema.

Questa tesi si propone di definire una metodologia CAE che miri a prevedere i problemi legati al rumore interior-borne sin dalle prime fasi di sviluppo di un nuovo veicolo, cioè nella fase di definizione del layout cosiddetto Body-in-White (BiW). La metodologia proposta si basa sull'analisi dell'ERP che sta per potenza irradiata equivalente. Questo parametro combina la velocità normale del pannello strutturale vibrante alle proprietà del materiale del fluido. Questa relazione è riportata nell'Equazione 1:

$$ERP = \rho_F c_F \int_A \left|\hat{v}_{S,n}\right|^2 dA \qquad 1$$

dove ρ_F indica la densità del fluido, c_F è la velocità del suono nel fluido e $\hat{v}_{S,n}$ rappresenta la velocità normale di un nodo strutturale appartenente al pannello vibrante. Questa equazione si basa sull'assunto di considerare la velocità di una particella fluida uguale alla velocità del nodo corrispondente del dominio solido strutturale. Sono state condotte diverse analisi su semplificato per calibrare il modello

FE per cogliere adeguatamente il comportamento dinamico dei sistemi BiW e dei suoi componenti. Gli approcci semplificati suggeriscono la possibilità di ottenere informazioni sul comportamento acustico dei pannelli che circondano un volume fluido senza considerare gli elementi fluidi. La figura 2 (a) mostra il modello semplificato di una piastra semplicemente supportata e una cavità fluida rettangolare. La figura 2 (b) presenta i risultati di un'analisi della risposta in frequenza caratterizzata da un'eccitazione esterna che carica la lastra di alluminio normalmente nel suo baricentro.

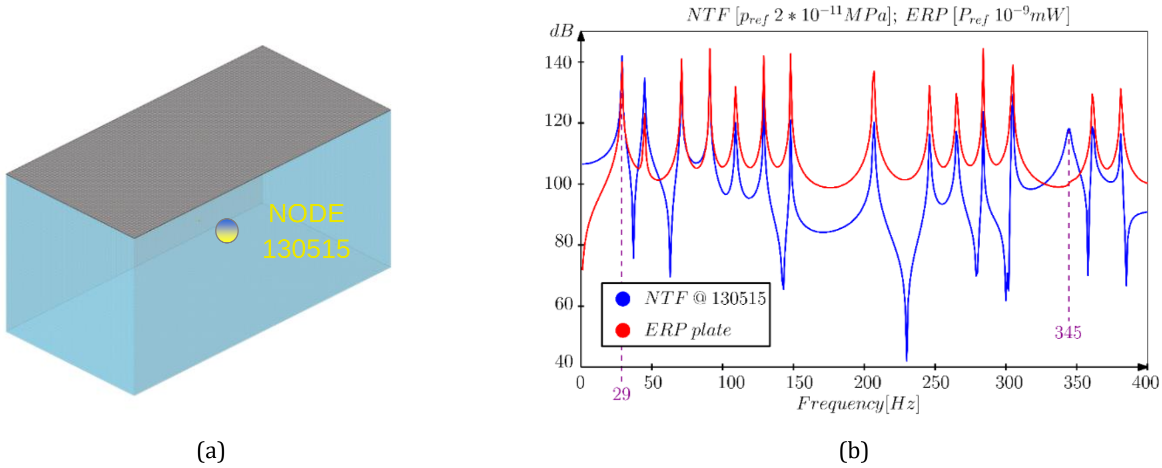

Figure 2: (a) Modello FEM di una piastra semplicemente appoggiata accoppiata ad una cavità acustica; (b) analisi di sensitività della cavità parallelepipeda, confronto tra ERP del pannello e NTF al nodo 130515

Un aspetto di primaria importanza per questa attività di ricerca è la buona corrispondenza tra gli andamenti dell'ERP della lastra e del campo di pressione. Questo è solo un aspetto qualitativo, che può fornire un'indicazione complessivamente coerente della frequenza naturale dei modi normali di piastra che generano i picchi di risonanza del rumore. L'ERP può cogliere adeguatamente il comportamento dinamico della componente strutturale che perturba il campo di pressione nel dominio del fluido.

La metodologia si propone di descrivere il comportamento acustico dei pannelli che circondano l'abitacolo del veicolo nelle configurazioni BiW in termini di ERP. A tal fine è stato definito un nuovo fattore di partecipazione per discriminare i pannelli più influenti che contribuiscono a irradiare la potenza all'interno dell'abitacolo del veicolo. L'Equivalent Panel Participation Factor (EPPF) è definito nelle seguenti equazioni:

$$EPPF = \frac{ERP_i}{ERP_{tot}} \cdot R_{Lin,ave} \qquad 2$$

Il primo termine è il rapporto tra la potenza irradiata dell'i-esimo pannello e l'ERP totale valutato ad una determinata frequenza. L'ERP totale è la somma dell'ERP di tutti i pannelli, come mostrato nella seguente equazione:

$$ERP_{TOT} = \sum_{i=1}^{N=\#\,panels} ERP_i \qquad 3$$

Il fattore $R_{Lin,ave}$ è un indice di correlazione lineare medio tra due indici di correlazione lineare. Tali indici quantificano la relazione tra porzioni di curve definite in un limitato intervallo di frequenze rispettivamente destro e sinistro attorno alla frequenza specifica in esame:

$$R_{Lin,ave} = \frac{1}{2}\left|\frac{cov(ERP_i, ERP_{tot})_{lh}}{\sqrt{D(ERP_i)_{lh}} \cdot \sqrt{D(ERP_{tot})_{lh}}} + \frac{cov(ERP_i, ERP_{tot})_{rh}}{\sqrt{D(ERP_i)_{rh}} \cdot \sqrt{D(ERP_{tot})_{rh}}}\right| \qquad 4$$

La formulazione dell'indice di correlazione lineare considera il rapporto tra la covarianza dell'ERP dell'i-esimo pannello relativo all'ERP totale nell'intervallo delle frequenze e il prodotto della radice quadrata della media dei due ERP considerati (Eq. 5-6- 7).

$$cov(ERP_i, ERP_{tot}) = \sum_{lx=i\pm eps=1}^{lx=eps=15} (ERPi_{lx} - \overline{ERPi_{lx}}) \cdot (ERP_{tot} - \overline{ERP_{tot,\ lx}}) \qquad 5$$

$$D(ERP_i) = \sum_{lx=i\pm\varepsilon=1}^{lx=\varepsilon=15} (ERPi_{lx} - \overline{ERPi_{lx}})^2 \qquad 6$$

$$D(ERP_{tot}) = \sum_{lx=i\pm\varepsilon=1}^{lx=\varepsilon=15} (ERP_{tot,\ lx} - \overline{ERP_{tot,lx}})^2 \qquad 7$$

Per semplicità in Figura 3 viene riportato un esempio di confronto tra il Total ERP e l'ERP del pannello del tetto del veicolo. È stato studiato il picco di Total ERP a 82 Hz ed è stato considerato un intervallo intorno a ε = 15 Hz.

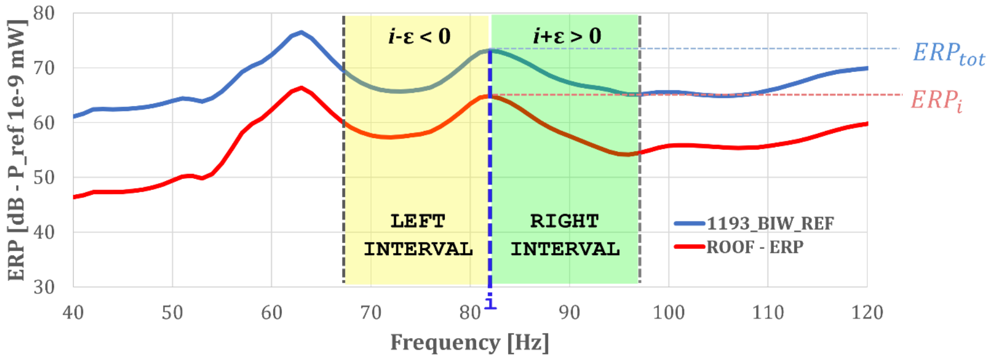

Figure 3: Confronto tra ERP del tetto ed ERP totale.

The linear correlation index gives information about how the i-th panels (red curve) influence the shapes of the Total ERP (blue curve) in the around interval considered. This coefficient described the relationship of the two curves on the hypothesis of linearity. The two different short intervals of frequency around the peak under investigation could better approximate the linearity condition. The extrapolation of the dominant panels of the BiW was obtained considering the average of the all the peaks of the load-cases. The dominant panels extrapolated are reported in the following histogram:

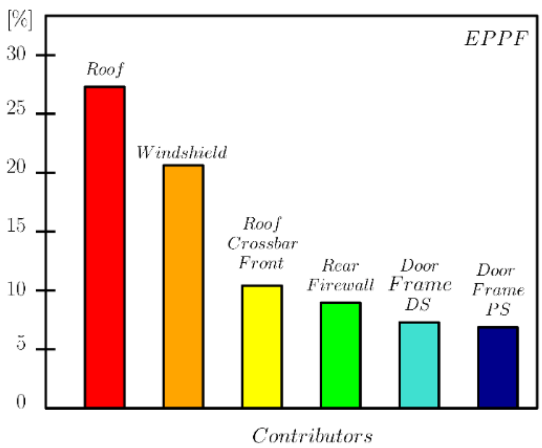

Figure 4: Pannelli che contriuiscono maggiormente ai picchi di ERP totale, per il caso di carico considerato.

I passi successivi della metodologia consistono nella modifica strutturale dei pannelli discriminati ed eventualmente delle loro strutture. La prima modifica progettuale riguarda un'ottimizzazione della forma delle diverse zone della panca. Queste zone definiscono lo spazio progettuale della prima fase di ottimizzazione. L'obiettivo è spostare a frequenze più alte il primo modo del sistema al variare della forma della piastra. Durante ogni iterazione, l'algoritmo di ottimizzazione sposta i nodi dello spazio di progettazione nella direzione normale alle shell. In questo modo è possibile creare nervature lungo la superficie dello spazio di progettazione con geometria sia libera che vincolata. Il vantaggio di questa peculiare tecnica di ottimizzazione è l'ottenimento di strutture a spessore sottile con un maggiore momento d'inerzia senza aumentare lo spessore e, di conseguenza, la massa. La figura 5 riporta il risultato ottimizzato.

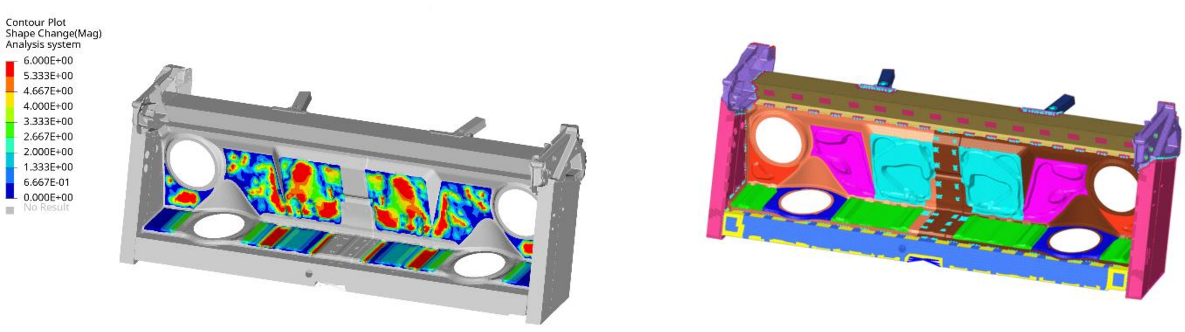

(a) (b)

Figure 5: (a) Risultati dell'Ottimizzazione Topografica; (b) Modello FEM del nuovo layout ottimizzato

Altre analisi di ottimizzazione sono state eseguite per ottenere una nuova configurazione BiW cercando di migliorare il comportamento acustico dei pannelli più influenti minimizzando l'incremento del peso. Le modifiche progettuali sono elencate nella seguente tabella T1:

T 1: Riassunto delle modifiche adottate al nuovo BIW

COMPONENTS	**REFERENCE [kg]**	**NEW CONFIGURATION [kg]**
ROOF	5.04	7.18
ROOF DAMPING LAYER	0.99	1.29
BENCH	3.81	3.87
REAR FIREWALL	1.87	1.90
FRONT ROOF CROSSBAR	2.17	2.44
COWL	1.98	2.34
REAR ROOF CROSSBAR	2.02	2.39
UPPER DOOR FRAMES	3.39	3.60
TOTAL	**21.26**	**25.01**

Per semplicità, le componenti elencate nella tabella sono riportate nella seguente Figura 6, in cui le componenti modificate da una specifica ottimizzazione numerica sono evidenziate in rosso e le altre in azzurro.

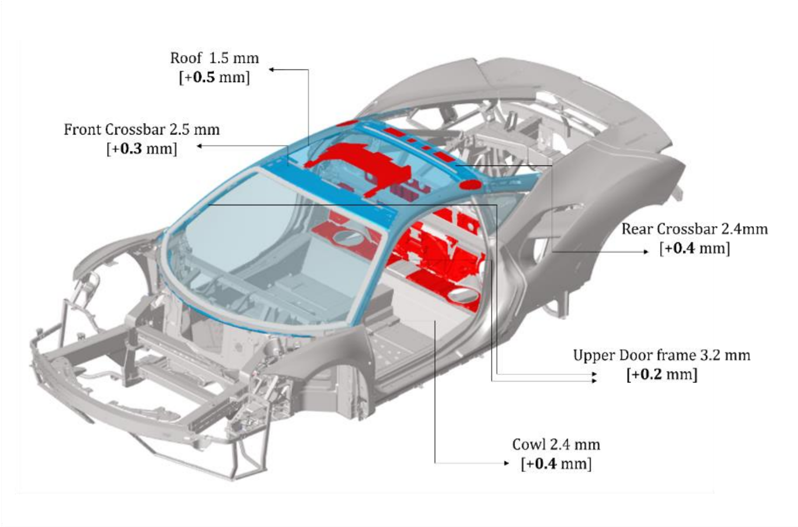

Figure 6: Nuova configurazione BIW: componenti ottimizzati sono evidenziati in rosso, i componenti a spessore aumentato in azzurro.

La nuova configurazione di BiW viene finalmente valutata in configurazione TB. Pertanto, le analisi di frequenza acustica sono state eseguite per estrapolare l'NTF dei punti di attacco di ciascuna sospensione, come mostrato in Figura 7.

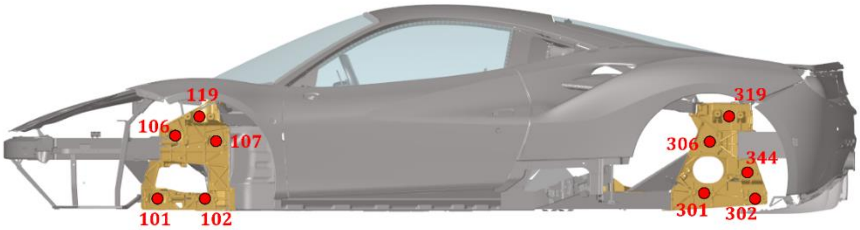

Figure 7: Nodi di attacco sospensioni alle shocktower anteriore e posteriore.

I risultati sono riportati nella seguente Figura 8. La nuova configurazione TB viene confrontata con il modello di riferimento.

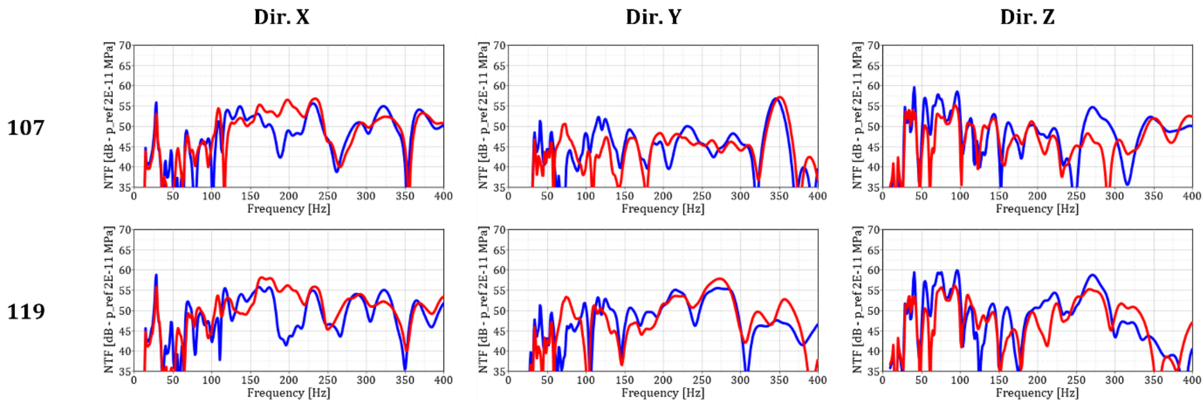

Figure 7.4: Funzione di trasferimento del rumore generato dalle shocktower anteriore. In blu è raffigurato l'andamento del modello TB base di riferimento e in rosso la nuova configurazione che accoglie tutte le modifiche strutturali sviluppate.

I risultati in direzione X evidenziano un comportamento coerente della nuova configurazione TB rispetto al modello di riferimento. Da queste curve si possono osservare due tendenze principali. Tra i 10 Hz ed i 100 Hz, in cui la nuova configurazione è globalmente a livelli di pressione sonora inferiori rispetto al riferimento. Questo comportamento è coerente con le osservazioni estrapolate dallo studio del Total ERP della configurazione BiW. Quest'ultimo è il range tra 150 Hz e 250 Hz che mostra gli andamenti opposti, ma il livello complessivo della pressione è vicino al target acustico. Il comportamento della risposta acustica dei carichi dalla direzione Y e dalla direzione Z è migliore rispetto al modello di riferimento. I picchi più alti della pressione del modello di riferimento vengono ridotti, avvicinandoli notevolmente ai livelli target. Questi risultati confermano le previsioni formulate nelle analisi di configurazione BiW nella fase iniziale della metodologia. Non ci sono prove per associare la riduzione a un livello target alla quantità alla potenza irradiata equivalente totale delle configurazioni BiW. La metodologia offre al progettista uno strumento utile per orientare il progetto più vicino ai target acustici senza considerare tutti i sottosistemi necessari che caratterizzano il comportamento dinamico del TB e che definiscono la cavità acustica.

Contents

Preface 3

Summary 5

Riassunto 11

1 – Introduction 20

1.1 – The design of a new vehicle 22

2 – Noise, Vibration and Harshness 25

2.1 – A brief introduction to Noise 25

2.2 – Noise, Vibration and Harshness in Automotive 27

3 – Structural Vibrations 30

3.1 Dynamic response of multi d.o.f. systems 30

3.2 Modal Analysis 36

3.3 Damping 38

3.4 Modal Truncation 42

4 Fluid-structure interaction 45

4.1 – General Theory 45

4.2 Application to the FE method 46

4.3 Mesh sensitivity 51

4.4 Examples with fluid cavities 53

5 – Structural Dynamics, effect of wall-fluid interaction 57

5.1 Introduction 57

5.2 Equivalent Radiated Power (ERP) 57

5.3 Example: box model with single plate 61

5.4 Acoustic Panel Participation Factor 65

6 - Definition of new methodology approach for CAE acoustic analyses 71

6.1 - Selection of the influent panels of BiW 78

6.2 – EPPF: Equivalent Panel Participation Factor 80

6.3 - The improvement the dynamic behaviour of the panels 87

6.3.1 - Structural optimization analyses of the bench 88

6.3.2 - Structural optimization analyses of the roof 93

6.3.3 - Structural optimization analyses of the rear firewall 95

6.4 - Definition of new BiW configuration 100

7 - Results 103

8 – Conclusions and Future Works 108

Bibliography 111

Appendix – A.1 118
Appendix A.2 125

1 – Introduction

The search for better driving comfort represents an increasingly important challenge for OEMs in recent years. Since the companies approach more and more market segments, more targets need to be satisfied to meet the needs of diverse customers. Therefore, companies need to raise the bar on the techniques adopted to define and achieve the performance targets of their products. All this is done in a context of great industrial competition, which leads to continuous product improvements, and facing a constant increase in the minimum safety requirements regulated by the competent bodies.

The competitiveness of an industry may be enhanced with the development of methodologies for both product design and process, or with the diversification of the offer. This last aspect requires the understanding of the customer's wishes even when the markets of interest change. The contingency of these factors implies the need to develop products with an increasing number of requirements and a continuous search for product innovation. This situation has been well defined in the automotive field for some time.

Cars established as the primary means of transport in the second half of the twentieth century. Its actual appearance dates to the beginning of the century as a luxury alternative to horse-drawn carriages. The birth of this type of vehicle is mainly attributable to the development of internal combustion engines, as well as to the industrial revolution. The requirements of these first vehicles depended mainly on their primary function of autonomous transport. These requirements were met by developing an internal combustion engine, transmission systems, tank housing with its fuel system, passenger seating and driving system. All these subsystems were obviously mounted on a chassis, which was, in fact, a carry-over of the pre-existing chassis of traditional carriages. These characteristics made this new type of vehicle sufficiently attractive for a small exclusive market of particularly wealthy people. This result may be deduced by analysing the problem from a technical, an economic and a socio-historical points of view.

From a technical point of view, back in those days, the OEMs struggled to achieve high production volumes and were unable to expand their market by reaching a higher number of possible customers. This difficulty is attributable to a still immature industrial conversion of production processes. The production of vehicles required high craftmanship, which resulted in the development of an expensive and limited-edition product. In addition, there were problems with efficiency, reliability, and performance.

From a sociological and historical point of view, it is not surprising that car owners belong to the upper class during the first decades of automobile history. This is the result of the unaffordable economic outlay for most of the population. In addition to its function, which was very discontinuous in the early periods, the automobile symbolises the man of the early decades of the twentieth century oriented towards futuristic and industrial visions, also belonging to new social classes that are gradually more and more influential.

It can be concluded that the car was born as a symbol of exclusivity, belonging to prominent personalities in step with the times. This mechanism can also be found today, not only in the automotive field but in about all consumer goods in which the exclusivity of some good gives rise to the desire for the same product to a gradually wider market, obtainable in a surrogate form. The good is the projection of the desire of belonging to the elite, to compensate for that innate sense of lack, made tangible by what one cannot have. Therefore, the development of mass society and industry allows this weird mechanism inherent in society and/or probably in the individual to transform the very concept of consumer goods and, therefore, the automobile.

The car is no longer just a means of transport, but it will necessarily have to meet a much higher number of characteristics and requirements, among which the function is only one of them. The technological development of automobiles has been driven by the need to create more performing vehicles from the point of view of speed and, therefore, engine power, with the consequent development of all subsystems, particularly the chassis, to exploit the available power. Furthermore, a fundamental impetus can be attributed to Taylorism and Fordism as production philosophies that have made it possible to make the car a mass commodity by exponentially increasing production volumes. This result was possible thanks to new materials that better matched the new production systems, such as steel and aluminium alloys that have more efficiently replaced the wood relegated only to some luxury interior finish and no longer in the chassis and bodywork components.

The industrial success of the automobile has naturally prompted governments and individuals to intensify investments in this sector and, therefore in its research and development. An example is the case of FIAT in Italy and in the development of the iconic 500, which represents the symbol of the Italian economic boom following World War II. FIAT 500 was always proposed as a small car, therefore an economical car in a specific market segment. This aspect is fundamental for understanding the design choices of any vehicle; in this case, the need to contain costs by maximizing the number of vehicles is a predominant priority over the others. Despite this, many technological innovations have been noted that have distinguished the new models, starting from the first of 1957. Important developments have been noted, such as, for example, the positioning of the engine at the front, the adoption of an independent wheel suspension system, attention to the style of the bodywork.

The 500 also came out in different versions, such as the familiar and more capacious "Giardiniera" which varied from the classic engine and wheelbase. The interesting part is that the two models shared the same starting platform. This modularity of the components is a crucial aspect, today taken to extremes, to keep low costs, while offering competitive products. With the following models, the overall dimensions of the FIAT 500 have increased, and this is due to ergonomics and safety requirements. Over time, knowledge on the adopted materials and components has also increased, leading to the overall improvement of performance in terms of weight the individual subsystems and therefore efficiency in fuel consumption, as well as durability and reliability. A further technological advance derives from the electronics of the control systems, which have substantially improved fuel consumption, safety, and comfort. An example is the system controlling the behaviour of the suspension systems by varying the behaviour of the shock absorbers as the driving conditions change.

The proliferation of cars in the last decades of the twentieth century is considered among the factors that have raised terrestrial pollution beyond the warning levels. This alert has diverted the automotive world towards more sustainable solutions, which are affecting the industry on various levels.

First, the advent of the electrification of vehicles is gradually supplanting the traditional internal combustion engine with hybrid and full-electric systems. For example, from 2020, the 500e, the electrified version of the iconic 500, entered the market. In addition to the variation of the propulsion system, countermeasures were also adopted in the materials used in the various components of the vehicle. In fact, sustainable and recyclable materials, such as aluminium and composite materials with natural constituents, such as linen or hemp fibre, have been more and more adopted to replace traditional materials in interior finishes, as well as in those areas where the structural function is practically absent.

Finally, in the last 30 to 40 years, the world has substantially changed, not only from the industrial but also from the social point of view, with the advent of computers and the internet. This tool minimized distances and offered unprecedented support to the designers. CAD and CAE software have substantially reduced the development time of a new product, minimising errors and allowing the possible analyses to be increased exponentially in the same amount of time. The advent of these tools has marked a real breaking point with the past. Now more than ever, the design of a new vehicle requires careful planning to monitor and guide all the stages of the process through the imposition of targets at every level. Over the years, improvements have also been made in managing the projects themselves, or at least the underlying philosophies have changed. For example, the "lean" mentality born in Japan has had a great success and developed worldwide like a wildfire. This approach aims to determine a production volume defined by demand while avoiding production waste, analysing each design and production phase to minimize possible sources of errors, predicting risks, and trying not to waste.

1.1 – The design of a new vehicle

This paragraph will briefly describe the design phases of a new vehicle, focused on the chassis development, which is the primary structural subsystem. The project starts from the conceptual phase, in which the market surveys are carried out. Here, the company determines the main characteristics that the new vehicle must have. This is connected to the work of the style department, which will outline the main shapes and dimensions of the new vehicle.

Then, the project enters the conceptual design phase, in which the main technical choices take shape. In addition, macro-characteristics are established by defining the primary targets, such as the overall weights, dynamic performance, ergonomics, comfort levels and innovative design solution. All these targets are decided according to the available budget.

Afterwards, the project moves to architecture phase, in which the components are developed at various levels. Depending on the type of car to be developed, there may be entirely new components, for which the appropriate material and production process will also have to be defined. Other components may be carry-overs deriving from previous vehicles on to the same platform or sharing in any case integrable characteristics. Within an OEM, this situation occurs very frequently, as it allows a considerable reduction of costs by avoiding the reinvestment of time and money in producing similar components. The design of a vehicle needs knowledge on production and assembly, as well as the simulation of the component's virtual approval.

Once the architecture phase is closed, each component designed up to this point is to be considered as approved, thus it becomes complicated and expensive to make macro-changes to the project in the subsequent phases of the architecture. Virtual analyses through CAD and CAE tools play a predominant role during the setting and the architecture phase. The more the simulation models can simulate the actual behaviour, the more it will be possible to make a specific component or subsystem more defined. In each phase, each subsystem of the vehicle need to comply with the required. After this phase, the first vehicle called mulotype begins to be developed, often as a set of pre-existing components, and with the presence of only the subsystems that characterize the new vehicle. This substantial compromise is due to the fact that it is almost impossible to get every new component right away. It is still possible to assess whether the vehicle in this set-up has characteristics consistent with expectations. After this phase, the prototypes are set up in which the vehicle is effectively congruent in all its parts with the new design with any updates and changes evaluated during the analysis of the mulotype. Finally, the pre-production phase is reached, it immediately precedes the actual series phase in which the new vehicles that will go on the market are produced. In this phase prior to the series, the vehicle is deliberated one last time in all its parts, and all its performance and therefore, the intention is to obtain a final experimental resolution. In this phase, obviously, the experimental aspect is given by the tests performed in various laboratories. The test benches, and the road tests have a greater impact than what is decided at the virtual level by the simulation models. In general, it can be observed how the design of a new vehicle develops through these successive phases, parallelizing within each of these. The design, development and tuning of each part of the vehicle, each of which must be subject to several constraints and targets. Therefore, the complexity and number of procedures and phases are evident, which must be carried out within the timescales planned. Furthermore, different strategies or alternative scenarios must be envisaged right from the start, as far as some problems arise that lead to delays in the development flow. We wanted to describe in this paragraph the subsequent phases of the development of a vehicle to highlight how it is necessary to be able as much as possible to intercept the possible macro-problems in the early stages of the project, such as the setting and the architecture. This implies that the vehicle performance is determined as much as possible in every aspect. Therefore, the simulation models are as close as possible to reality, and they need to mimic the real behaviour as faithfully as possible.

This thesis aims to define a CAE methodology to predict problems related to in-borne noise since the earliest stages of development of a new vehicle, i.e., during the definition of the so-called Body-in-White (BIW) layout.

The standard CAE practice consists of the analyses of the acoustical behaviour of the vehicle's Trimmed-Body (TB) configuration in the frequency domain. The interior-borne-noise prediction is generally studied in the frequency range between 0 to 400 Hz. Even in the vibroacoustic design of vehicles, the computing of NVH (Noise Vibration Harshness) behaviour with FEA (Finite Element Analysis) now is a common approach. For a typical TB model, the level of details is very high, and the model can easily consist of millions of elements. The computational time is very high with this kind of model. In recent years, the increment of computational power has been very notable, but this cannot be the solution to the problem because much power brings out the potentiality of better accuracy and a better physical estimation, and this is always chosen. Otherwise, many different techniques exist to perform detailed dynamic analysis in a short time [1], [2]. It is necessary to model the fluid and the fluid-structure coupling to calculate the acoustic performance of vehicles. Several authors studied the fluid-structure interaction and the FE models of fluid materials in literature. In particular, Everstine G. C. [3] evidences the analogy between the elasticity equations and those describing scalar fields, like the Helmholtz equation, Laplace equation, Poisson equation, heat transfer equation and the laws governing hybrid problems, like fluid-structure interaction for acoustic problems.

Moreover, Graggs [4] derives the formulation for a cubic finite element by considering Hermite polynomials as shape functions to describe the velocity potential at the nodes. To monitor and predict the problems of structurally transmitted and amplified noise, it is fundamental to adequately describe the dynamic behaviour of panel-like structures in simplified problems. In this way, it is possible to compare and adequately calibrate the FE model with the exact solution. These components have been intensely studied in the literature [5]–[8] and are particularly interesting in automotive, as they are the main structures composing unibody frames and moving parts of the body. Thin-walled components are typically investigated and modified to reduce the interior structure-borne noise. The principal technique employed to detect the significant panels is the acoustical panel participation [9], [10].

The proposed study is based on the Equivalent Radiated Power (ERP) analysis of vibrating components as a tool to discriminate the components likely to cause most of the noise in the passenger compartment. This quantity is known in the literature and is used for acoustic applications, as well as for the automotive field [11]–[14]. In this project, this quantity is the basis for developing a new methodology, which aims to identify the highest radiating areas of the interface between the vehicle structure and the acoustic cavity. The link between the vibration of structural components and the perturbation of the pressure field of the fluid, that wets these components, allows to free oneself from the modelling of the acoustic cavity. Thus, the dynamic behaviour of these components, emphasized by normal modes, is studied by evaluating the radiated power content over frequency directly in BiW models.

Once the problematic components are identified, numerical optimization techniques are proposed to meet the performance targets, reducing the number of calculations required by conventional methods (e.g. trial and error loops). This approach, based on the analysis of the ERP, is challenging, and it was also suggested by Luegmair M. in his works [Luegmair]. This methodology offers the possibility of developing a Trimmed-Body model with an improved level of acoustic comfort by reducing the development time of a new vehicle.

2 – Noise, Vibration and Harshness

2.1 – A brief introduction to Noise

The noise includes many phenomena, and it is use in different disciplines to describe all the annoying sensations related to the sound. In recent years, attention to problems related to noise and vibrations in the automotive field has grown in terms of comfort and driveability. If, on one hand, the final customer has become more aware of the risks related to noise and vibrations, the legislation has intervened by introducing severe limitations to protect people from the harmful effects of prolonged exposure to high levels of noise and vibrations. The onset of noise in a vehicle is closely related to vibrations. A sound can only be produced in two ways: 1) the vibration of solid objects, and 2) the turbulence of the air. Therefore, the actions that can be undertaken in the engineering field to monitor and to reduce the noise levels in the automotive field concern the study of vibrational phenomena. In this chapter, after having exposed some basic concepts of acoustics and vibrations, the problems related to noise and vibrations in motor vehicles will be described, paying attention to the problems associated with internal combustion engines.

Sound is characterized by the propagation of pressure waves in an elastic medium due to the rapid succession of compressions and expansions of the medium itself due to a vibrating element. The frequency and the speed with which the pressure disturbance propagates depend on the same elastic medium, which can be solid, liquid or aeriform. When an element vibrates in an elastic medium such as air, the particles of the surrounding medium also begin to oscillate around their equilibrium position and, in the volume of air surrounding the sound source, tiny variations in pressure are produced (from 10^{-5}Pa to 10^{-2} Pa). The sound waves are transmitted in the medium causing a variation in the medium's density, and they originate the pressure variations from the equilibrium condition. At a certain distance from the sound source, pressure variations above (compressions) and expansions of atmospheric pressure occur below ($p_{atm} = 1.013 \cdot 10^{-5}$Pa)[15].

When the pressure waves reach the human ear, the eardrum membrane begins to vibrate and, through a complex system of nerve impulses, are perceived by the brain, giving rise to the auditory sensation. One of the parameters that characterize the sound is the frequency f. It represents the number of oscillations made in a second. We speak of a sound phenomenon when the frequency is included in the range of 20 Hz ÷ 20,000 Hz, or the range in which it is conventionally assumed that the human ear is sensitive. Signals with frequencies below 20 Hz are called infrasounds, while signals above 20,000 Hz are called ultrasounds. Generally, a sound does not correspond to a pure tone, characterized by a single emission frequency, but by a complex signal of many frequencies that give rise to a continuous spectrum. Other physical parameters necessary for the description of the acoustic phenomena are the period T and the wavelength λ which represent the time interval and the space necessary to perform a complete oscillation, respectively. The relationships between these parameters are:

$$f = \frac{1}{T} \tag{2.1}$$

$$T = \frac{2\pi}{\omega} \tag{2.2}$$

$$\lambda = \frac{c}{f} \tag{2.3}$$

$$\lambda = cT \tag{2.4}$$

where $\omega = 2\pi f$ is the pulsation and c is the speed of sound with in the fluid domain. This speed does not depend on the oscillation frequency, but only on the thermodynamic conditions of the medium in which the perturbation propagates. For air, approximate formulas that determine the value of the speed of sound as a function of the temperature are:

$$c \cong 20.05 T[K] \qquad 2.5$$

where T is the temperature expressed in Kelvin,

$$c \cong 331.4 + 0.6t[°C] \qquad 2.6$$

and where t indicates the temperature in °C.
The fundamental physical quantities in acoustics are pressure, power and sound intensity. The sound pressure p_i depends on position and the time is the variation in atmospheric pressure produced by the sound phenomenon for the static pressure p_{atm} of the unperturbed domain:

$$p - p_{atm} = p_i \qquad 2.7$$

where p and p_{atm} represent the values of the pressure existing in the medium in the presence and absence of the sound wave, respectively. In general, the sound pressure assumes minimal values compared to the static pressure, and for this reason, we tend to characterize the sound pressure p_i through its RMS value, equal to the square root of the Root Mean Square (RMS) value. This relation is collected in the definition of the Effective Pressure shown (p_{eff}) in Eq. 2.8:

$$p_{eff} = \sqrt{\frac{1}{T}\int_0^T {p_i}^2 \, dt} \qquad 2.8$$

An omnidirectional source radiates the energy uniformly into an isotropic medium such as air. The pressure amplitude decreases moving far away from the omnidirectional source because the energy is distributed over a wider emission surface (wavefront). In any space position, the acoustic field can be described with a magnitude characterized by direction and amplitude that represents the amount of energy that flows through the unit of surface S in the unit of time. This quantity is called sound intensity I and it is measured in W/m^2.

$$I = \frac{p_{eff}}{\rho c} \qquad 2.9$$

The sound intensity I is a vector, and it depends on the direction of the surface considered. The amount of sound energy that the acoustic source can radiate in the unit of time is called sound power P (measured in Watt, W). The following expression considers inviscid fluids at steady-state condition:

$$P = IS \qquad 2.10$$

Sound pressure is the most used parameter for measuring sound, as the change in atmospheric pressure is a relatively simple amount to detect. However, using a linear scale to measure sound pressure, the range of audible values is extensive. The range considers minimum values of *20* µPa, corresponding to the minimum level perceptible by the human ear, to a value of just over *100* Pa which identifies the pain threshold. Thus, it is preferred to express the acoustic parameters as a function of a relative logarithmic scale in decibel (dB). Therefore, the sound pressure level L_p is defined by the relation:

$$L_p = 10log\left(\frac{p^2}{{p_0}^2}\right) = 20log\left(\frac{p}{p_0}\right) \ [dB] \qquad 2.11$$

where p is the sound pressure (in Pa) and p_0 is the reference pressure of $2{\cdot}10^{-5}$Pa. The sound pressure level (SPL) describes the sound field and can be measured directly with a microphone. The following equations define the sound power level and the sound intensity level:

$$L_P = 10log\left(\frac{P}{P_0}\right) \quad [dB] \qquad 2.12$$

$$L_I = 10log\left(\frac{I}{I_0}\right) \quad [dB] \qquad 2.13$$

where P_0 is the conventional reference sound power of 10^{-12} W, and I_0 is the reference sound intensity equal to $10^{-12}\ W/m^2$.

These parameters describe the characteristics of the noise, which propagates in the medium perturbing the fluid system.

2.2 – Noise, Vibration and Harshness in Automotive

The analyses of the vibro-acoustic performance of a vehicle concern the NVH (Noise, Vibration and Harshness), and it is defined as the combination of three parameters:

- Noise;
- Vibration;
- Harshness.

During the different driving conditions, all vehicles are subjected to different dynamic forcing [16]–[18]; the vibration and noise induced by these stresses mainly affect the comfort and driving performance of a car and reduce the safety and reliability the vehicle itself. While it is possible to measure these properties, in some conditions, a subjective assessment of the vehicle's behaviour is required, or analytical tools are used to provide results in line with the driver's subjective impressions. These aspects are part of the "psycho-acoustic" field, which represents the study of the perception of sound. Vibrations inside a vehicle involve an extended range of frequencies, from 1 Hz during vehicle manoeuvres to about 10 kHz during acoustic excitations. A fundamental aspect to consider is that the induced vibration not only depends on the intensity of the excitation but also on the behaviour of the structure, which can amplify these effects due to structural and acoustic resonances. As indicated by Morello in [17], vibro-acoustic phenomena can be classified according to the frequency at which they occur. The following frequency bands can be defined to classify vibrational phenomena:

- Ride (0 ÷ 5 Hz): includes low-frequency accelerations due to vehicle manoeuvres and rigid body oscillations on the suspension;

- Shake (5 ÷ 25 Hz): includes the first resonances of the main subsystems connected to the vehicle chassis, such as the engine and suspensions.

- Harshness (25 ÷ 100 Hz): includes frame resonances as a flexible body.

The frequency range represents a partial overlap of frequencies perceived as vibration with noise. The ear often perceives vibrations with high acoustic intensity as pressure variations, and we refer to them as "boom".

• Noise (> 100 Hz): the hearing system perceives the vibration as noise. The pure vibration is considerably attenuated, and it can be slightly felt by contact (e.g. on the steering wheel). Hence, the frequency band above 100 Hz is referred to as noise.

Based on the noise propagation mechanism, it is possible to define two different types of transmission paths:

- Structure-borne: the various subsystems of the vehicle transmit the dynamic forces to the chassis directly through the connections and structural interfaces. These phenomena cause vibrations in the structure and at the frame panels. The structural vibrations are transmitted by air into the passenger compartment surrounding the car occupants, causing "interior noise".

- Air-borne: The pressure waves that propagate outside the vehicle induce vibrations in the panels or windows of the car and cause pressure waves inside the vehicle, thus generating noise.

In all cases, the transmission of noise occurs in the acoustic cavity, representing the air surrounding the vehicle's occupants. Therefore, the difference between structural or airborne noise is represented by the transmission path between the source and the panels surrounding the cavity inside the car. Generally, in a car, the structural noise transmission can be considered dominant at low frequencies (<500Hz), while the aerial transmission is predominant at higher frequencies, above 1000 Hz. The insulation attenuates the structural noise, while the airborne noise is reduced by absorption [18]. The driver feels vibrations at the interface with the vehicle, such as on the steering wheel, seat, floor, and pedals.
The main sources of noise and vibration in motor vehicles, which contribute significantly to the level of noise and comfort perceived by passengers inside the vehicle, are mainly linked to two factors: the powertrain that generates the motion of the vehicle (powertrain noise) [19] and the motion of the vehicle on the road (rolling noise)[20]–[23]. It stated that the noise level perceived by passengers in the passenger compartment and related to the powertrain is a combination of engine noise; noise related to the intake noise and exhaust systems; noise related to the cooling system (cooling system noise); gearbox noise and transmission noise. While the noise level linked to the motion of the vehicle on the road (the so-called rolling noise) has two main components: the noise linked to the interaction between tire and road pavement (road noise) and the aerodynamic noise caused by the airflow around to the vehicle (aerodynamic noise). Other noises inside a vehicle are related to the braking system (brake noise), while others are classified as squeaking, screeching and clicking.
Generally, the noise produced externally by a new vehicle, under normal operating conditions, is dominated by the noise linked to the motion of the vehicle on the road (rolling noise), which becomes

increasingly important as the cruising speed of the vehicle increases [23]–[26], exceeding the sound power level related to the powertrain. If we consider, for example, a car at a cruising speed below 20 km/h, the rolling noise has a negligible effect on the overall noise level produced by the vehicle, but at speeds above 60 km/h, this component becomes the dominant noise source. At speeds above 130 km/h, the vehicle noise is dominated by aerodynamic noise. Generally, the noise and vibrations perceived by passengers in the car compartment originate outside the passenger compartment and, before reaching the passenger compartment, can interact in some way with the structure of the vehicle itself and, in some cases, even with other noise sources.

When the noise reaches the interior via airways, we speak of air-borne noise, while if the noise reaches the interior of the compartment interacting with the vehicle structure, we speak of structure-borne noise. Most low-frequency noise is transmitted structurally, while high-frequency noise is transmitted by air. The structural sound paths are characterized by direct connections of the structure with the panels on the surface of the passenger cabin, where the energy is radiated into the internal acoustic space as noise. On the other hand, air routes refer to cases in which the sound generated outside the passenger cabin is transmitted through the vehicle panels inside the passenger compartment. At low frequency, road-noise is a classic example of noise that is transmitted by structural means: the interaction between the tire and the road pavement is the source of the vibrations that, transmitted through various paths consisting of combinations of suspension components, chassis, and body panels, reach inside the passenger compartment of the vehicle.

The structural transmission paths are also responsible for the low-frequency noise components produced by the motor[19], such as boom noise (for frequencies below 100 Hz) and moan noise (for frequencies from 100 to 200 Hz): the stresses produced by the motor are transmitted through the engine mounts to the vehicle chassis, and from the latter into the car compartment. Road noise at high frequencies is, on the other hand, an example of noise that is transmitted by air: the noise generated by the wheels propagates both under the vehicle, from where aerial paths then transmit it to the panels that make up the vehicle floor. It is all around the vehicle, from where it is transmitted to the windows and panels that make up the passenger compartment. The noise produced by the powertrain is also transmitted to the passenger cabin through aerial and structural routes. The sound energy generated by the surface's vibration of the powertrain components and by the aerodynamic loads inside its components is radiated into the passenger compartment through the air (air-borne noise). In contrast, the mechanical forces and vibrations induced by the components are transmitted through the attachment points to the vehicle structure and, from this, through structural paths, to the cabin (structure-borne noise).

The strategies adopted to reduce noise in motor vehicles include a wide choice of solutions depending on the noise source on which one wants (or must) intervene, how the noise is transmitted inside the passenger compartment and the type of application. In general, it is possible to state that the measures necessary to reduce noise inside a vehicle mainly concern: the treatment of noise sources, reducing noise transmission[27]–[29], the absorption of noise inside the passenger cavity[30], [31].

3 – Structural Vibrations

3.1 Dynamic response of multi d.o.f. systems

A dynamic response problem has two important differences from a static response problem. The first difference is the dependence of the problem from time, while the second difference is the presence of inertia and damping forces and moments, which vary according to the external loads. For a generic system with n degrees of freedom, on which a system $\underline{F}(t)$ of periodic external loads acts, the general dynamic equation system may be written in matrix form as:

$$\underline{\underline{M}}\underline{\ddot{x}} + \underline{\underline{C}}\underline{\dot{x}} + \underline{\underline{K}}\underline{x} = \underline{F}(t), \quad \underline{x} = \underline{x}(t) \qquad 3.1$$

The first member of the equation is composed by the sum of the elastic reactions $\underline{\underline{K}}\underline{x}$, the viscous damping forces and moments $\underline{\underline{C}}\underline{\dot{x}}$, and inertial reactions $\underline{\underline{M}}\underline{\ddot{x}}$. $\underline{\underline{M}}$ is the mass matrix of the system, which may be also modelled with concentrated parameters. $\underline{\underline{C}}$ is the viscous damping matrix, which is symmetrical and semi-positive definite, while $\underline{\underline{K}}$ is the stiffness matrix of the system. If the model of the system includes structural damping, $\underline{\underline{K}}$ has complex coefficients.

We make now two important assumptions. First, we assume the dynamic problem to be periodic. Periodic functions have their value repeated after a defined interval of time. Therefore, a *period* $T > 0$ may be identified so that:

$$f(x) \coloneqq f(x+T) \quad \forall x \in \underline{x} \qquad 3.2$$

Trigonometric functions are a common example of periodic functions, e.g.:

$$f(x) = \cos(x) \qquad 3.3$$

$$T = 2\pi \qquad 3.4$$

The period changes as the frequency changes:

$$f(x) = \cos(kx) \rightarrow T = \frac{2\pi}{k} \qquad 3.5$$

The second assumption concerns the linearity of the problem. For a stable dynamic system, in which the response is determined by a linear differential equation, if an external sinusoidal load is applied with its own amplitude and frequency, the steady-state response will be a sine function having the same amplitude as the external force.

The two assumptions made above are not always respected in practical applications, as many systems may not satisfy the hypothesis of linearity.

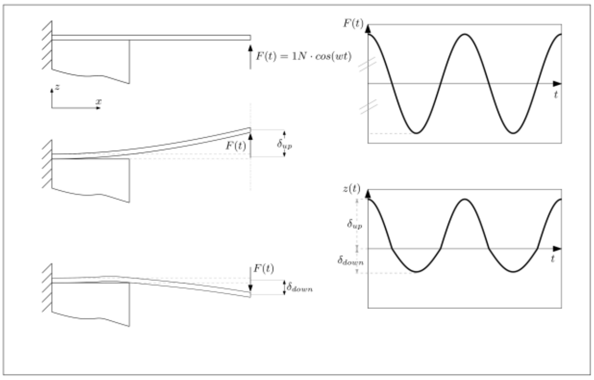

Figure 3.1: Non-linear example of a cantilever beam with a periodic force at the free edge

The cantilever beam in Figure 3.1 is partially in contact with a rigid surface. The free extremity of the beam is loaded by a harmonic force with unitary amplitude, and a frequency ω. This dynamic problem is periodic and non-linear. The loss of linearity occurs when the beam is close to its undeformed shape, i.e., when the vertical displacement of the free edge is around zero. Even though the external load is periodic with its mean value equal to zero, the amplitude of the deflection at the beam extremity is not the same if the deflection is positive or negative. This response is clearly due to the unilateral constraint. In this case, the hypothesis of linearity falls, and the response cannot be obtained from the superimposition principle. Therefore, the boundary conditions of the system have a primary influence on the solution of the dynamic problem. To sum up, in order to avoid nonsensical or misleading results, it is mandatory to check if the hypotheses, on which the solution methods are founded, are respected.

Integral transforms are linear mathematical instruments, particularly useful in structural dynamics. They are called *integral* because they are expressed by the integral, over certain extremes, of the original function, which is multiplied by a *Kernel* function. To solve differential problems, adopting integral transformations is often convenient, as the solution of the transformed problem may be found with great ease. Afterwards, the solution in the original domain may be obtained with the inverse transform. In general, the integral transform $h(v)$ of a function $g(x)$, is defined as:

$$h(v) = T[g(x)] = \int_a^b g(x)K(x,v)dx \qquad 3.6$$

$K(x,v)$ is the Kernel function, which defines the type of transform, along with the limits of integration. The inverse transform is a new integral transform, defined as:

$$g(x) = T^{-1}[h(v)] = \int_{a'}^{b'} h(v)H(x,v)dv \qquad 3.7$$

Integral transforms are most likely linear operators, for which the following properties are valid:

$$T[cg_1 + dg_2] = cT[g_1] + dT[g_2] \qquad 3.8$$

where

- $c, d \in \mathbb{R}$
- g_1, g_2: are functions depending on the variable x.

Among the transforms which benefit from the above property, great interest is given to those transforms which have an exponential kernel function:

$$K(x, v) = e^{\alpha x v}, \alpha \in \mathbb{R} \qquad 3.9$$

This kernel function allows a relatively easy calculation of the transformed of the derivative of any function, due to the easy solution of the integral of an exponential function:

$$T\left[\frac{dg}{dx}\right] = \int_a^b \frac{dg}{dx} K(x, v)dx = -\alpha v h(v) + g(b)e^{\alpha v b} - g(b)e^{\alpha v a} \qquad 3.10$$

Many complicated analytical calculations are avoided when using these particular transforms. One may simply calculate the product of the transformed function by a constant. This concept may be extended to the transform of higher order derivatives by writing:

$$\frac{d^n g}{dx^n} = h(v)(-\alpha v)^n + \cdots \qquad 3.11$$

In conclusion, these transforms allow to solve ordinary differential equations by transforming them into much simpler algebraic equations.

In structural dynamics, the D'Alembert equilibrium equations may be simplified with these relations. The integral transformations transform functions of time into functions of frequency. This linear operation is commonly addressed as the transformation from time to frequency domain:

$$h(v) = T[g(x)] = \int_a^b g(x)K(x, v)dx \qquad 3.12$$

Laplace transform is a most common transform adopted in mechanics. In structural dynamics, where the external loads are expressed with trigonometric functions, Fourier transform is extremely helpful. Considering a harmonic function, it can be expanded as a Fourier series in the trigonometric or exponential form. The Fourier coefficients are expressed according to the expansion.

$$f(t) = \frac{a_0}{2} + \sum_{n=1}^{\infty} a_n \cos(\omega_n t) + b_n \sin(\omega_n t), \qquad \omega_n = \frac{2\pi n}{T} \qquad 3.13$$

$$\begin{cases} c_0 = \dfrac{a_0}{2} \\ c_{-n} = \dfrac{a_n + jb_n}{2} \\ c_n = \dfrac{a_n - jb_n}{2} \end{cases} \qquad 3.14$$

$$f(t) = \sum_{n=1}^{\infty} c_n e^{j\omega_n t} \qquad 3.15$$

$$c_n = \frac{1}{T}\int_0^T f(t)e^{-j\omega_n t}dt \qquad 3.16$$

$f(t)$ is univocally determined once the coefficients c_n are known. On the other hand, from a known function, one may find c_n. The Fourier transform of the first and second derivative of a function are respectively:

$$T_{Ff}\left[\frac{df}{dt}\right] = j\omega F(\omega) \qquad 3.17$$

$$T_{Ff}\left[\frac{d^2 f}{dt^2}\right] = -\omega^2 F(\omega) \qquad 3.18$$

Fourier transform moves the dynamic problem from the time domain to frequency domain, the inverse transform allows to move the problem back to time domain. In addition, the representation of quantities in the complex plane is particularly simple for periodic problems. To give an example, a given complex vector a, having an amplitude A and frequency ω, is represented in the complex plane with a vector with module A, rotating at an angular speed ω:

$$a = Ae^{j\omega t} \qquad 3.19$$

$$\dot{a} = j\omega A e^{j\omega t} = j\omega A e^{j\left(\omega t + \frac{\pi}{2}\right)} \qquad 3.20$$

$$\ddot{a} = -\omega^2 A e^{j\omega t} = -\omega^2 a \qquad 3.21$$

The projections of a onto the real and imaginary axis have a harmonic evolution over time. The first derivative of a with respect to time has a 90° offset with respect to a, while the second derivative of a over time has a 180° offset with respect to a. The two derivatives of a rotate at the same angular speed as a (see Figure xx2).

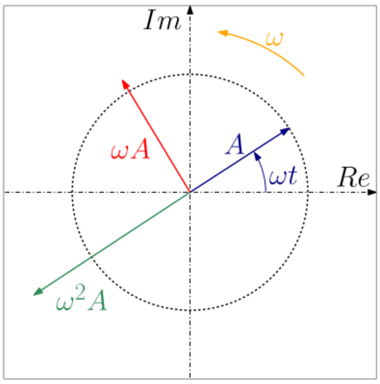

Figure 3.2: Rappresentazione grafica sul piano di Arnald-Gauss del vettore rotante a e delle sue derivate.

With this approach one may represent on the complex plane the forces acting on the dynamic system. Considering the single d.o.f. harmonic oscillator, it is excited by a harmonic external load, which has a constant amplitude. The oscillator is modelled with a mass m, a spring having a stiffness k, and a viscous damper with a damping coefficient c. The dynamic equilibrium equation is expressed as:

$$F - m\ddot{x}_p - c\dot{x}_p - kx_p = 0 \qquad 3.22$$

The sum of all the terms at the first member of eq. 22 must be zero in order to satisfy the equilibrium in steady-state conditions. The solution of this problem is graphically interpreted adopting Fourier Transform and representing in the complex plane the following vectors:

- x_p displacement
- F external force
- $-m\ddot{x}_p$ inertial load
- $-kx_p$ spring reaction force
- $-c\dot{x}_p$ viscous damping force

For the sake of simplicity, we consider a certain moment in time, at which the displacement of the harmonic oscillator x_p is aligned with the real axis. The inertial load has amplitude $m\omega^2 x_p$ and is aligned with x_p. The elastic reaction force of the spring is parallel and opposite to the displacement x_p, with an amplitude kx_p. The viscous damping force, which has amplitude $c\omega x_p$, has a 90-degree phase lag from x_p, that means that neither the inertial nor the elastic forces may balance the viscous force. The balance is guaranteed by the external load, as shown in figure 3.3. The external force anticipates the displacement vector x_p by a phase ϕ.

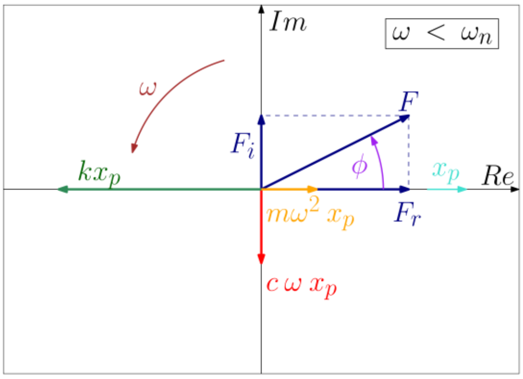

Figure 3.3: Single d.o.f oscillator represented on the complex plane

This balance configuration is valid whenever the frequency of the load is below the natural frequency of the system. Under this condition the elastic forces are higher than inertial forces (see Figure 3.3). In fact, if the exciter's frequency tends to zero, the viscous and inertial reactions tend to zero as well, and the force is balanced to the only elastic reaction of the spring. This is the so-called *static condition*. On the other hand, if the excitation frequency goes above the natural frequency of the system, the inertial reactions become higher than the elastic forces of the spring. Lastly, if the exciter varies with a frequency equal to the natural frequency of the system, bringing the system under *resonance*, the inertial reactions are equal to the elastic forces, and the external load are balanced by the only viscous reactions, as the exciter is offset by 90 degrees with respect to x_p.

Now, assuming the external forces to be periodic, they may be expanded in Fourier series. Due to the linearity hypothesis, the dynamic problems may be decomposed as the summation of a series of problems, in each of which the external load is one of the harmonics of the Fourier series decomposing the original external force.

Moving to a system with multiple degrees of freedom like eq 3.22, the solution may be simplified by representing the system of external forces $\underline{F}(t)$ as the real part of a complex vector, expressed in the exponential form:

$$\underline{F}(t) = Re[\underline{f}\,e^{j\omega t}], \Rightarrow \underline{f} \in \mathbb{C} \Rightarrow \underline{f} := \underline{f_0}\,e^{j\Phi} \qquad 3.23$$

$$\underline{F}(t) = \underline{f_0}e^{j\Phi}\cos(\omega t) + j\underline{f_0}e^{j\Phi}\sin(\omega t) \qquad 3.24$$

Amplitude $\underline{f}$ is, in the most general case, a vector of complex quantities. $\underline{F}(t)$ may be expressed with trigonometric functions (eq. 3.24). This notation is equivalent to expressing the system of external forces as a list of complex vectors in the complex plane, all of which are rotating at the same rotational speed but with slightly different relative angular position. To give an example, the i-th component of $\underline{f}$ is shown in figure xx.

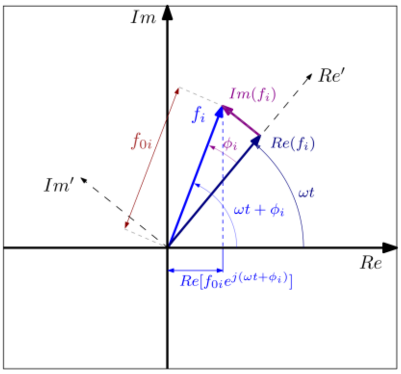

Figure 3.4: i-th component of $\underline{f}$ in the complex plane.

That component is a vector with an amplitude f_{0i}, it is rotating around the origin of the complex plane, with a rotational speed ωt and it is inclined by an angle ϕ_i from a component of $\underline{f}$, say the j-th one, which is in this case purely real. The angular position of the purely real components of $\underline{f}$ are represented by the rotating complex plane. The amplitude of f_i in the domain of time is the real part of f_i, as seen from the fixed complex plane:

$$Re\left[f_i e^{j\omega t}\right] = f_{0i}\,cos(\omega t + \varphi_i) \qquad 3.25$$

After the analysis of the exciting system of forces, the first member of eq. 3.22 is now the object of our study. Moving to the frequency domain, the problem is expressed as follows:

$$\left(-\omega^2\underline{\underline{M}} + \boldsymbol{j}\omega\underline{\underline{C}} + \underline{\underline{K}}\right)\underline{x} = \underline{f} \qquad 3.26$$

Finite element analysis allows the solution of the frequency response problem above, which is usually preceded by the investigation of the modes of vibration of the dynamic system. The study of the modes of vibration has primary importance on the approval of a structural component. Neglecting these aspects may have, in the worst case, catastrophic consequences, like the French bridge *Pont d'Angers*, which collapsed in 1850 during the transit of a battalion of soldiers. The reason of the failure, which was not apparent back in the day, was the excitation developed by the synchronized march of the soldiers. This excitation had a frequency close to one of the natural frequencies of the bridge, and led it to resonance. To avoid this inconvenience, nowadays, soldiers break ranks when crossing a bridge.

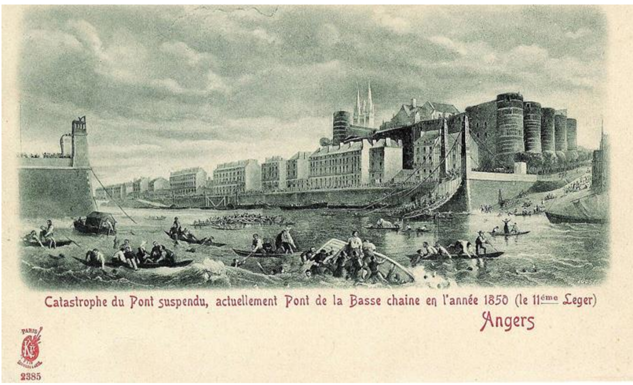

Figure 3.5: Pont d'Angers, 1850. *https://it.wikipedia.org/wiki/Ponte_Angers#/media/File:Pont_de_la_Basse-Cha%C3%AEne_(7).jpg*

3.2 Modal Analysis

Modal analysis aims at obtaining the periodic modes of vibration occurring without any external loads or damping. As no structural damping is considered, the stiffness matrix has real coefficients only. After the Fourier transform of the dynamic equation, one obtains:

$$\left(-\lambda \underline{\underline{M}} + \underline{\underline{K}}\right) \underline{x} = \underline{0}, \qquad \underline{x} \neq 0 \ \wedge \ \lambda = \omega^{2} \tag{3.27}$$

In order to satisfy the equation, at least one of the two terms of the first member must be zero. Put aside the non-trivial solution, which describes the undeformed structure, the solutions of the problem are found when the frequency equals one of the natural frequencies of the system. These frequencies are found by imposing:

$$det\left(\underline{\underline{K}} - \lambda \underline{\underline{M}}\right) = 0, \ \Rightarrow P(\lambda) = 0, \ deg\big(P(\lambda)\big) = n \tag{3.28}$$

Eq. 3.28 is the characteristic equation of the dynamic problem; the determinant of the dynamic matrix is a polynomial in which λ has degree *n*. The roots of $P(\lambda)$ are the eigenvalues of the dynamic problem. Being $\underline{\underline{M}}$ and $\underline{\underline{K}}$ symmetrical with only real coefficients, the roots are all real, and represent the natural frequencies of the problem. An eigenvector $\underline{x_i}$ is associated to each eigenvalue, the eigenvectors correspond to the mode shape, i.e. the shape with which the dynamic system vibrates at the corresponding eigenvalue. The solution of the problem is a series of eigenvalue-eigenvector couple $(\lambda_i, \underline{x_i})$, there are as many couples as many unconstrained degrees of freedom the system has. The effect of constraints in the system is included in the system's mass and stiffness matrices, thus identical structures with different constraint systems will generally have different solutions. Eigenvectors may be normalized by multiplying them by an arbitrary constant. Any consideration about the amplitude of the modes makes no sense, if the initial conditions are not known.

The eigenvectors associated to the modes of vibration are orthogonal to each other, with respect to the mass and the stiffness matrix of the system:

$$r \neq s \wedge \lambda_r \neq \lambda_s \Rightarrow \begin{cases} \underline{x_r}^T \underline{\underline{M}}\, \underline{x_s} = 0 \\ \underline{x_s}^T \underline{\underline{K}}\, \underline{x_r} = 0 \end{cases} \tag{3.29}$$

Eigenvectors are frequently normalized with respect to the mass matrix, many finite element software adopt or allow this option. The normalization constant μ is defined as follows.

$$\mu^2 = \frac{1}{\left(\underline{\hat{x}_i}\right)^T M \left(\underline{\hat{x}_i}\right)} \Rightarrow \begin{cases} \underline{\hat{x}_j}^T \underline{\underline{M}}\, \underline{\hat{x}_i} = \delta_{ij} \\ \underline{\hat{x}_j}^T \underline{\underline{K}}\, \underline{\hat{x}_i} = \delta_{ij} \cdot \omega_i^2 \end{cases} \tag{3.30}$$

The normalized eigenvectors, multiplied by the mass matrix, result in 0 or 1. On the other hand, multiplying the eigenvectors by the stiffness matrix results in the square of one of the system eigenvalues, or zero.

Eigenvectors may be grouped in a matrix, called Modal matrix $\underline{\underline{X}}$ multiplying the modal matrix at the left and right of $\underline{\underline{M}}$ results in the identity matrix, while doing the same operations for $\underline{\underline{K}}$ results in a diagonal matrix $\underline{\underline{\Lambda}}$ having the system's eigenvalues on the main diagonal. Therefore, the normalized eigenvectors are an orthonormal base for the dynamic problem. A system of modal coordinates $\underline{\xi}(t)$ may be associated to such base. Moving from the original coordinates to modal coordinates one obtains a diagonal form of the dynamic problem:

$$\begin{cases} \underline{\underline{M}}\,\underline{\ddot{x}} + \underline{\underline{K}}\,\underline{x} = \underline{0} \\ \underline{x}(t) = \underline{\underline{\hat{X}}}\,\underline{\xi}(t) \end{cases} \Rightarrow \underline{\underline{M\hat{X}}}\,\underline{\ddot{\xi}} + \underline{\underline{K\hat{X}}}\,\underline{\xi} = \underline{0} \Rightarrow \underline{\underline{I}}\,\underline{\ddot{\xi}}(t) + \underline{\underline{\Lambda}}\,\underline{\xi}(t) = \underline{0} \tag{3.31}$$

The solution of this system is extremely easy in practice, as the system is made of n uncoupled equations, which may be seen as a series of single-d.o.f. oscillators vibrating with one of the mode shape of the system.

The analysis of the frequency response is adopted whenever the dynamic system under exam is excited by an external load. After the settlement of the first transitory, the steady-state response remains over time. This analysis is performed entirely in the frequency domain. Following the results of modal analysis, eq. 3.1 gives:

$$\left(-\omega_i^{2}\underline{\underline{M}} + \underline{\underline{K}}\right)\mu_i\underline{\hat{x}_i} + j\omega\underline{\underline{C}}\mu_i\underline{\hat{x}_i} = \underline{f} \Rightarrow \mu_i = \frac{1}{j\omega_i}\frac{\underline{\hat{x}_i}^T\underline{f}}{\underline{\hat{x}_i}^T\underline{\underline{C}}\,\underline{\hat{x}_i}} \tag{3.32}$$

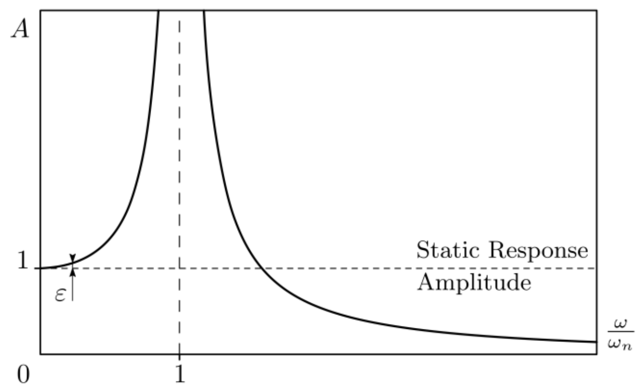

Figure 3.6: Frequency response of 1 d.o.f. system

Figure 3.6 shows the amplitude of the frequency response of the single d.o.f., as a function of the frequency of the excitation. If the excitation frequency is much lower than the natural frequency of the oscillator, the amplitude of the response may be approximated with the amplitude of the response to a static load. The approximation has an error (ε) which becomes progressively lower as the exciter frequency tends to zero. If the system has no damping, the oscillation amplitude under resonance is infinite, by introducing damping, the amplitude of the response under resonance has a finite peak, which increases as the damping intensity decreases.

3.3 Damping

To approach the solution of a dynamic response problem, some assumptions must be made on the damping matrix. Damping is a dissipative phenomenon that decreases the free vibration amplitude over time and limits the vibration amplitude under resonance. Damping can be generally classified in: viscous damping, hysteretic damping and Coulomb friction damping. Viscous damping is generally due to the surrounding fluids, or by specific components. It consists in a reaction force proportional to the vibration speed, the energy dissipated through a cycle is proportional to the frequency and to the oscillation amplitude. Structural damping is typical of structural materials and derives from local plastic deformations at a microscopic level, even though the material is globally working in the linear elastic field. Coulomb damping shows mechanisms similar to hysteretic damping but is associated to dry friction between surfaces in relative motion. Damping is mostly due to hysteresis and friction, however, being the modelling of these phenomena complicated, damping is generally approximated with viscous damping models. The entity of hysteretic damping may be evaluated in terms of energy, by calculating the work done by an external harmonic load on the system. As Figure 3.3 shows, damping is the only action that balances the imaginary part of the external load. Considering a single d.o.f. oscillator, the external force anticipates the displacement by a phase φ:

$$f = Asin(\omega t) \ \Rightarrow \ x = Bsin(\omega t - \varphi) \qquad 3.33$$

$$L_0 = AB\omega \int_0^T sin(\omega t) sin(\omega t - \varphi) dt = AB\pi sin\varphi \qquad 3.34$$

Eq. 3.34 expresses the work of the external force in a single cycle ($T = \frac{2\pi}{\omega}$). This work is maximum if φ reaches 90° or 270°. In fact, in these conditions, the damping force balances the entire external force. On the other hand, the dissipated work is zero, if the force is in phase or in counterphase with the displacement (i.e. φ is equal to 0° or 180°). The work dissipated by the viscous damper may be expressed, under the conditions of maximum dissipation, as:

$$L_v = \pi c \omega B^2 \qquad 3.35$$

$$B = \frac{Asin\varphi}{c\omega} = B_m \qquad 3.36$$

Eq. 3.36 expresses the amplitude of the response under maximum dissipation. That value depends on the amplitude of the external load, and it is inversely proportional to the damping coefficient, as shown in Figure 3.7:

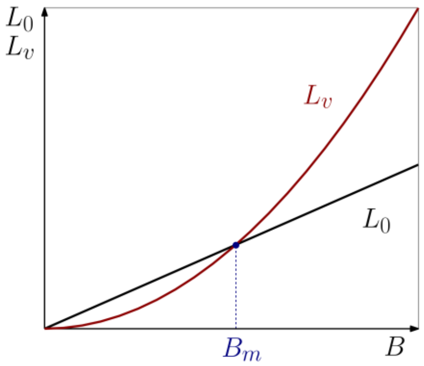

Figure 3.7: Amplitude of the response under maximum dissipation identified by the balance between the wok of the external load, and the work of the viscous damper.

Hysteretic damping originates from a resistance inside the structural material, which determines some phase lags between excitations and deformations, therefore, in the system's intrinsic stiffness. Based upon this observation, the work dissipated by hysteretic damping may be expressed as:

$$L_i = \pi k B^2 \eta \;\; \Rightarrow \; \eta \coloneqq sin\varphi \qquad 3.37$$

$$c_s = \frac{\eta k}{\omega} \Rightarrow -m\omega^2 X + k(1 + j\eta)X = F \Rightarrow \; k_c = k(1 + j\eta) \qquad 3.38$$

where η is the structural damping coefficient, which is usually substituted by an equivalent viscous damping coefficient, which is more easily manageable in practice. The equivalent viscous damping coefficient (c_s) is expressed by equating the work dissipated by the two damping phenomena. The effect of structural damping is evident if c_s is substituted in the dynamic equation. Eq. 3.38 shows that the only structural damping contribution is linked to the stiffness of the system. Therefore, structural damping is considered as the imaginary part of the system's stiffness. This dissipation behaviour may be understood by expressing the amplitude of the external force as a function of the oscillator's displacement, as shown in Figure 3.8:

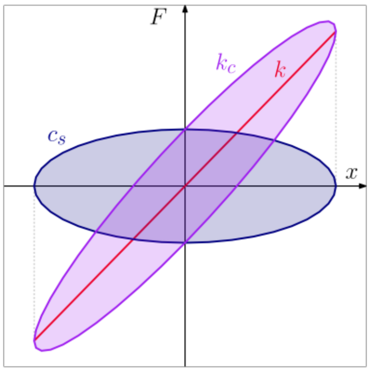

Figure 3.8: Hysteretic damping work per unit cycle.

The effect of damping is the result of the coexistence of two terms: the first one is the energy dissipation ellipse in blue, limited by the amplitude of the harmonic load and response. The second term is the real part of the stiffness matrix, which does not perform work on the system. It is shown in figure 3.8 as a segment inclined with a slope equal to the stiffness of the system. The overall damping is the sum of the two contributions and it is shown by the purple inclined ellipse. Regardless its nature, damping in structural problems is usually small, and its effect on the structural response is not macroscopic. Thus, it is possible to model the damping effect using the viscous model. There are various ways to model damping in a mechanical system. One of the handiest ways to do so is allowing the diagonalization of the damping matrix, like what happens with the mass and stiffness matrices, obtaining thus the decoupling of the balance equation in modal coordinates.

Among all the models which allow such diagonalization, a popular model is Rayleigh proportional damping. This model describes the effects of viscous damping with acceptable accuracy for many applications. The model assumes that damping effects are one order of magnitude lower than those of inertia and stiffness. In this model, the damping matrix is expressed as a linear combination of the mass and stiffness matrices:

$$\underline{\underline{C}} = \alpha \underline{\underline{M}} + \beta \underline{\underline{K}} \Rightarrow \underline{\underline{\hat{x}}}^T \underline{\underline{C}}\, \underline{\underline{\hat{x}}} = \alpha \underline{\underline{I}} + \beta \underline{\underline{\Lambda}} \qquad 3.39$$

As for the other matrices, the eigenvectors of the problem are orthogonal to each other with respect to $\underline{\underline{C}}$. Therefore, $\underline{\underline{C}}$ is diagonalized by the modal matrix $\underline{\underline{X}}$, and like for the free vibration problem, the shift to modal coordinates simplifies the dynamic problem in n decoupled equations, where n is the number of degrees of freedom of the system. The n equations represent n single-d.o.f. harmonic oscillators vibrating with the shape of the corresponding normal mode, just like was for the analysis of free vibrations, with the only exception that the i-th harmonic oscillator of the sequence have a modal damping ratio ζ_i associated to the i-th normal mode. Each modal damping ration is defined according to the corresponding natural frequency ω_i:

$$\zeta_i = \frac{1}{2}\left(\frac{\alpha}{\omega_i} + \beta\omega_i\right) \qquad 3.40$$

Equation 3.40 shows that the dependence of modal damping ratio from the same coefficients that defined the damping matrix. Figure 3.9 shows modal damping as a function of frequency.

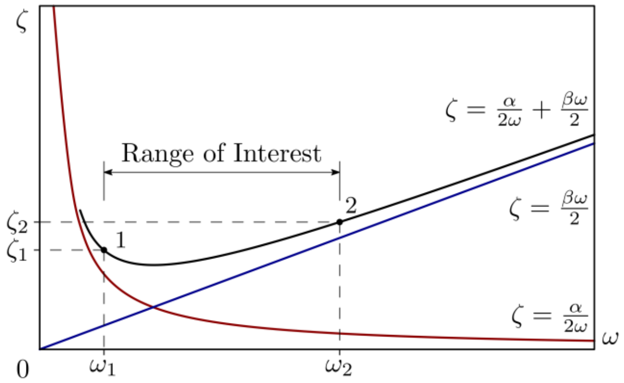

Figure 3.9: Modal damping ratio as a funtion of frequency.

$\underline{\underline{C}}$ may be proportional to just one of the other two matrices defining the dynamic problem. Two extremal cases:

- $\beta = 0 \Rightarrow \zeta_i = \frac{\alpha}{2\omega}$: damping is proportional to the sole mass matrix and it is inversely proportional to the frequency.
- $\alpha = 0 \Rightarrow \zeta_i = \frac{\beta\omega}{2}$: damping is proportional to the stiffness matrix only. This time, the damping ratio goes linear with the frequency.

Frequency response analysis through modal decomposition aims at obtaining a transformation of the dynamic problem by exploiting the modal base, typically normalized with respect to mass matrix. The system of decoupled equations is:

$$\left[-\omega^2 \underline{\underline{I}} + j\omega\left(\alpha\underline{\underline{I}} + \beta\underline{\underline{\Lambda}}\right) + \underline{\underline{\Lambda}}\right]\underline{\xi} = \underline{q} \qquad 3.41$$

The term at the second member of equation 3.41 is the product between the amplitude of the external load and the modal matrix; it is thus the projection of the system of external loads into the vectorial space defined by the normal modes, also called modal *space*. The steady-state response of the system is the linear combination of the solutions of the decoupled equation (ξ_i), which is made on account of the principle of superimposition. The solutions of the decoupled equations may be expressed in time or frequency domains.

$$\xi_i(t) = |\xi_i| \, cos(\omega t + \psi_i - \phi_i) \qquad 3.42$$

The amplitude $|\xi_i|$ and the two phase lags (ψ_i and ϕ_i) of the solutions ξ_i are expressed as follows:

$$|\xi_i| = \frac{|q_i|}{{\omega_i}^2} \frac{1}{\sqrt{\left[1 - \left(\frac{\omega}{\omega_i}\right)^2\right]^2 + 4{\zeta_i}^2\left(\frac{\omega}{\omega_i}\right)^2}} \qquad 3.43$$

$$\psi_i = arg\ (q_i);\ \phi_i = arg\ \left(1 - \left(\frac{\omega}{\omega_i}\right)^2 + 2j\zeta_i\frac{\omega}{\omega_i}\right) \qquad 3.44$$

3.4 Modal Truncation

Modal decomposition allows the solution of a system when the system has a reasonable number of degrees of freedom, and hence of normal modes. This is usually not true in Finite Element analysis, especially when dealing with systems made up of many mechanical components. In these cases, only a limited part of the normal modes of the system is extracted with the modal analysis and adopted for the solution of the system. This procedure is often called *modal truncation*. The modes that are excluded from the modal basis are not included in the response of the system. This is equivalent to applying some implicit boundaries to the model, since some particular motions of the model are somewhat impeded. Truncating the modal basis introduces an approximation in the solution, which must be considered not to obtain misleading results. Many studies emerged around the 80s and 90s to reduce such approximation, such as Mode Acceleration Method (MAM) and Modal Truncation Augmentation Method (MTAM). Dickens *et al.*[32] compare these methods finding out that MTAM may be integrated with greater ease in numerical software addressing frequency response analysis. In addition, MTAM is adopted in todays Finite Element solvers, and is presented very clearly by many authors [33]–[36].

The exact response of the system is the combination of the normal modes selected in the truncated modal basis and all the other non-retained modes:

$$x(\omega) = \underline{\underline{\hat{X}}}\underline{\xi}(\omega) = \underline{\underline{\hat{X}}}_r\underline{\xi}(\omega)_r + \underline{\underline{\hat{X}}}_{nr}\underline{\xi}(\omega)_{nr}, \qquad 3.45$$

- $\underline{\underline{\hat{X}}}_r$ retained modes,
- $\underline{\underline{\hat{X}}}_{nr}$ non-retained modes.

MTAM aims at defining some *residual modes*, which are fictitious modes to be added to the truncated modal basis. Residual modes are orthogonal with respect to the mass and stiffness matrices, but they are not the result of the generalized eigenvalue problem defining normal modes. As the modal base is truncated, a part of the external load has no projection onto the modal space. Considering the sole part of the external load that is projected in the truncated modal space ($\underline{q}$) would induce an error[33], [35], [37]. To reduce this error, the non-projected part of the external load is balanced by a fictional mode having a natural frequency much higher than the modal basis. The high natural frequency of the fictional mode ensures that in the frequency range defined by the truncated modal base, the dynamic response to the fictional mode is similar to a quasi-static, being the inertial forces much low (see Fig. 3.6). This solution helps in balancing the inertial and elastic contribution to the response, which is generated by modal truncation. This technique is also known as *quasi-static compensation* of modal force. It requires as many residual vectors as many degrees of freedom are excited by the external system $\underline{F}$. The effectiveness of this method may be proven in many ways. Take, as an example, the cantilever plate, loaded within its middle plane. The modal base is truncated at the plate's fourth mode, and all the modes of the base consider the out-of-plane vibrations of the plate. Being these modes characterised by motion in a direction perpendicular to the external load, the projection of the external load in the modal space will result in a null system of forces, which would then result in a wrong solution. The following plots compare the solutions considering the direct solution method (blue curve), the modal decomposition with (red curve) or without (green curve) residual modes. If the modal base does not contain all the significant modes for the solution, the result is much different from the analytical solution. A practical way to prevent the truncated modal base from being too poor is including the modes associated to a natural frequency up to twice the maximum frequency of the external load under exam. Combining this tip with MTAM, the frequency response of the system is calculated with good approximation up until the maximum frequency of interest for the external load. Furthermore, the computational time and effort is much lower, if compared to what the direct solution method needs.

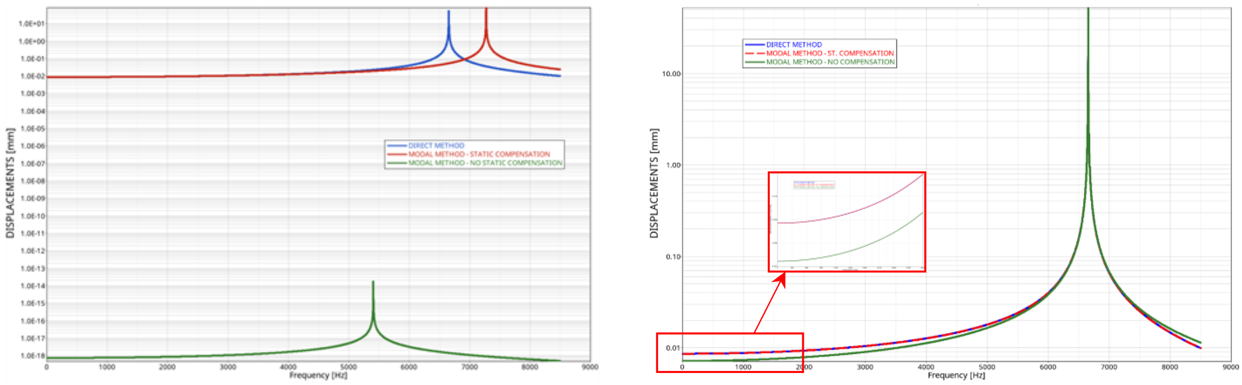

(a) (b)

Figure 3.10: (a) Effect of the residual vector on an insufficient modal base. (b) Correct application of modal truncation and static compensation.

Modal superimposition has become a standard instrument for seismic analysis [36], as well as for vibro-acoustic problems in automotive [37]. The method is robust both from the theoretical, and from the practical point of view. The determination of the main modes to represent the response of the dynamic system is up to the analyst.

There are other ways to calculate the frequency response of a dynamic system. *Direct method* aims at directly solving the dynamic equation (with or without damping) in the frequency domain. The term "direct" denotes that no coordinate transformation is performed. The equation system is solved using a step-by-step method.

There are also hybrid methods which embrace the best of the opportunities offered by modal decomposition and the direct method. The main method of this kind is Lanczos, which may be adopted for Finite Element models. This method employs peculiar numerical techniques like Sparse Decomposition, which increases calculation speed while reducing the computational burden.

In general, there is no absolute best method between modal decomposition and direct method, the choice between the two depends on the accuracy and to the available time for the calculation. Table T 3.1 summarizes when one method is to be preferred.

T 3.1: Modal method vs Direct method

CONDITION	**MODAL**	**DIRECT**
Small model		X
Large model	X	
Few excitation frequencies		X
Many excitation frequencies	X	
High excitation frequencies		X
Non-modal damping		X
Higher accuracy		X

4 Fluid-structure interaction

4.1 – General Theory

Noise propagates from the source to the receiver through pressure waves within a solid or fluid medium. Identifying the laws governing sound transmission is necessary in describing noise perceived by the occupants of a vehicle, considering both the fluid and the structural problem. Finite element modelling of Fluid-structure interaction is at the basis of this thesis. Vibro-acoustic problems with fluid-structure interaction have been addressed since the second half of the 20th century. At first, attention was paid on theoretical problems, addressing their applicability in practice, which is crucial to acknowledge the effectiveness of these studies. Foxwell [38] and Warbuton [39] study how an acoustic field within a fluid may affect the vibration of a shell. On top of that, Pretlove [40] deal with the interaction between a fluid acoustic cavity and a simply supported plate. In these studies, the authors adopted a common approach, which attempts at determining the equations of motions by dividing the fluid and structural domain. Basically, this approach consists in finding the normal modes of structural components as if they were in the vacuum, solving then the wave propagation equations of the fluid domain. The interaction between the two domains is modelled with an equilibrium equation at the interface of the two domains.

Following these early works, studies tried to unify the solution of the two domains by the describing the problem in terms of displacement [Gladwell and Zimmermann [41]; Gladwell[42] or pressure field [43]. Craggs [4] simulates the behaviour of a window interacting with the air volume enclosed in a room subject to sonic boom. The solution is obtained through the Finite Element (FE) modelling of the problem by means of shell and fluid elements. For the structural domain, shell elements lead to the resulting displacement field, while fluid elements aim to obtain the pressure field within the fluid. The main advantage of this approach is the more immediate experimental validation of the numerical results. In fact, experiments in structural dynamics are mainly focused on the displacement field, alongside with its derivatives over time; while, the pressure field is the quantity of general interest in acoustic. The equation of motion of a plate, which vibrates in a three-dimensional space is:

$$\rho h\ddot{w} + \frac{Eh^3}{12(1-\nu^2)}\nabla^4 w = p_E(x,y,t) - p_A(x,y,t) \qquad 4.1$$

where:

- ρ = density of the material;
- h = thickness of the plate;
- w= time dependent displacement's variable;
- E = modulus of elasticity;
- ν = Poisson coefficient;
- p_E= pressure arising from the external perturbation work;
- p_A= pressure arising from the work done by the acoustic field (negative because it is opposed to the external work)

The pressure field is described by the wave propagation equation, expressed as follows:

$$\nabla^2\phi - \frac{1}{c^2}\cdot\frac{\partial^2\phi}{\partial t^2} = 0 \qquad 4.2$$

In which:

- ϕ = velocity potential,
- c= speed of sound in the fluid medium.

To complete the description of the fluid-structure interaction, the only missing part is the description of the interface between the two domains:

$$\rho\dot{w} = -\frac{\partial\phi}{\partial n} \tag{4.3}$$

where n is the direction normal to the interface.

The equation of motion of the fluid domain expresses the pressure field after a differentiation over time, by applying the following identity:

$$p = -\rho\frac{\partial\phi}{\partial t} \tag{4.4}$$

$$\nabla^2 p - \frac{1}{c^2}\cdot\frac{\partial^2 p}{\partial t^2} = 0 \tag{4.5}$$

Therefore, the expression of the pressure gradient at the interface between fluid and structure is:

$$\rho\ddot{w} = -\frac{\partial p}{\partial n} \tag{4.6}$$

The analytical solution of these problems may be tackled for some notable cases only. For more general cases, numerical approaches are adopted to approximate the exact solution.

4.2 Application to the FE method

FE analysis of acoustic systems requires the discretization of the acoustic volume into nodes and elements. Any acoustic volume may be enclosed by rigid, deformable or damping walls. Alternatively, the acoustic radiation of a structure may be examined in an anechoic or free environment. Analytical methods may be adopted to calculate acoustic fields and structural vibrations for the simplest systems only. These systems include limited geometries, like rectangles, circles, and their three-dimensional counterparts [44]. Considering geometries of higher complexity, the literature converges towards numerical analyses, like FE or Boundary Element Method (BEM). FE analysis of acoustic systems has several applications, among which we have the analysis of internal sound fields, the sound radiation arising from structural vibrations, panel sound Transmission Loss (TL), and the design of sound insulating system. FE methods are mainly linked to structural problems as well as – particularly for linear problems – the solution of Navier elasticity equation. Commercial software allow the approximate solution of such equations by discretizing a domain and solving the problem at the nodes of the finite elements. However, Everstine G. C. [3] evidences the analogy between the elasticity equations and those describing scalar fields, like Helmholtz equation, Laplace equation, Poisson equation, heat transfer equation and the laws governing hybrid problems, like fluid-structure interaction for acoustic problems. These laws describing linear physical problems may be represented by a single general relation, in which the unknown terms are to be specified:

$$\nabla^2 \phi + g = a\ddot{\phi} + b\dot{\phi} \qquad 4.7$$

in which ∇^2 is the Laplace operator. g, a and b are generally dependent on the position in space, while ϕ is the unknown scalar field, which appears also in its time derivatives. Everstine G. C. [45] proposes as an example the Navier elasticity equation for structural field, which is in the direction x:

$$\left(\frac{\lambda + 2\mu}{\mu}\right) u_{xx} + u_{yy} + u_{zz} + \left(\frac{\lambda + \mu}{\mu}\right)\left(v_{xy} + w_{xz}\right) + \frac{1}{\mu} f_x = \frac{\rho}{\mu}\ddot{u} \qquad 4.8$$

in which u, v and w are the Cartesian components of the displacement field, λ and μ are Lamé elasticity constants – μ being the shear modulus – and f_x is the force per unit volume along x, ρ is the material density and u_{xx} is the second partial derivative of u with respect to x. Navier's equation along x may be obtained from the 4.8 by introducing:

$$\left(\frac{\lambda + 2\mu}{\mu}\right) = 1 \qquad 4.9$$

$$v \equiv w \equiv 0 \qquad 4.10$$

$$a = \frac{\rho}{\mu} \qquad 4.11$$

$$g - b\dot{\phi} = \frac{1}{\mu} f_x \qquad 4.12$$

The same approach may also be adopted for the boundary conditions, which are crucial in the definition of fluid-structure interaction problems:

$$a_1 \frac{\partial \phi}{\partial n} + a_2\phi + a_3\phi + a_4\ddot{\phi} + a_5 = 0 \qquad 4.13$$

where n is the normal vector pointing outwards from the domain boundary.

FE methods consider a coupling between structures and fluids like air or water. In acoustic fluid-structure interaction problems, the equations of structural dynamics must be considered along with the mathematical description of the acoustic system, which is done by means of Navier-Stokes equation of conservation of the momentum of the fluid. Some hypotheses may be done in describing the fluid motion:

- the acoustic pressure in the fluid medium is determined by wave equation,
- the fluid is assumed to be compressible: density variations are due to pressure variations
- the average fluid flow is absent,
- the density and pressure may vary along the elements, and the acoustic pressure is the excess over the average pressure,
- FE analyses are limited to relatively low acoustic pressures, so that the density variations from the average are small [44].

Graggs [4] derives the formulation for a cubic finite element by considering Hermite polynomials as shape functions to describe the velocity potential at the nodes. The same approach may be extended to plate elements.

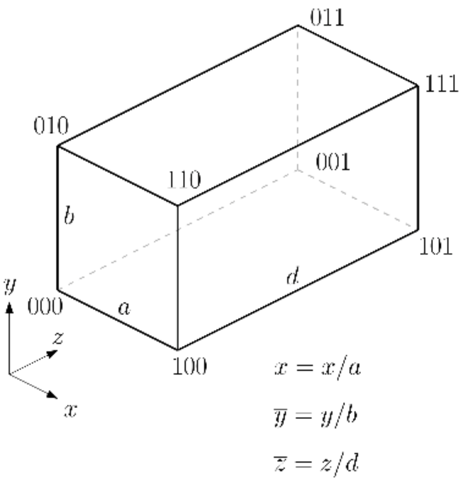

Figure 4.1: Fluid element.

The velocity potential at the nodes depends on the value of the polynomial and on the unknowns ϕ, $\frac{\partial\phi}{\partial x}$, $\frac{\partial\phi}{\partial y}$ and $\frac{\partial\phi}{\partial z}$. The expression of the potential within the element is:

$$\begin{aligned}\phi(x,y,z) = \sum_{i,j,k=0}^{1} \phi_{i,j,k} g_p(\bar{x}) g_q(\bar{y}) g_r(\bar{z}) + \sum_{i,j,k=0}^{1} \frac{\partial\phi}{\partial \mathrm{x}_{i,j,k}} g_\alpha(\bar{x}) g_q(\bar{y}) g_r(\bar{z}) \\ + \sum_{i,j,k=0}^{1} \frac{\partial\phi}{\partial \mathrm{y}_{i,j,k}} g_p(\bar{x}) g_\beta(\bar{y}) g_r(\bar{z}) + \sum_{i,j,k=0}^{1} \frac{\partial\phi}{\partial \mathrm{z}_{i,j,k}} g_p(\bar{x}) g_q(\bar{y}) g_\gamma(\bar{z})\end{aligned} \qquad 4.14$$

$$p = 2_i + 1$$
$$q = 2_j + 1$$
$$r = 2_k + 1$$
$$\alpha = 2_i + 1$$
$$\beta = 2_j + 1$$
$$\gamma = 2_k + 1$$
$$g_1(\varepsilon) = 1 - \varepsilon^2 + 2\varepsilon^3$$
$$g_2(\varepsilon) = \varepsilon - 2\varepsilon^2 + \varepsilon^3$$
$$g_3(\varepsilon) = 3\varepsilon^2 - 2\varepsilon^3$$
$$g_4(\varepsilon) = \varepsilon^3 - \varepsilon^2$$

The potential may also be expressed in a more compact form as:

$$\phi = \boldsymbol{\phi}_e{}^T \{g_x, g_y, g_z\} \qquad 4.15$$

and similarly for the displacement field of shell element:

$$w = \mathbf{w}_e{}^T \{f_x, f_y\} \qquad 4.16$$

The equation of motion of the fluid element is obtained by imposing condition of minimum to the action integral (applying thus Hamilton's theorem) for any arbitrary variation of the velocity potential, which must withstand the following condition:

$$\delta\phi_e = 0, \text{per } t = t_1 \ \wedge \ t = t_2 \qquad 4.17$$

The action integral is defined by kinetic energy T, the strain energy V and the virtual work of the external forces (B_E) and the opposing virtual work at the interface (B_A):

$$J = \int_{t_1}^{t_2} [T - V + (B_E - B_A)]dt. \qquad 4.18$$

In a more expanded form, the action integral has the expression shown in eq 4.19, which considers the velocity potential by substituting the displacement u:

$$J = \int_{t_1}^{t_2} \left[\frac{1}{2}\rho \iiint (grad(\phi))^2 dx\, dy\, dz - \frac{1}{2}\frac{\rho}{c^2}\iiint \phi^2 dx\, dy\, dz + \iint (-\rho\phi_s u_s) dx\, dy\right] dt. \qquad 4.19$$

The integrand function identifies the acoustic Lagrangian L. Considering the velocity potential and the Finite Element displacement field (Eq. 4.15, 4.16), and applying the condition of stationarity to the variational formulation (Eq. 4.17), the equation of motion simplifies to:

$$\delta J = \int_{t_1}^{t_2} \left[\rho\delta\mathbf{\phi}^T \boldsymbol{S}_e \phi + \left(\frac{\rho}{c^2}\right)\boldsymbol{P}_e \ddot{\mathbf{\phi}} - \rho\boldsymbol{\theta}_e \ddot{\mathbf{w}}\right] dt = 0. \qquad 4.20$$

The equation of motion of fluid elements is obtained with steps similar to those adopted to express the motion of solid elements:

$$\left(\frac{1}{\rho c^2}\right)\boldsymbol{P}_e \ddot{\boldsymbol{P}}_e + \left(\frac{1}{\rho}\right)\boldsymbol{S}_e \boldsymbol{P}_e = \rho\boldsymbol{\theta}_e \ddot{\mathbf{w}} \qquad 4.21$$

The approximated equation of motion of the fluid element is comparable with the wave equation characterised by a volume source:

$$\left(\frac{1}{c^2}\right)\ddot{\boldsymbol{P}} - \nabla^2 p = \rho\frac{\partial q_s}{\partial t}, \qquad 4.22$$

In which q_s indicates the acoustic source, which may be seen as a source of volume flow. A term concerning the acceleration [4] is at the first member. It is worth to note that the above relations are valid for a single fluid element; therefore, when assembling a model, its consistency must be ensured with respect to adjacent elements, in terms of pressure and pressure gradient at a node that belongs to two or more finite elements [46].

The equation of motion of the structural domain, *i.e.* the plates that surround the fluid domain, is expressed as:

$$\boldsymbol{M}_e \ddot{\boldsymbol{w}}_e + \boldsymbol{K}_e \boldsymbol{w} = \boldsymbol{F} - \boldsymbol{\theta}^T \boldsymbol{P}_e, \qquad 4.23$$

The vibro-acoustic problem is characterised by the coupling of the two domains, as well as by the definition of the interaction between them. The coupled problem may be rationalized in the following matrix form, considering the assembled matrices describing the discretised systems:

$$\begin{bmatrix} \boldsymbol{M} & \boldsymbol{0} \\ \boldsymbol{0} & \boldsymbol{P} \end{bmatrix} \begin{bmatrix} \ddot{\boldsymbol{w}} \\ \ddot{\boldsymbol{P}} \end{bmatrix} + \begin{bmatrix} \boldsymbol{K} & \boldsymbol{\theta}^{\boldsymbol{T}} \\ \boldsymbol{0} & \boldsymbol{S} \end{bmatrix} \begin{bmatrix} \boldsymbol{w} \\ \boldsymbol{P} \end{bmatrix} = \begin{bmatrix} \boldsymbol{F} \\ \boldsymbol{0} \end{bmatrix}, \qquad 4.24$$

This time an external force on the structural domain of the system is considered, and any acoustic source is assumed to be zero. The problem is in general not symmetrical, which means that the solution of the associated eigenvalue problem may take a high computational effort. The submatrix θ^T represents the interaction between the fluid and structural domain, which is very important in this problem. The interface conditions given by Eq. 4.6 require the application of a force at each node of the fluid domain at the interface. The condition is expressed in terms of $\rho A\ddot{w}_n$, where A is a fraction of the area of the elements adjacent to that node, and $\ddot{w}_n$ is the acceleration of the fluid particle normal to the interface. The dual condition implies the application of fluid pressure on the structure at the interface. This pressure is converted in a system of forces $-pA$ at the nodes of the structure. These observations are valid even when the consistent formulation for the mass matrix of the finite elements is employed, as proposed by Zienkiewicz [47], [48] .

The solution of the problem may be obtained adopting the modal superimposition method, thus, solving a preliminary modal analysis. The following pages of this section will deal with the solution of some notable problems, in which analytical results will be compared to the results of numerical simulations, to prove the accuracy of the simulations. These problems are widely analysed by Everstine G. C. [45]. Before treating these cases, the modal analysis of a simple, hexahedral fluid cavity will be presented. The analytical solution of such problem is known. The associated eigenvalue problem is:

$$[\boldsymbol{S} - \boldsymbol{\omega}^2 \boldsymbol{P}]\boldsymbol{p} = \boldsymbol{0}, \qquad 4.25$$

The cavity presents rigid and non-viscous walls, therefore one obtains:

$$\frac{\partial p}{\partial n} = \boldsymbol{0}, \qquad 4.26$$

where S is six eigenvalues equal to zero, corresponding to six eigenvectors, which may be seen like the six rigid body modes associated to structural problems. In these cases, a uniform static pressure field occurs in the cavity. Without these trivial solutions, the following generic solution is obtained:

$$\lambda_{lmn}{}^2 = \pi\left(\frac{l^2}{a^2} + \frac{m^2}{b^2} + \frac{n^2}{d^2}\right), \qquad 4.27$$

where l, m and n are characteristic wave numbers, one for each direction in space. a, b and d are the dimensions of the cavity (see Figre 4.1). The corresponding eigenvectors are expressed as:

$$\varphi_{lmn} = cos\left(\frac{l\pi x}{a}\right) \cdot cos\left(\frac{l\pi y}{b}\right) \cdot cos\left(\frac{n\pi z}{d}\right), \qquad 4.28$$

4.3 Mesh sensitivity

The exact analytical solution of more complex acoustic cavities is either impossible to find, or too complicated to be obtained with numerical approximations. However, some information may still be taken – accepting some approximation – by using FE methods, which is particularly winning in its software implementation. An important aspect concerns the sensitivity of the solution to the element density at which the fluid domain is discretized. Table T 4.1 reports the natural frequencies resulting from the analytical solution and five numerical simulations. Figure 4.2 shows the discretization of the five fluid domains, which is heavily refined to assess the sensitivity of the solution.

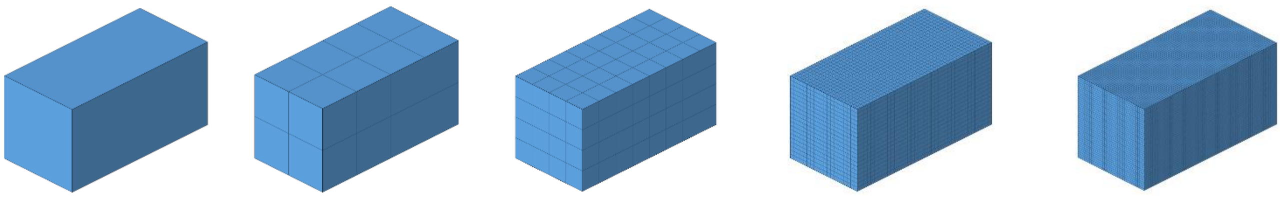

(a) Single element | (b) 16 el.: 4 in $\hat{x}$, 2 in $\hat{y}$, 2 in $\hat{z}$ | (c) 128 el.: 8 in $\hat{x}$, 4 in $\hat{y}$, 4 in $\hat{z}$ | (d) 16000 el.: 40 in $\hat{x}$, 20 in $\hat{y}$, 20 in $\hat{z}$ | (e) 128000 el.: 80 in $\hat{x}$, 40 in $\hat{y}$, 40 in $\hat{z}$

Figure 4.2: FE models of a hexahedral acoustic cavity at five discretization sizes.

The cavity has: $a = 40mm$, $b = 20mm$ and $d = 20mm$, and contains a fluid in which sound propagates at a unitary speed (c). The first seven nonzero natural frequencies are listed in the following table:

T 4.1: First natural frequencies of the acoustic cavity.

Models Frequency ($\times 10^{-2}$ Hz)	**Fig 4.2 (a) 1**	**Fig 4.2 (b) 16**	**Fig 4.2 (c) 128**	**Fig 4.2 (d) 16000**	**Fig 4.2 (e) 128000**	**Analytical Solution [Hz]**
λ_1	1.3783	1.2823	1.2580	1.2503	1.2501	**1.2500**
λ_2	2.7566	2.7566	2.5646	2.5026	2.5006	**2.5000**
λ_3	2.7566	2.7566	2.5646	2.5026	2.5006	**2.5000**
λ_4	3.0820	3.0403	2.8566	2.7975	2.7957	**2.7951**
λ_5	3.0820	3.0403	2.8566	2.7975	2.7957	**2.7951**
λ_6	3.8985	3.8985	3.6270	3.5392	3.5365	**3.5355**
λ_7	4.1350	4.1040	3.8389	3.7587	3.7522	**3.7500**

It is clear how the adoption of an adequate element size is needed in order not to overestimate the results. The element size should be sufficiently lower than the size of the acoustic cavity, as the effect pressure of pressure waves on the scalar pressure field may not be detected if the element size is too large. Focusing on the first fluid mode, which consists of a longitudinal wave, the error between the simulations and the analytical solution decreases as the number of elements increases in the direction of the pressure wave.

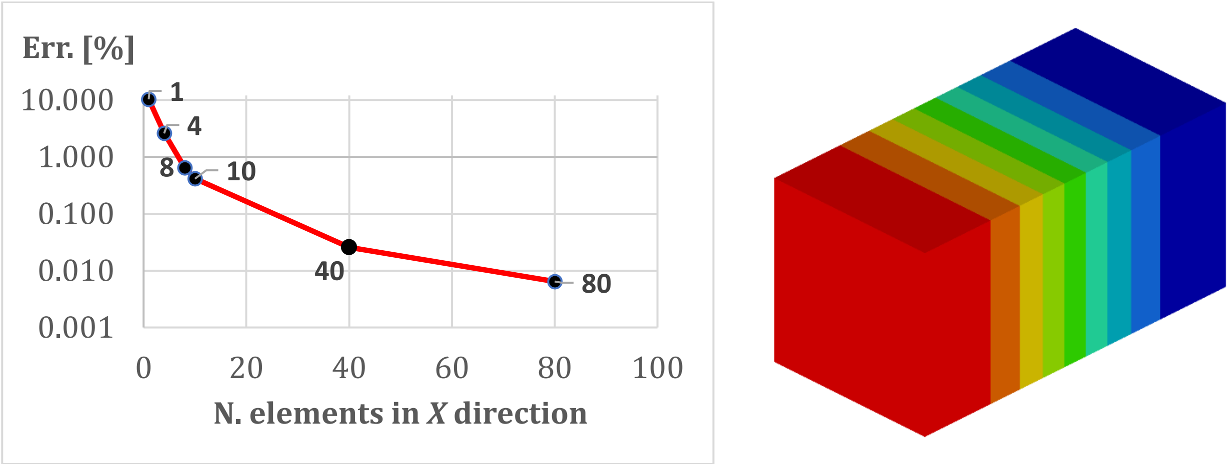

(a) (b)

Figura 4.3: (a) Mesh sensitivity over the first fluid mode of the acoustic cavity (b).

To summarize, the discretization of the fluid domain depends on the type of fluid domain, and it should not alter the simulation results. The discretization density depends on the frequency of the external excitation, as well as on the properties of the fluid domain. A general rule of thumb suggests considering at least six elements to represent properly a wave. Therefore, given the minimum wavelength in the domain, the minimum number of elements is obtained as:

$$N_{elements} = \frac{\lambda}{6} = \frac{c_0}{f_{max}} \qquad 4.29$$

For instance, in the automotive field, these precautions must be considered, both for analyses in which the vehicle is modelled entirely, or in partial configurations during its design and development. During these phases, the dynamic behaviour is investigated for the virtual delivery of the vehicle. In these cases, the number of elements in the model tends to exceed the million, therefore a trade-off is necessary to obtain the results in a reasonable time. The computational effort can be managed by focusing on the accuracy of the results on relevant components, rather than the element size. In fact, the maximum frequency of the excitation – which determines the maximum size of the elements – is typically an input of the model and it cannot be limited. For purely structural and linear problems, *i.e.* when the superposition principle is valid, it is useful to exploit any symmetry of the model. This way, apart from any scaling of the results, the number of degrees of freedom of the model may be reduced by at least a half. This practice is less feasible in dynamics as it involves the exclusion of some normal modes of the structure during the modes' extraction phase. In any case, if the objective of the analysis is studying a specific behaviour of the system, this approach may still be considered. From the fluid domain viewpoint, the analyst could resort to defining specific boundary conditions to obtain the effect of symmetry or skew-symmetry. In the first case, a rigid wall must be applied to the boundary elements at the symmetry plane, while, in the second case, the antisymmetric effect is obtained by imposing zero pressure at the geometric symmetry plane.

4.4 Examples with fluid cavities

Interesting problems generally concern frequency response analyses in which the acoustic cavity amplifies the amplitude of the response of the structural system around its natural frequencies. The state of rest of the system is usually altered by a mechanical excitation, but sometimes there may also be an acoustic source. One of the classic examples of mutual fluid-structure interaction is the hollow cylinder, filled with gas and mechanically forced by a piston like that one of Figure 4.4 (a). This example is interesting as the analytical solution of the problem is known; thus, the analytical and the numerical results can be easily compared.

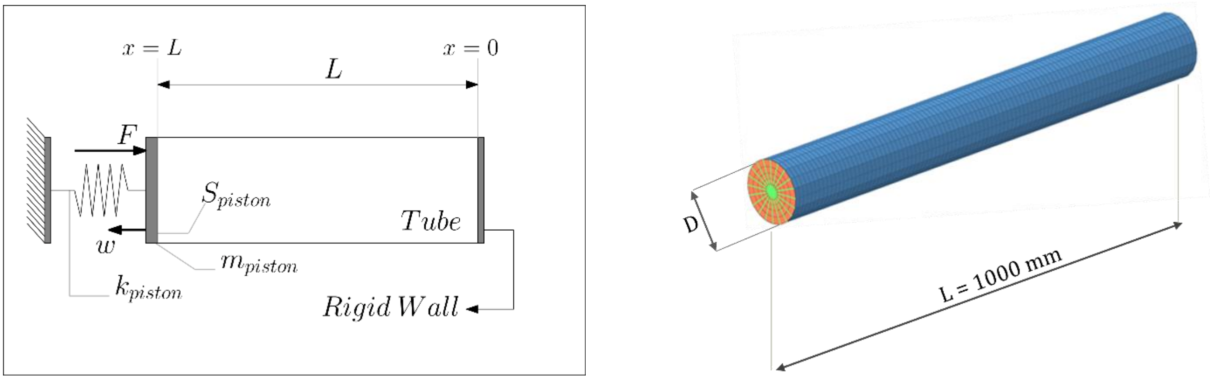

(a) (b)

Figure 4.4: Cylinder dynamic scheme (a) and FE model (b).

The problem may be modelled as mono-dimensional, as the axial length of the cylinder is much larger than the diameter of its cross section. The cylinder contains a pumping system, which is made up of a piston with its own mass (m_{piston}) linked to a linear spring with a defined stiffness (k_{piston}). The piston causes a harmonic perturbation to the fluid system inside the cylinder, which is assumed to have perfectly rigid walls. It is reasonable to think that the problem is periodic in its steady-state behaviour. Thus, it is useful to study the dynamic problem in the frequency domain. Considering the fluid within the cylinder, the pressure field for a 1D domain may be modelled with Helmholtz equation, associated to the relative boundary conditions:

$$\nabla^2\hat{p}(x) + k^2\hat{p}(x) = 0 \tag{4.30}$$

where:

$$k = \frac{\omega}{c_0} \tag{4.31}$$

and ω is the exciter's frequency. The pressure field along the cylinder axis is subject to specific conditions at one extremity of the cylinder ($x = 0$), which is closed by a rigid wall, and at the other extremity ($x = L$), where the piston vibrates:

$$\frac{d\hat{p}}{dx}(0) = 0, \tag{4.32}$$

$$\frac{d\hat{p}}{dx}(L) = \rho_0\omega^2\hat{w}, \tag{4.33}$$

and $\hat{w}$ represents the axial displacement of the piston.

The two conditions of Eq. 4.32-33 define the interaction between the fluid domain and the solid structure. In both cases, perfect adhesion is assumed between fluid particles and the solid wet surfaces. Therefore, in a steady-state balance conditions, no variation of the pressure field is admitted at the rigid extremity, while the oscillating piston determines a variation in volume for the fluid, hence, of pressure, in accordance with the oscillation. No condition is assumed at the lateral surface of the cylinder, in both radial, and tangential direction, as the problem is modelled as one-dimensional. As long as the axial length is higher than its inner diameter, this simplification is reasonable. The solution of Helmholtz equation determines the axial pressure field, which is:

$$\hat{p} \; = \hat{A}cos\,(kx), \qquad 4.34$$

where the amplitude $\hat{A}$ is calculated considering the interaction with the piston (Eq. 4.33):

$$\frac{d\hat{p}}{dx}(L) = -\hat{A}ksin(kL) = \rho_0\omega^2\hat{w} \;\; \Rightarrow \;\; \hat{A} = -\frac{\rho_0\omega^2}{ksin(kL)}\hat{w} \qquad 4.35$$

Therefore, the evolution of the fluid pressure field is expressed as:

$$\hat{p} = -\frac{\rho_0\omega^2}{ksin(kL)}\hat{w}cos\,(kx) \qquad 4.36$$

The only remaining unknown variable is the displacement of the piston ($\hat{w}$), which may be determined from the equation of motion of the single d.o.f. harmonic oscillator equation:

$$\left(k_{piston} \; - m_{piston}\omega^2\right)\hat{w} = S_{piston}\hat{p}(L) + \hat{F}_{ext} \qquad 4.37$$

from which, the amplitude of the displacement is obtained as:

$$\hat{w} = \frac{S_{piston}\hat{p}(L) + \hat{F}_{ext}}{\left(k_{piston} \; - m_{piston}\omega^2\right)} \qquad 4.38$$

introducing $\hat{w}$ in eq. 4.36:

$$\hat{p} = -\frac{\rho_0\omega^2}{ksin(kL)} \cdot cos(kx) \cdot \frac{S_{piston} \cdot \hat{p}(L) + \hat{F}_{ext}}{\left(k_{piston} \; - m_{piston}\omega^2\right)} \qquad 4.39$$

As previously mentioned, the solution of the problem has been replicated using the FE simulations, with the aim of verifying the correctness of the simulation under different types of perturbation of the fluid system. The external excitation can be introduced by modelling the piston and applying the desired harmonic load $\hat{F}_{ext}$. Alternatively, an arbitrary displacement law could be imposed directly to the piston. A third possibility could be the definition of a point sound source that generating a pressure equivalent to the pressure generated by the piston. This method would eliminate one of the two fluid-structure interactions.

This exercise allows to approach the possible sources of noise within a complex physical system, like a vehicle. The analytical result is valid whenever the hypothesis of a one-dimensional problem stands. In the engineering practice, the characteristic dimensions of the fluid tube must be properly calibrated. The problem was numerically simulated FE methods by appropriately discretizing the fluid column. The cylinder had an axial length of 1000 mm while the diameter of the cross section is chosen to be 0.06 times the cylinder axial length. The mesh of the fluid domain is generated by revolution, the solid elements farthest from the axis having a characteristic size of 5 mm, in order not to increase the approximation of the results (Figure 4.5 a).

(a) (b)

Figure 4.5: Detail view of: the mesh of fluid volume(a) and of modelling of piston (b).

The geometry of the piston is omitted from the model; however, its mass and the stiffness of the spring to which it is linked have been consistently inserted in the model (Figure 4.5 b). Four-noded iso-parametric plate elements are used to discretise the surface wetted by the fluid in the interface area and the mass of the piston. The piston is attached to a six-dimensional spring element, setup to respond to the translation of the piston along the axis of the cylinder only. A rigid element connects one end of the spring to the plate elements representing the face of the piston. In this way, no other elastic elements are placed in series with the spring, and the displacement of the piston is exactly the displacement of one extremity of the spring. The other extremity of the spring is fixed. A harmonic force is imposed to the piston. The amplitude of such force varies with frequency. Table T 4.2 summarises the details of the mesh of the model, which has been tuned adopting Altair® Hypermesh pre-processor. The FE simulation is then solved using Altair® OptiStruct.

T 4.2: FE model details.

Components	Elements type	Material	Property
Fluid Domain	Hexahedral 8 nodes	Air - MAT10	PSOLID + PFLUID
Walls	Isoparametric 4 nodes	Steel - MAT1	PSHELL, T = 2 mm
Spring	CBUSH	\	PBUSH, K1 = 100 N\mm
RBE2	1D rigid link	\	\

The frequency response analysis is carried out adopting modal superimposition method. Normal modes of the harmonic oscillator and of the fluid domain are determined adopting Lanczos method [5], [6], [49], the modal basis has been truncated at 2000 Hz. The cut-off frequency should allow to obtain a sufficiently accurate solution up to an excitation frequency of 1000 Hz, as it was discussed in the previous chapter. With this assumption, the modal basis considers a reasonable amount of fluid normal modes, and with the help of a residual mode for static compensation, the model is able to capture all the dynamic effects of the frequency response analysis for all the excitation frequencies below 1000 Hz. Figure 4.6 shows the coherence between the numerical and analytical solution. The analytical solution is obtained adopting a self-built MATLAB script [44].

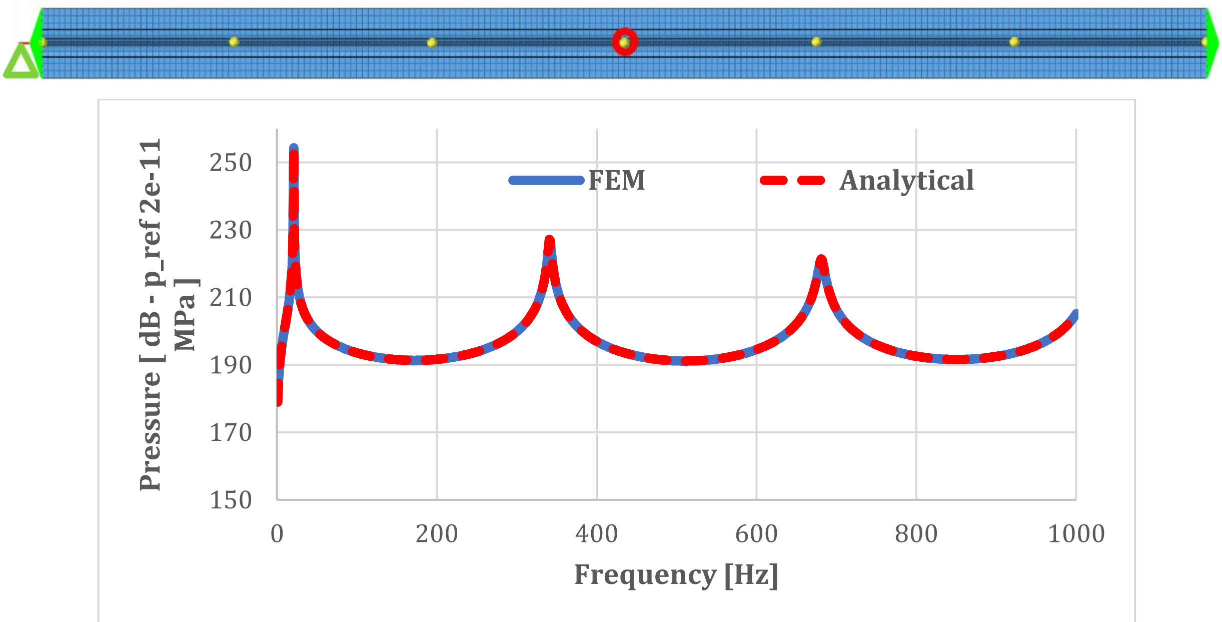

Figure 4.6: Comparison between the analytical and FE results of the pressure field over the excitation frequency.

Figure 4.6 presents the pressure field within the fluid, this distribution has been sampled at a node on the axis of the cylinder, which is highlighted in the inset of Fig. 4.6. Pressure is reported in decibel (dB) and it refers to the minimum pressure audible by the human ear. Resonance peaks are easily distinguished and they show the influence of fluid modes on the response of the system, which would otherwise settle around 190 dB. In this case, the external force has an amplitude varying with frequency to make the piston an acoustic source of $S_{source} = 10^9\ mm^3/s$. This quantity has the dimension of a volumetric flow. The amplitude of the force is:

$$\hat{F}_{ext} = m_{piston} \cdot v_{max} \cdot \omega \qquad 4.40$$

$$v_{max} = \frac{4 \cdot S_{source}}{\pi \cdot D^2} \qquad 4.41$$

As it was anticipated, the effect of the external load could be imposed by directly considering a constant acoustic source equal to S_{source}, or by imposing a maximum speed equal to v_{max} to the piston, or by a force ensuring the uniform acoustic flow along the frequency range. It is immediate to note that in the last case, which was adopted in the system, the amplitude of the external load must be linear with frequency:

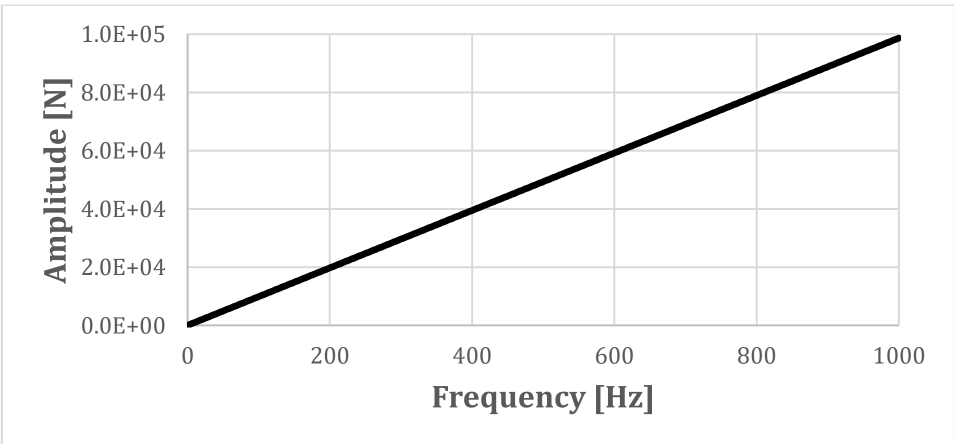

Figure 4.7: Amplitude of the external load over the considered frequency span.

5 – Structural Dynamics, effect of wall-fluid interaction

5.1 Introduction

This section illustrates the study of the dynamic behaviour of plate-like structures with small thickness. These components have been deeply studied in the literature [7], [14], [50]–[52] and are particularly interesting in automotive, as they are the main structures composing unibody frames and moving parts of the body. Therefore, the vibrational behaviour of these structures is analysed. In an automotive body, these structures are typically welded or riveted to more rigid structures like extrusions or castings with three-dimensional geometries. Welding seams and rivets are highly rigid connections. The excitations from the road or the engine mounts trigger the vibration of these structures, determining in many cases non-negligible noise levels in the passenger compartment. The rigid connections and the compliance of these panels, which naturally have out-of-plane modes, make them the main amplifiers of road and engine noise. Noise increase arises from the excessive vibration of these structures, as well as from the pressure field in the fluid medium, especially in correspondence with the natural frequencies of the panels.

To monitor and to predict the problems of structurally transmitted and amplified noise, it is fundamental to properly describe the dynamic behaviour of panel-like structures. The following pages propose a comparative study on the vibration of a simply supported plate, which has been performed with analytical method and Finite Element (FE) simulation. In fact, simply supported plates, or Levy-type plates [8], [11]–[13], are some of those plate-like structures, for which a closed-form solution is known for out of plane normal modes.

5.2 Equivalent Radiated Power (ERP)

The dynamic behaviour of these components, emphasized by normal modes, are studied by evaluating the radiated power content over frequency. This quantity is known in the literature and is used for acoustic applications, as well as for the automotive field [53]–[56]. In this project, this quantity is the basis for the development of a new methodology, which aims at identifying the highest radiating areas of the interface between the vehicle structure and the acoustic cavity. Radiating power is associated to the velocity of the fluid particles, when they are excited by some source of structural vibrations. By exploiting the properties of fluid-structure interaction problems, the analysis of the fluid particles motion may be put aside, considering instead the only dynamic behaviour of the structural radiating surfaces, which are wetted by the fluid. To this end, the Equivalent Radiated Power (ERP) may be introduced as:

$$ERP = \rho_F c_F \int_A \left|\hat{v}_{S,n}\right|^2 dA \qquad 5.1$$

Where ρ_F is the density of the fluid, c_F is the speed of sound through the fluid, $\hat{v}_{S,n}$ is the velocity of the fluid particles normal to the radiating surface.

This relation is derived by considering the acoustic intensity $\vec{I}$ in the frequency domain, which is a complex quantity, obtained by multiplying the pressure p by the velocity $\vec{v}$ of fluid particles:

$$\vec{I} = p\vec{v} \qquad 5.2$$

By considering an area $\vec{A}$, oriented with a normal $\vec{n}$, the acoustic power P may be defined as the real part of acoustic intensity, integrated in the area:

$$P = Re \int_A \vec{I} d\vec{A} \qquad 5.3$$

Eq. 5.3 describes the acoustic power P in the fluid domain. The interaction between fluid and structure is regulated by the interface between the two domains. The two-domain description may be bypassed to evaluate the acoustic power on the basis of the following simplification:

- The surface of a plane and rigid plate is assumed to radiate the fluid with plane waves only.

Plane waves may be described in a single dimension and show pressure in phase with velocity. From these characteristics, the following relation arises for acoustic impedance Z:

$$Z = \frac{\hat{p}}{\hat{v}} = \rho_F c_F. \qquad 5.4$$

where $\hat{p}$ and $\hat{v}$ are the amplitude of pressure and the velocity waves, respectively. Subscripts F denote that the relative quantities are characteristics of the fluid. From Eq. 5.4, the definition of acoustic intensity may be redefined, leading to a new expression for acoustic power:

$$P = \rho_F c_F \int_A \vec{v}^2 d\vec{A} \qquad 5.5$$

Based on the previous assumption, the condition at the fluid-structure interface may be exploited, considering the velocity of a fluid particle (v_F) to be equal to the velocity of the structure normal to the interface ($v_{S,n}$):

$$v_{S,n} = v_F \qquad 5.6$$

Through this fundamental relationship, the speed of the structure normal to the interface can be considered for the calculation of a radiating power equivalent to the acoustic power of the fluid. As a first approximation, accepting the limitations arising from these assumptions, the dynamic behaviour of the panels surrounding an acoustic chamber may be described, in the frequency range of the eventual excitation. The panels may be then classified based on the ERP trend over the excitation frequency. The link between ERP and radiated noise is even more evident if the radiated power is considered in sound units (dB), as presented in the previous pages.

To evaluate this approach, the ERP of a plate is presented, adopting the common method employed of frequency response analysis via FE methods. An aluminium plate, simply supported on its perimeter is loaded at its centre of gravity by a unitary harmonic force with constant amplitude in the range between 0 and 400 Hz. The plate has the following characteristics:

Table 5.1: (a) Features of the aluminium plate under investigation; (b) FE model of the plate

	Symbol	Value	Units
Aspect Ratio	a/b	2	/
Length	a	1000	mm
Width	b	500	mm
Thickness	h	1	mm
Modulus of Elasticity	E	71000	MPa
Density	ρ	2700	kg/m^3
Poisson Ratio	ν	0.33	/

(a)

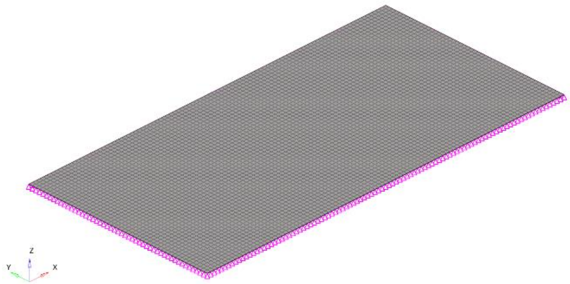

(b)

The FE model has been defined by discretizing the plate with four noded iso-parametric elements having an average size of 10mm. The plate has 5000 elements and 5151 nodes. The frequency response analysis is carried out using the modal superimposition method. AMSES sub-structuring algorithm has been adopted in determining the normal modes of the plate [5], [6], [49]. The objective of the analysis is to evaluate the ERP in decibel (dB), so that ERP can be compared with the trend of a hypothetical Sound Pressure Level (SPL) of a node within of a fluid domain. To obtain this evaluation, it is necessary to impose some constant conditions:

- Air density: 1.2 kg/m^3,
- Speed of sound through air: $3.4 \cdot 10^2\ m/s$,
- ERP Loss Factor: 1,
- Reference ERP: $1.0 \cdot 10^{-9}\ mW$.

As said before, the reference ERP is a conventional parameter that is used for deriving the sound power value of a part. The ERP Loss Factor considers any loss that may occur at the interface between fluid and structure. For the moment, the influence of this factor is neglected, therefore, zero losses are assumed. The analysis has been analytically replicated in the Matlab environment, in order to validate the results of a commercial finite element solver with a good level of confidence. The frequency response has been obtained with the modal decomposition method and therefore extracting the natural frequencies and associated normal modes from the free oscillation problem [57] with modal analysis:

$$\nabla^4 w(x,y) - \rho h \omega^2 (x,y) = 0 \qquad 5.7$$

$$k^2 = \omega^2 \frac{\rho h}{D}; \qquad D = Eh^3/[12 \cdot (1-\nu^2) \qquad 5.8$$

$$w(x,y) = A_{mn} sin \frac{m\pi x}{a} sin \frac{n\pi y}{b} \qquad 5.9$$

$$\omega_{mn} = \sqrt{\frac{D}{\rho h}} \left[\left(\frac{m\pi}{a}\right)^2 + \left(\frac{n\pi}{b}\right)^2 \right] \qquad 5.10$$

the frequency response is then obtained by composing the normal modes basing on their participation to the external load, at each frequency [58], as in 5.11:

$$w(r_S, \omega) = \sum_{m=1}^{N_S} w_m(\omega) \phi_m(r_S) \qquad 5.11$$

in which N_s denotes the number of structural modes from the modal analysis. The amplitude of the response at a specific node depends on the position r_S of the node – and therefore on the coordinates (x, y) of the reference system used – and on the forcing frequency. It should be noted that the m-th normal mode will have higher relevance, on the specific node at a specific exciter pulsation as higher of the value assumed by the Modal Participation Factor (MPF) w_m.

MPF links the specific normal mode to the direction of the forcing, thus pointing out how much the forcing at a specific frequency is able to excite a specific normal mode of the structure. So, for example, if the specific mode is characterized by a purely out-of-plane displacement field, it will not participate, and therefore w_m will be null, if the direction of the external exciter is within the plane of the plate. The aim of the study is to evaluate how the FE solver calculates the ERP of the structure under analysis. For this purpose, a self-built code has been developed with the aim of extracting from the FE model the node IDs and their relative coordinates. On top of that, the nodal connectivity matrix for each 4-noded iso-parametric elements has been also extracted. In this way, it is possible to analytically evaluate the nodal velocity resulting from the frequency response analysis, under the same conditions – and therefore with the same degree of accuracy – of the FE simulation.

Within the frequency range of the analysis, the normal modes of the plate are mostly described by out-of-plane motion, consequently we referred to the exact solution of the plate simply resting on all four sides, describing the solution as displacement field normal to the plate [59], [60]. The ERP considers the speed of the generic point in a direction normal to the plate surface. As the frequency range and modes vary, this normal is generally not the normal to the reference plane of the undeformed plate. A code has been developed to calculate a normal associated with each point of the plate corresponding to a node of the FE model, considering the deformed shape of the plate. An area with its relative normal needs to be associated to each node, as they indicate how much power is radiated from that node.

From the extracted connectivity matrix, two pairs of vectors, each sharing the tail (anchor node) has been defined as in Fig. 5.2b. The cross products of these vector pairs determine two vectors normal to the deformed element. The element normal is the average of the newly derived vectors. This operation introduces an approximation which the effect decreases as the mesh size decreases. This approach has been used as quadrilateral elements may not have a unique normal. At this point, the nodal normal has been defined as the average of the normal to all the elements connected to the specific node (see Appendix A.1).

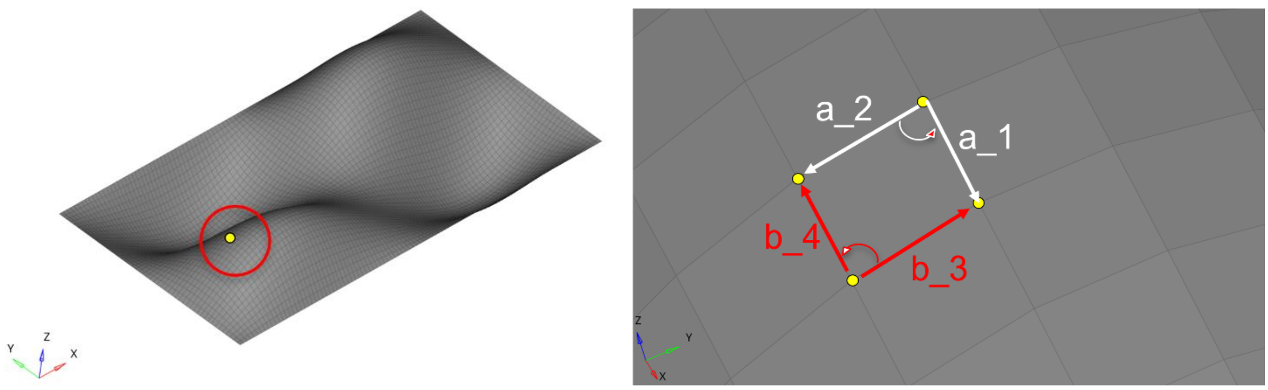

Figure 5.2: nodal normal at the generic node, inside a deformed plate.

A local area is associated to each node, considering also how many elements are connected to the node itself:

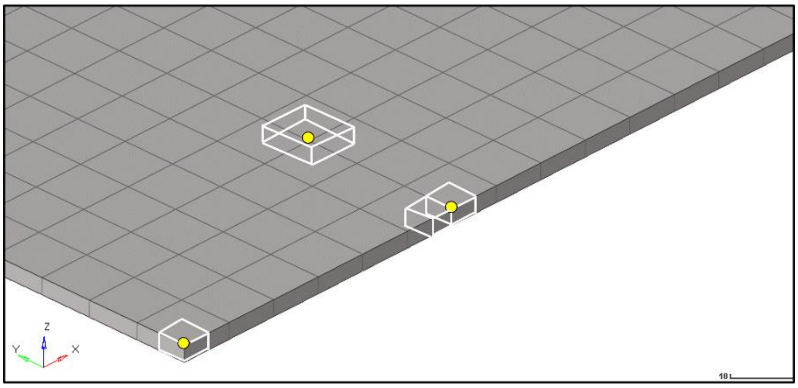

Figure 5.3: definition of the nodal local area.

This procedure ensures a good correlation between the analytical ERP definition and its FE counterpart:

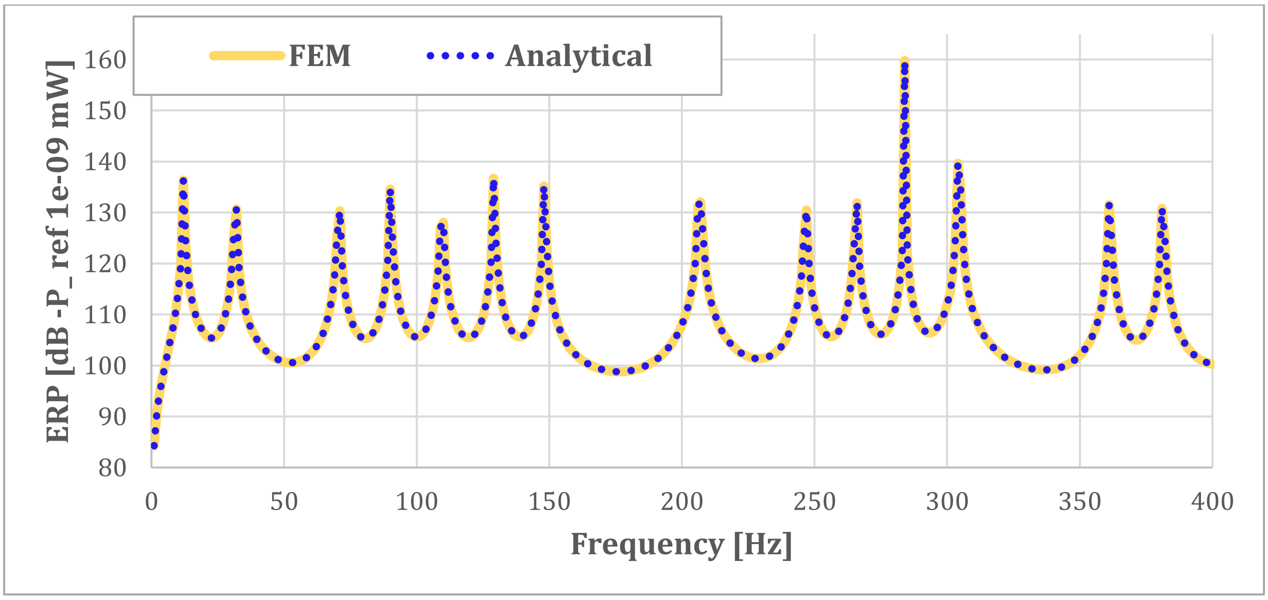

Figure 5.4: comparison between analytical and numerical ERP of aluminium plate.

5.3 Example: box model with single plate

The literature widely discusses the analysis of simplified models with a manageable mathematical description, the solution of which may be extracted with analytical calculations [46], [60]–[63]focus on the analysis of noise resulting from the interaction between vibrating walls and a fluid volume within an acoustic cavity. The potential of these conceptual problems is to understand and to highlight the behaviour of the system in a univocal way, as well as to obtain, in some cases, an experimental comparison.

In this work, once the problem has been analysed from the point of view of both fluid and structure, a coupled model of a plate and a prismatic acoustic cavity is analysed, prior to the investigation on a high-performance vehicle. The purpose of this test is to obtain a further comparison between analytical and numerical results on the frequency response problem. A plate with the same characteristics as the one reported in Table 5.1 has been constrained and loaded as in the previous example. Meanwhile, the acoustic cavity has two dimensions equal to those of the plate and extends by 500 mm in the direction normal to the plate. With these dimensions, the first normal mode of the cavity is a pressure wave aligned to the long side of the plate. The FE model of the system is represented in Figure 5.5:

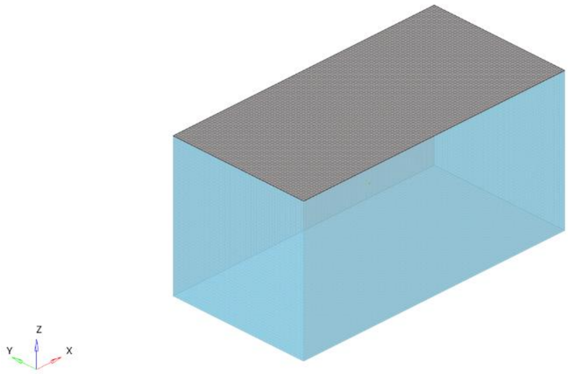

Figure 5.5: FE model of simply supported plate coupled to the rectangular acoustic cavity.

The plate-air coupling is considered in a weak form, in the sense that structural and fluid normal modes may be calculated independently, coupling then the response of the two systems by means of a linear combination, adjusted according to the interface conditions. This practice reduces simulation time, by accepting negligible errors. On the other hand, the literature reports widely about strong form coupling. Cazzolato et al. [44] reports that for a structural component immersed in water, the solution method must consider cross-fluid terms, i.e., the coupling between fluid modes.

The boundaries of the fluid domain that do not wet the plate undergo rigid wall conditions. The results of the FE simulation and the analytical solution are reported in Figure 5.6. Good accordance is found between the results.

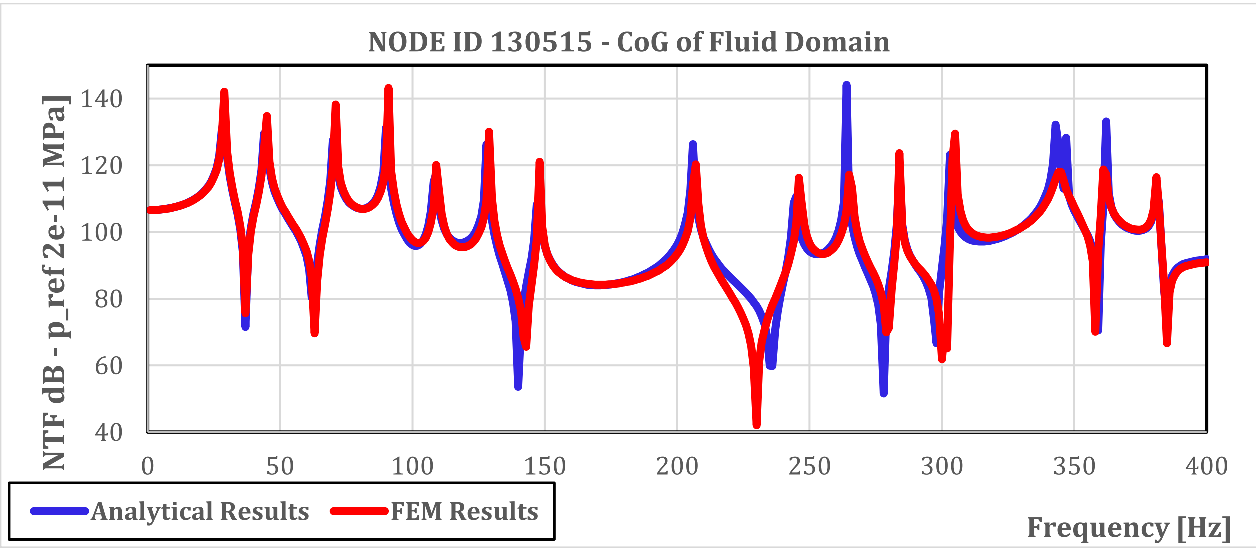

Figure 5.6: Noise Transfer Function (NTF): comparison between analytical and numerical results.

The results show the amplitude of the noise at the centre of gravity of the fluid cavity. The presence of resonance peaks is distinctly noted, as well as the use of a structural damping coefficient of the material ($\eta_S = 0.03$) and of the fluid ($\eta_F = 0.005$) to make the amplitude of pressure peaks finite.

An aspect of primary importance for this research activity is the good correspondence between the trends of the ERP of the plate and of the pressure field [64], [65]. This is only a qualitative aspect, which may give an overall consistent indication of the natural frequency of the plate normal modes generating the noise resonance peaks. These natural frequencies must be critically monitored in practice. In the analysed frequency range, the modal base presents two fluid modes – apart from the rigid modes – the first being at 170 Hz and the second being at 341 Hz. The first mode does not seem to affect the pressure trend, as a valley of pressure in the noise transfer function between 150 and 200 Hz. The same valley is found in the panel ERP trend as shown in Fig. 5.7. This effect depends on the position of the node studied in the fluid domain. A peak of the pressure field at 341 Hz occurs. This is not found in the case of the single plate. This difference could be attributed to the effect of a normal mode of the fluid cavity.

Figure 5.7 compares the fluid pressure and the panel's ERP directly. Two peaks are highlighted, at the frequency of 29 Hz and 345 Hz, respectively.

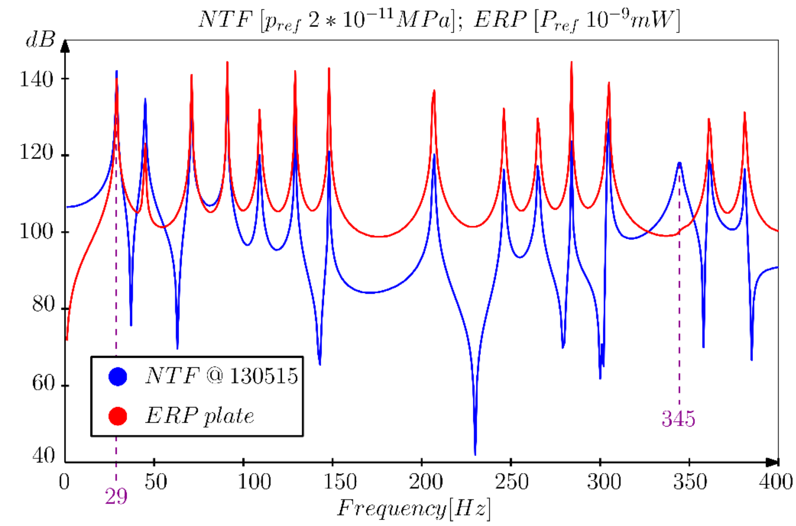

Figure 5.7: box type cavity sensitivity analysis: comparison between NTF @ 130515 and ERP of the plate.

The first, low-frequency peak corresponds to the maximum pressure amplitude throughout the entire frequency range. Pressure is expressed as Noise Transfer Function (NTF) which is mathematically defined as the ratio between the amplitude of the pressure (output) and the amplitude of the external forcing (input), expressed in this case in decibels. The chart shows, an excellent correspondence between NTF and ERP at 29 Hz. It can be inferred that the pressure peak is a consequence of the "pumping" action of the plate under resonance, towards the cavity. Conversely, a pressure peak in the NTF is detected at 345 Hz. This peak is not detected by the ERP curve of the plate. To better understand these phenomena, it is useful to evaluate the factors of modal participation of the fluid and of the plate:

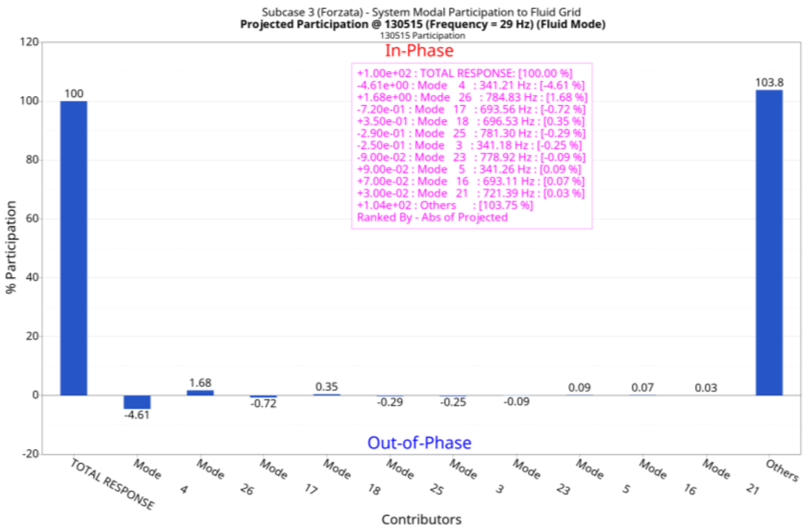

Figure 5.8: fluid modal participation factors @ 29 Hz.

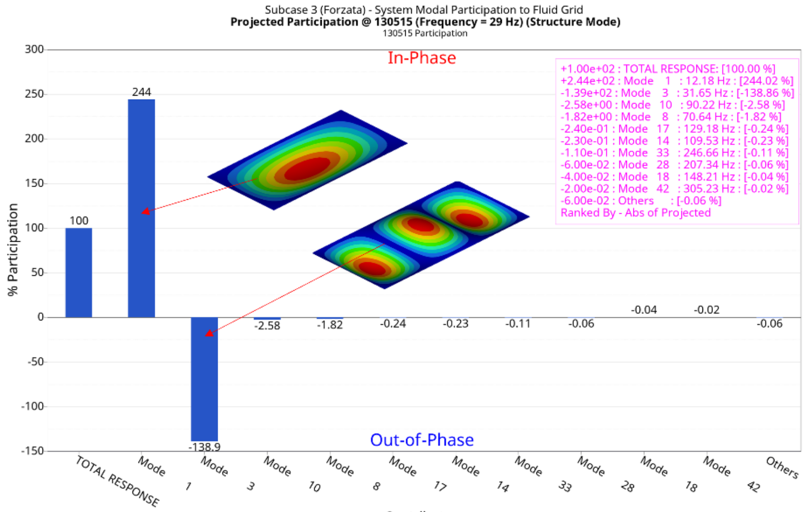

Figure 5.9: structural modal participation factors @ 29 Hz.

The histograms in Figs. 5.8 and 5.9 show the modes which contribute to the pressure trend at the sample node (130515) at 29 Hz. A percentage is given to each contribution, the sum of all the contributions makes up the response, which is shown to be 100% in the first column of both histograms. Modes with positive or negative contribution are noted. The sign denotes if the mode participates in phase or counterphase with the external forcing. Figure 5.8 shows how the contribution of the fluid modes is in first approximation zero – that contribution is almost entirely made up by the "others" which includes the sum of the modes not represented – and the first structural modes are the main cause of the pressure peak (see Fig. 5.9).

If we analyse the modal contribution to the pressure peak at 345 Hz, which is not captured by the power radiated by the plate, we notice some differences. As expected, this time, the fourth acoustic normal mode is the sole responsible of the increase in pressure, therefore, no contribution may be detected by the structural modes.

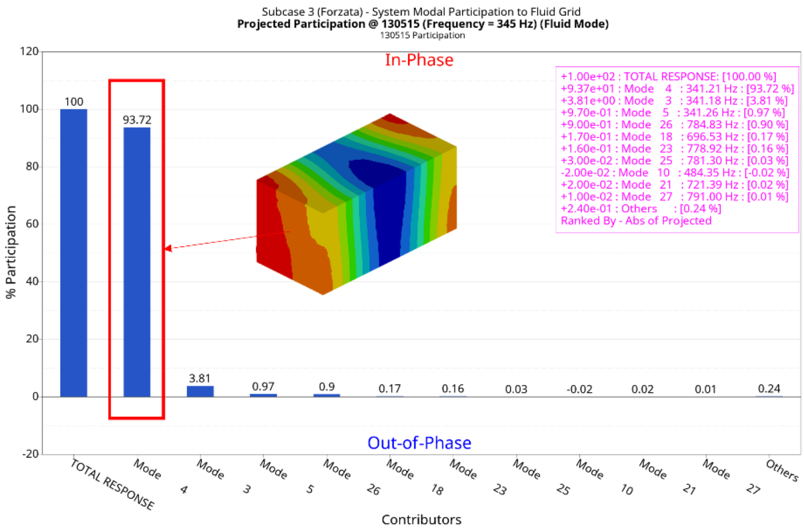

Figure 5.10: Fluid modal participation factors @ 345Hz.

5.4 Acoustic Panel Participation Factor

The modal participation factor is particularly convenient to discern which of the vibrating modes are responsible for the noise peaks, and therefore which modes need to be damped or shifting in frequency[66]–[68]. In systems like the Trimmed Body configuration of a vehicle, which includes a high number of degrees of freedom, the modes in the modal basis are particularly complex to analyse and their shape increase in complexity as the frequency increases. This leads to high local differences in shape, but some repetitive and similar trends between the modes may be globally found. Consequently, it will be difficult to find a condition in which one single normal mode is the solely responsible of a pressure peak at a given frequency. In addition, the graphic mode extrapolation for FE models with millions of nodes is most of the time largely expensive from a computational point of view. It is usually convenient to evaluate the participation factors, extrapolating then, from a subsequent modal analysis, the limited number of significant modes determining the resonance peaks. This approach minimises the required and analysed data, at the cost of a double calculation of the modal base.

In any case, there is also another modal participation factor, called acoustic participation factor, or *panel participation factor*. In general, the acoustic cavity of a vehicle is enclosed by surfaces with finite stiffness, instead of rigid walls. Therefore, the noise perceived inside the passenger compartment could depend on the vibration of not just a single, externally excited plate, but also on the vibration of other deforming panels. The panel participation factor quantifies the contribution of a single panel to the acoustic response. The following Section will define this parameter of interest, presenting an application to the model shown in Fig. 5.5 in which the prismatic acoustic cavity is fully enclosed by aluminium panels.

This parameter has been widely used in the automotive field to identify the causes of noise in the passenger compartment, as reported by Wang Y. et al. [69] and Han X. Et al. [67]. The acoustic panel participation factor can be obtained by considering the coupled dynamic equations [70]:

$$\begin{bmatrix} -\omega^2 M_s + i\omega C_s + K_s & A \\ \omega^2 A^T & -\omega^2 M_F + i\omega C_F + K_F \end{bmatrix} \begin{pmatrix} x \\ p \end{pmatrix} = \begin{pmatrix} 1 \\ 0 \end{pmatrix} \quad 5.12$$

Under a unit external load applied to the structure, the pressure field may be determined as a function of the exciter's frequency:

$$p(\omega) = -\omega^2 A^T (-\omega^2 M_F + i\omega C_F + K_F)^{-1} x \quad 5.13$$

Assuming that the cavity is enclosed by a certain number of thin-walled structures, which may be identified as panels, the displacement amplitude $x_{mn}(\omega)$ of node n, which belongs to panel m may be defined. The acoustic pressure caused by the local vibration of node n may be expressed as:

$$p_{mn}^{node}(\omega) = -\omega^2 A^T (-\omega^2 M_F + i\omega C_F + K_F)^{-1} x_{mn} \quad 5.14$$

Considering the effect of all the nodes of the panel, the sound pressure radiated from panel m may be quantified as:

$$p_m^{panel}(\omega) = \sum_{n=1} p_{mn}^{node}(\omega) \quad 5.15$$

The total acoustic pressure may be built by summing for all the panels enclosing the cavity (Eq. 5.16). Alternatively, one may determine how much of the total pressure is determined by a subset of panels.

$$p(\omega) = \sum_{m=1} p_m^{panel}(\omega) \tag{5.16}$$

The panel acoustic participation relative to panel m may then be evaluated as:

$$PAP_m(\omega) = \frac{p_m^{panel}(\omega)p(\omega)}{|p(\omega)|} = p_m^{panel}(\omega)cos(\alpha_m) \tag{5.17}$$

The acoustic panel participation factor (PAP) indicates the projection of the sound pressure generated by the m-th panel $p_m^{panel}(\omega)$ onto the direction of total pressure $p(\omega)$. The two vectors in the complex plane are distanced by a phase α_m.

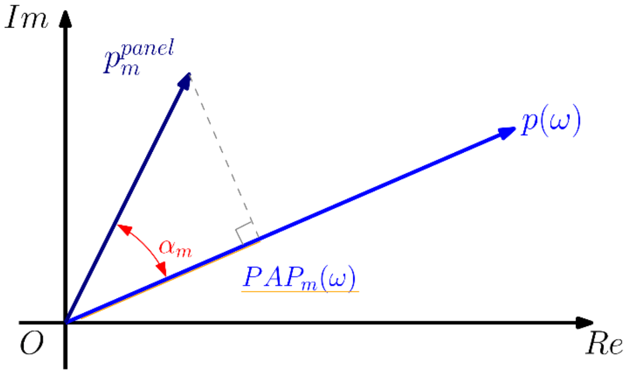

Figure 5.11: PAP representation.

The final part of this chapter will present several sensitivity analyses on the box-type model [69]. In these cases, non-rigid plates will be placed at the external faces of the acoustic cavity. The objectives of these tests are to derive the influence of the acoustic cavity in the vibration mechanisms of the thin-walled plates, as well as to evaluate the influence of the plates' properties. Furthermore, the acoustic panel participation factor and the ERP will be used to discriminate the behaviour of the different plates.

The first numerical test considers a box-type cavity filled by air in standard conditions. The cavity is surrounded by four rigid plates, and two flexible aluminium plates called Z^+ and Z^-, where the names depend on the normal direction, which goes outwards from the plate.

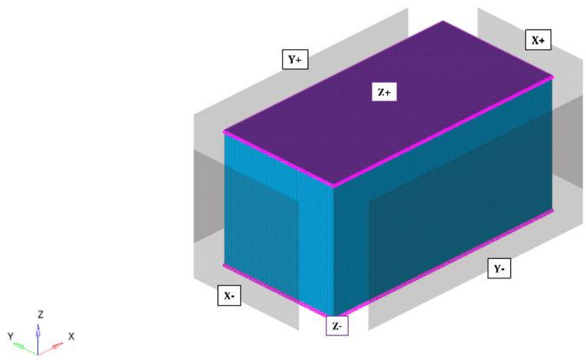

Figure 5.12: box-type FE model characterized by two flexible plates (Z^+ and Z^-) and four rigid walls (X^+, X^-, Y^-, Y^+).

The plates Z^+ and Z^- are simply supported, and plate Z^+ is loaded by an external harmonic force, with unit amplitude. The results of the reference model are reported in Fig. 5.13.

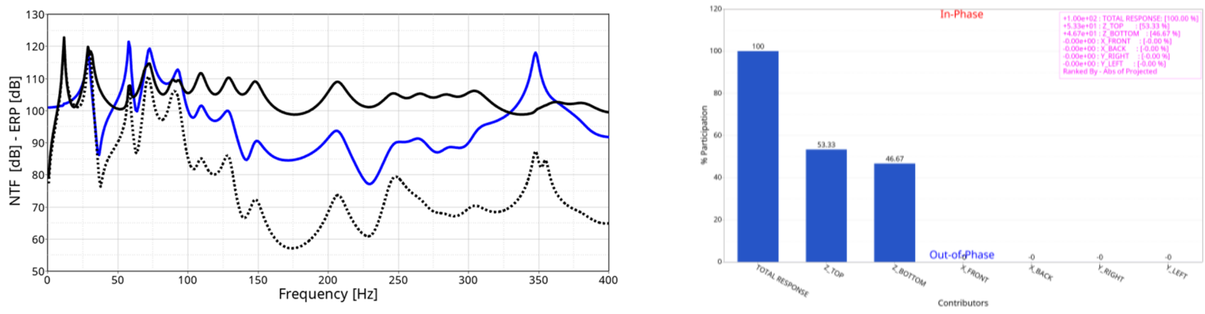

(a) (b)

Figure 5.13: (a) comparison between NTF (blue curve) and ERP of Z^+ (black curve) and Z^- (black dotted curve) plates pf reference model. (b) Panel participation factor (PFP) of plates related to the 130515 fluid node of the acoustic cavity at 348 Hz.

The results report the sound pressure at the centre of gravity of the box (node 130515), just like the previous example. Figure 5.13(a) shows the behaviour of sound pressure (blue curve) and the ERP of Z^+ (continuous black curve) and Z^- (dotted black dotted curve) plates, respectively. The normal modes of the plates cause the peaks of sound pressure, and they are detected either in the NTF curve and in the ERP curves. In particular, ERP seizes sound pressure peaks coherently with the NTF, but it does not provide precise information about the amplitude of sound pressure.

The ERP trend of Z^- plate is in good agreement with the trend of sound pressure, and it can represent the peak at 348 Hz caused by the fluid cavity mode. This interesting result shows the influence of the acoustic cavity. In fact, the acoustic cavity transmits the load caused by the vibrations of Z^+ to Z^-. Therefore, the behaviour of Z^- keeps track of both structural and fluid modes. Figure 5.13(b) shows the acoustic panel participation factors to the sound pressure at 348 Hz. In this simple example, this parameter does not distinguish any dominant panel between Z^+ and Z^-. On the other hand, it is observed that the rigid plates (X^+, X^-, Y^+, and Y^-) do not participate to the sound pressure peak at 348 Hz. This result is also valid through the entire frequency range.

A practical aim is usually in reducing the pressure peaks which are above a certain limit; thus, increasing the stiffness of the flexible plates could be the suitable to solve the problem. Some sensitivity analyses have been performed to highlight the influence of the mechanical properties of the plates.

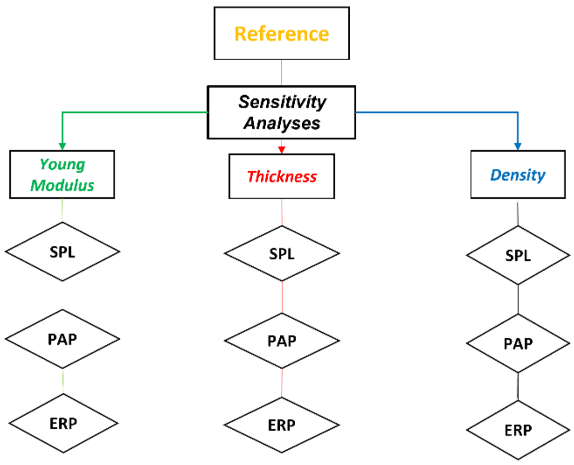

Figure 5.14: summary of sensitivity analyses.

First, the material of the plates is varied. Hypothetical materials having a Young Modulus augmented 2 and 3 times, like titanium and steel, have been considered.

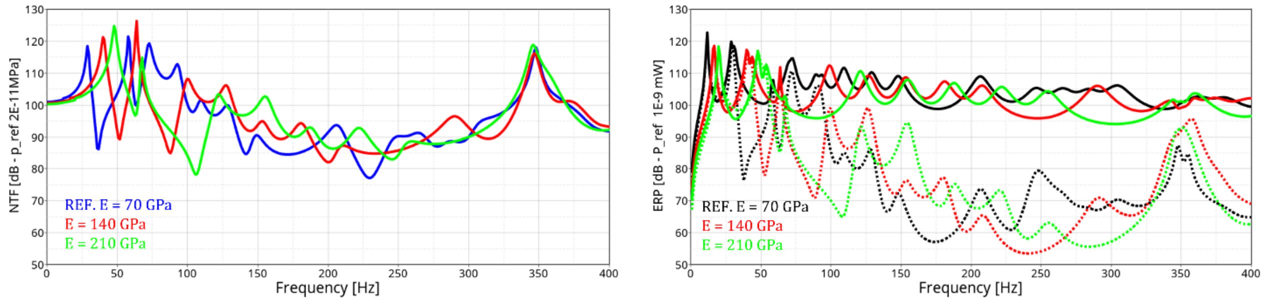

(a) (b)

Figure 5.15: (a) comparison between NTF results. (b) Influence of Young modulus in terms of ERP behaviour.

The influence of an increased Young Modulus shows a variation of the structural modal base. The normal modes of the plates are shifted to higher frequencies. On the other hand, the fluid modes do not present any variation, as they depend on the air properties and on the geometry of the cavity, which has been left unchanged. The same observation might be reported considering thicker plates of 2 mm and 3 mm:

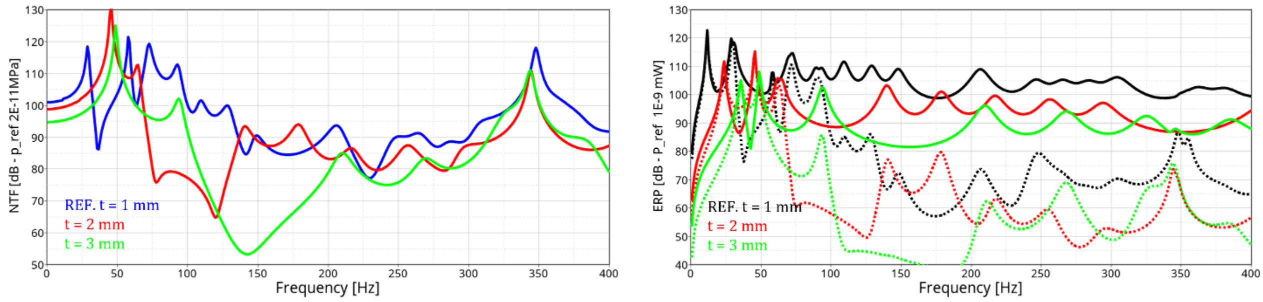

(a) (b)

Figure 5.16: (a) Comparison between NTF results. (b) Influence of plates thickness in terms of ERP behaviour.

From the results shown above, it is intuitive to consider that a stiffer structure will have normal modes at higher frequencies and will usually vibrate with lower amplitudes. In fact, as a first approximation, a natural frequency is the square root of the ratio between modal stiffness and the modal mass. Thus, it may be rationalized that a material characterized by higher density – being the other properties unchanged – will present lower natural frequencies.

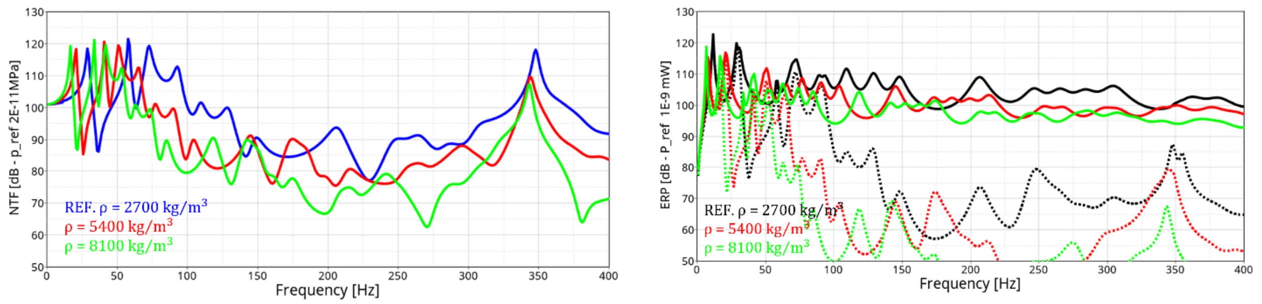

(a) (b)

Figure 5.17: (a) Comparison between NTF results. (b) Influence of density of the plates in terms of ERP behaviour.

In general, a vehicle designer modifies the shape, the thickness and the material of the panels to obtain the desired acoustic performance, which usually consists in having the panel's normal modes at a desired frequency. These observations may be done observing the general expressions of a plate's natural frequencies:

$$f_n = \frac{1}{2\pi}\sqrt{\frac{D}{\rho h}} \cdot \left[\left(\frac{n\pi}{L_x}\right)^2 + \left(\frac{m\pi}{L_y}\right)^2\right] \quad 5.18$$

The thickness, Young Modulus and density can be highlighted manipulating Eq. 5.18:

$$D = \frac{Eh^3}{12(1-\nu^2)} \quad 5.19$$

$$f_n{}^2 = \frac{1}{4\pi^2}\frac{D}{\rho h} \cdot \left[\left(\frac{n\pi}{L_x}\right)^2 + \left(\frac{m\pi}{L_y}\right)^2\right]^2 \quad 5.20$$

$$C_1 = \left[\left(\frac{n\pi}{L_x}\right)^2 + \left(\frac{m\pi}{L_y}\right)^2\right] \quad 5.21$$

$$\frac{\rho_0 f_n{}^2}{E_0 h_0{}^2} = \frac{1}{48\pi^2(1-\nu^2)}\frac{E}{E_0} \cdot \left(\frac{h}{h_0}\right)^2 \cdot \frac{\rho_0}{\rho} \cdot C_1{}^2 \quad 5.22$$

$$C_2 = [48\pi^2(1-\nu^2)]^{1/2}, \qquad C_3 = \frac{\rho_0}{E_0 h_0{}^2} \quad 5.23$$

$$f_n = \left[C_3 \cdot \beta \cdot \alpha^2 \cdot \frac{1}{\gamma} \cdot \frac{C_1{}^2}{C_2{}^2}\right]^{1/2} \quad 5.24$$

$$\begin{cases} \beta = {}^{E}/_{E_0} \\ \alpha = {}^{h}/_{h_0} \\ \gamma = {}^{\rho}/_{\rho_0} \end{cases} \quad 5.25$$

The ρ_0, E_0 and h_0 parameters represent the nominal values of the plates, respectively. Figure 5.18 shows the variations of natural frequencies function of α, β and γ.

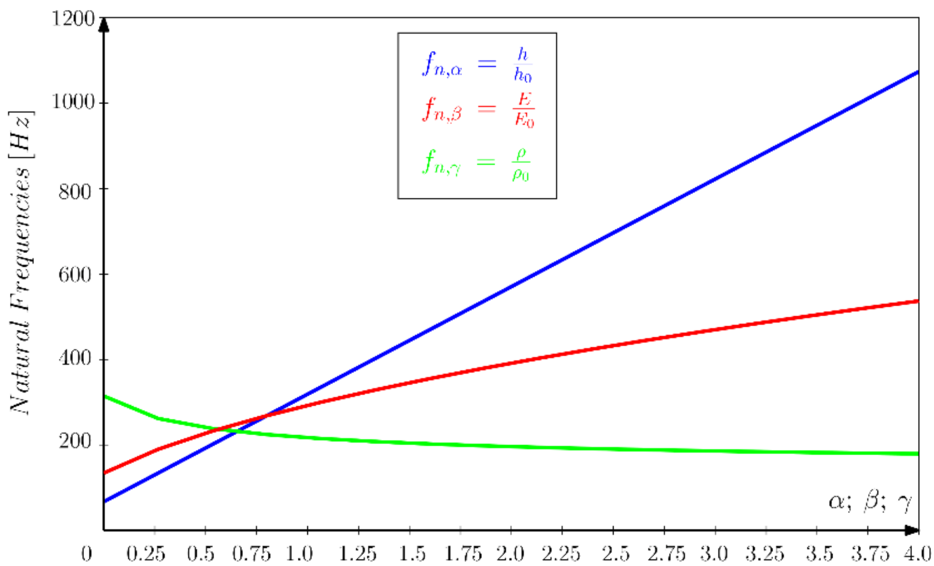

Figure 5.18: Influence of the thickness, Young Modulus and density of plates on natural frequencies.

6 - Definition of new methodology approach for CAE acoustic analyses

The experimental approach guided vehicles' design as a unique method to guarantee the proper behaviour for each subsystem and performance during automotive history. In the last few decades [71], CAE simulation models and analyses have become more and more relevant, supporting experimental tests. The computing powers have increased dramatically, and more and more problems can be managed in a reasonable time. FE models can describe the actual acoustic behaviour and mimic the quasi-static test performed in specific anechoic chambers. This research activity deals with the simulation of the acoustic performance of a vehicle in Trimmed Body (TB) configuration. TB configuration considers all the vehicle components except the powertrain, the driveline, the steering system, and the suspensions.

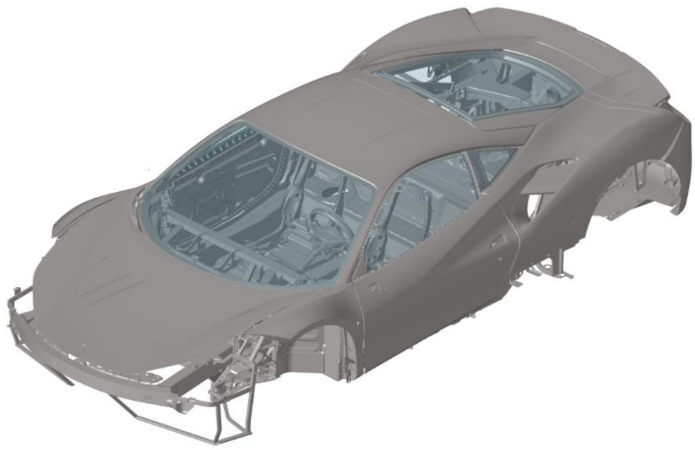

Figure 6.1: F142M Trimmed-Body (TB) configuration.

The friction in the contacts between components is, in general, the origin of noise transmitted and sometimes amplified in terms of vibrations by the vehicle. The full-vehicle configuration that collects all the vehicle subsystems can simulate the actual NVH performances in different driving scenarios. Multi-body models are suitable for these analyses in which the equations of motion are solved in the time domain. These models describe the dynamic behaviour of the main structural subsystems in terms of inertia, damping and stiffness properties. These analyses allow extracting the dynamic loads exchanged in the kinematic connections interposed between the subsystems. For these reasons, it might describe the vehicle's acoustic behaviour in TB configuration applying the specific dynamic loads at the corresponding hardpoints. OEM defines internal best practices for the experimental test and virtual approvals.

The ride simulation analyses are provided in the frequency domain for the NVH performance, including acoustic behaviour. The Fourier transform considers the hypothesis of linearity; thus, it permits analysing the vehicle using unit loads for the load-cases of interest. This practice results suitable to saving time during the design workflow of a new vehicle. In fact, it is more efficient to develop the vehicle's NVH performance even if the actual loads have not still evaluable. Therefore, the TB must accomplish the acoustic targets based on unit-loads cases. In the next phase of the project, it might evaluate the actual sound pressure level due to realistic amplitudes of the external excitations.

Several numerical techniques could reconstruct the overall sound pressure levels in the vehicle cabin, and all these techniques were widely studied in the literature. One of the most promising techniques is the Blocked Forces method [72]–[74]. It consents to avoid the complex simulations, or the experimental measures of the contact forces exchanged between the road profile and the tyres. In fact, this method evaluates the forces at the upright, which could be obtained by measuring a single suspension system in a specific bench test [75], [76]. This experimental technique could be simulated by developing the FE model of the complete suspension systems. In particular, the tyre model is included in the internal acoustic cavity to seize the proper dynamic behaviour [75], [77], [78]. The resulting FE model of the vehicle for ride simulation could be simplified by the dynamic condensation of the TB model [1], [2], [79]–[81]. The dynamic model includes the acoustic cavity to evaluate the behaviour of the sound pressure level at the ears of the receivers. The analysis, in this simplified full-vehicle configuration, permits applying the Transfer Path Analysis (TPA). This technique was born for the experimental detection of the vibration paths, particularly for the vehicle cabins' noise paths [82]. In this way, it is paid attention on the noisier paths and the structural modifications are applied to achieve the comfort targets.

The research activity concerns the analyses of the TB, in which it is possible to encounter the acoustic cavity, during the earlier phase in the vehicle design workflow. The acoustic cavity is defined by structural components that surround the cabin.

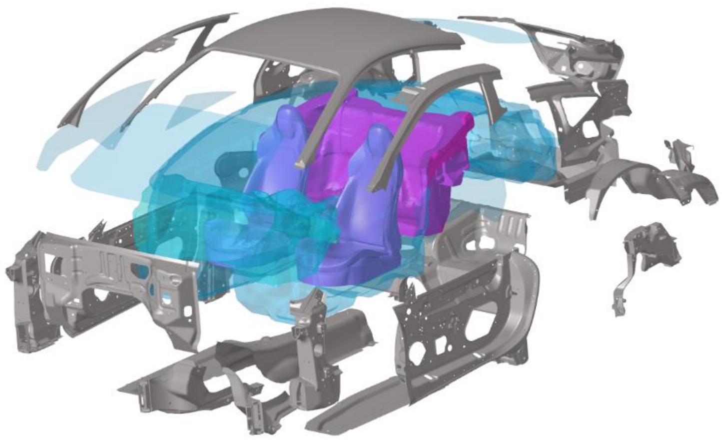

Figure 6.2: Exploded view of the interface zone between the acoustic cavity and structural counterpart of the vehicle cabin of F169.

Despite this, TB configuration is modelled just in an advanced phase of the design process flow. In that phase, almost all the components had been already deliberated. This common practice is reasonable because it is necessary to properly describe the inertia, the stiffness, and the damping properties to seize accurately the vehicle's acoustic behaviour. On the other hand, applying significant modifications to structural components costs high. This means to return to a previous phase of the design and start a loop for re-check and re-obtain the approvals for all the vehicle's performances, not only for the NVH counterpart. A robust design process has to avoid this inefficient situation; thus, it is necessary to define already in the early stages of the design NVH targets. The most significant component is the spaceframe in Body-in-White (BiW) configuration.

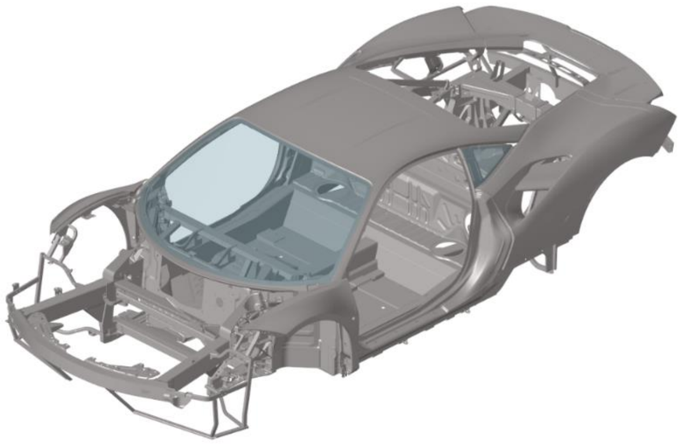

Figure 6.3: F142M Body-in-White (BiW) configuration.

In this earlier process phase, the vehicle's cabin is not closed because the door's subsystem is not collected in the frame's assembly. For this reason, it is not possible to define the acoustic cavity and evaluate the sound pressure level in the BiW configuration. This phase describes the structure's dynamic behaviour as global structure modes, dynamic stiffness, and panels mobility.

The former is essential to obtain the modal map of the vehicle at the final phase of the design process. This analysis compares the main vibrations of all sensitive subsystems to avoid different coupling modes and troublesome resonances peaks. In particular, the modes usually extrapolated are the first torsional mode and the first flexural modes. These remarkable modes are also important parameters to describe the stiffness of the chassis.

The second concerns the amplitude of the displacements of the loaded node. This analysis consents to detect possible drop-down of the dynamic stiffness due to the excitation of a specific mode of vibration in the chassis [83]–[86]. In general, anytime this phenomenon occurs a peak of the pressure amplitude in the TB acoustic analyses.

The latter describes a method to monitor local vibrational phenomena of plate-shaped components. The previous analyses consider a global behaviour or local stiffnesses, so it is helpful to develop a methodology to evaluate the dynamic behaviour of the panels of the spaceframe.

The dynamic stiffness could identify a local behaviour and could not accurately represent the acoustic performance. This parameter is usually evaluated in all the possible loaded attachment points of the spaceframe. In this way, it is possible to describe the reaction of the chassis to the external excitations and define minimum targets to design efficient local structures (e. g. the shock towers for the suspension's loads) in terms of stiffness to mass ratio.

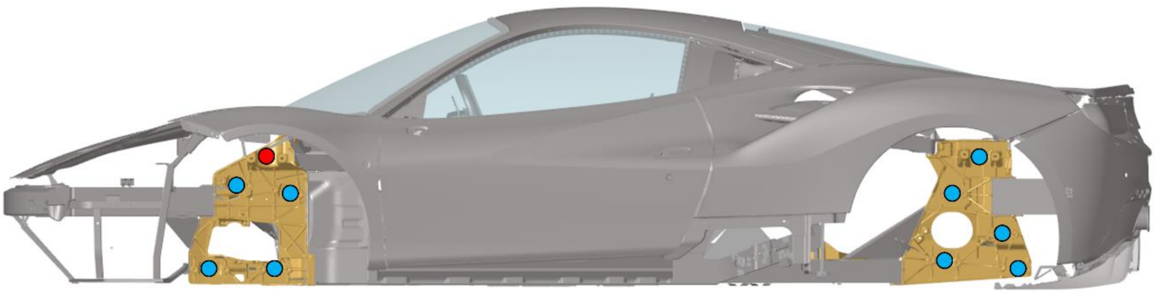

(a)

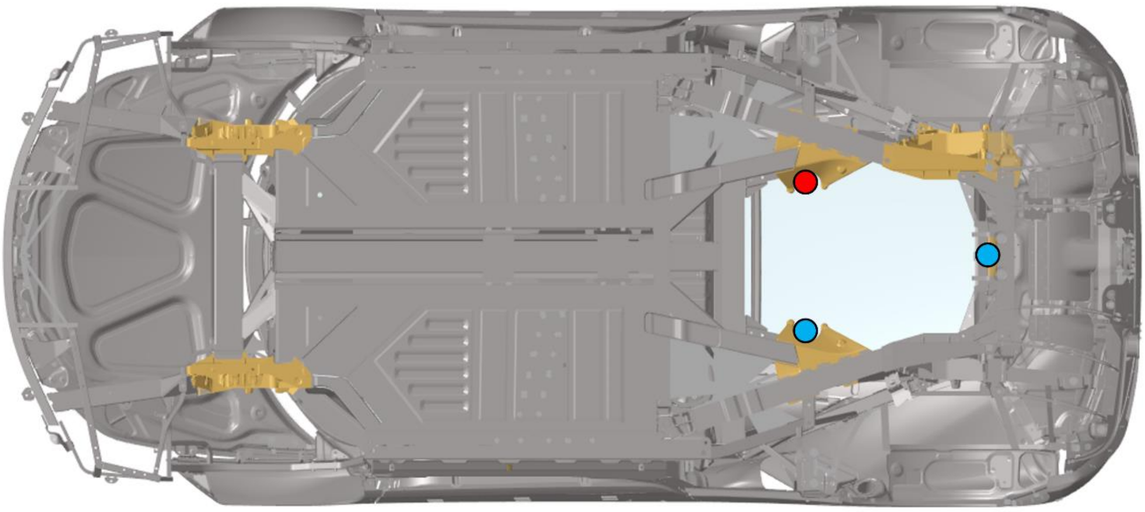

(b)

Figure 6.4: F142M Body-in-White (BiW) configuration, Loaded nodes in dynamic stiffness analysis: (a) Side view; (b) View from below. [The results of dynamic stiffness of the reds nodes are showed in the next figure].

The following figure shows the dynamic stiffness of the front shock absorber and of the internal combustion engine (ICE) connection. The two stiffnesses are collected along the $\hat{z}$ direction, which is conventionally normal to the ground's plane.

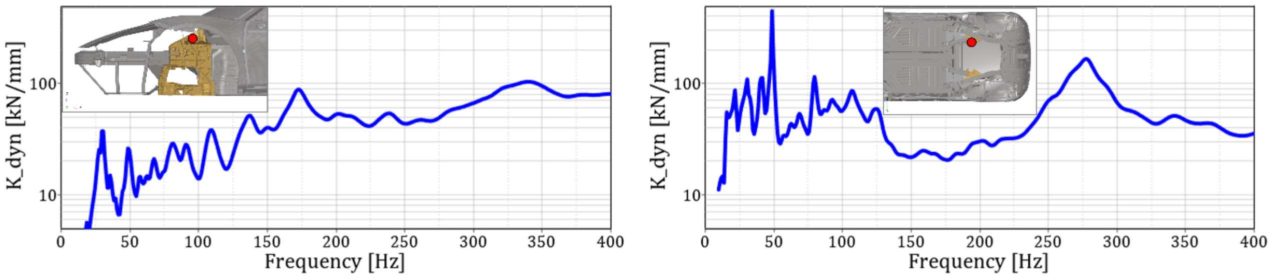

(a) (b)

Figure 6.5: Dynamic stiffness of shock absorber's hardpoint (a), and ICE's hardpoint (b).

The dynamic behaviour of the stiffness represented in Figure 6.5 is inversely proportional to the displacement amplitude. The curve shows the influence of the mode of vibrations on the structural properties of the components involved.

In general, correspondence of mode of vibrations in-phase and direction with the external loads causes an amplification of the displacement of the loaded node. Consequently, the dynamic stiffness presents a drop-down that indicates a neighbourhood of frequencies at which the performance worsens (e.g. Figure 6.5 (a) drop-down at 100 Hz).

On the other hand, in the case of anti-resonance peaks, the dynamic stiffness increases. Thus, dynamic stiffness is an essential requirement to describe all the loaded points adequately.

The panel mobility analysis is suitable for thin wall structures. The shape of these components determines significant vibrations, particularly in the out-of-plane direction that is the most compliant direction from the moments of inertia point of view. The panel mobility is a typical test to characterize the glass windscreen or the underbody panels experimentally. The method provides the measure of the velocity of the loaded points of a panel. A grid of samples is selected to extrapolate the average behaviour of the panel under investigation and eventually focus on the most compliant local area. FE models can simulate the velocity response of the loaded grids in the frequency domain, which mimics the experimental test. This approach could be too inaccurate in some cases.

First, the FE model's grids could mismatch the experimental samples of points in terms of coordinates. For components with complex geometry, this uncertainty could present a poor agreement between the prediction of FE analyses and the experimental test. The latter concerns the inaccurate representation of the acoustic behaviour of the vibrating panel. In particular, its accuracy is strictly dependent on the number and position of the sample's points. The ERP could represent the panel's average behaviour without the risk of obtaining misleading results. These two approaches could be compared considering a general underbody panel in two different configurations.

The first is a panel bolted to the structural components of the chassis. Two wide holes characterise the second. This layout could be suitable for maintenance if the panel is located under the ICE or the gearbox.

On the other hand, the panel without any holes could improve the aerodynamic performance. The panels are bolted on F142M in BiW configuration, in the zone of the ICE subframe. The simulation analysis considers the panel mobility of five interior nodes of the panels and two typical external unit-load at the rear shock tower of the driver's side. Both load-cases applied the load at the shock absorbers attachment's node in $\hat{y}$ and $\hat{z}$, respectively. The following figure shows the two FE models analysed.

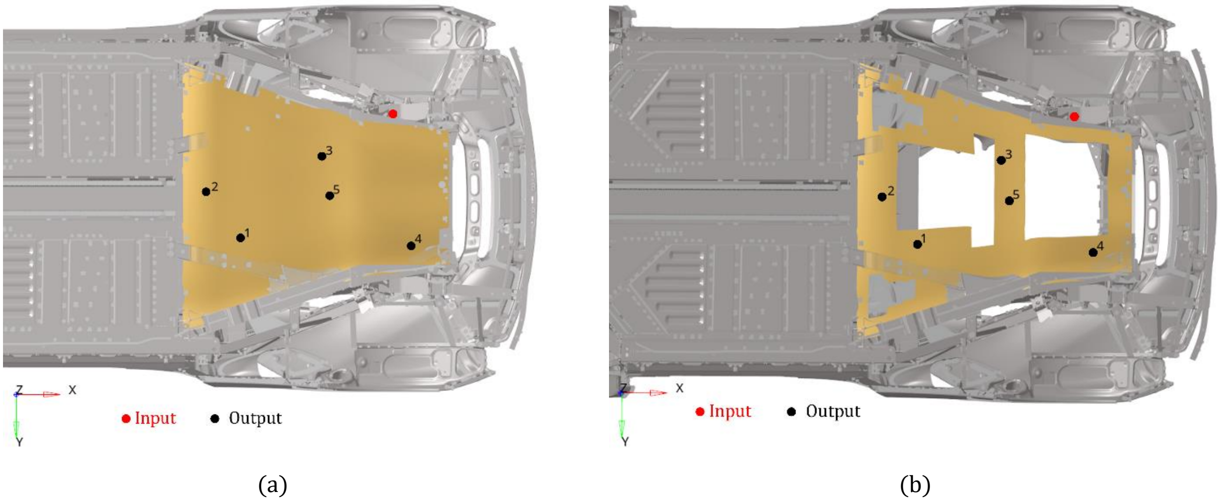

Figure 6.6: FE models of the rear underbody panel bolted on F142M - BiW: (a) Full panel, (b) Hollow panel.

The modal decomposition method is applied to solve the frequency response analyses. The external excitations considered frequencies between 10 to 200 Hz, and the modal basis extrapolates all the modes until 400 Hz. The radiated power of the panel is monitored in the cases excited by the unit-loads applied on the shock tower. This assumption intends mimicking the noise amplified by the panel during a drive or the quasi-static test in the anechoic chamber. The comparison of the two layouts is presented below.

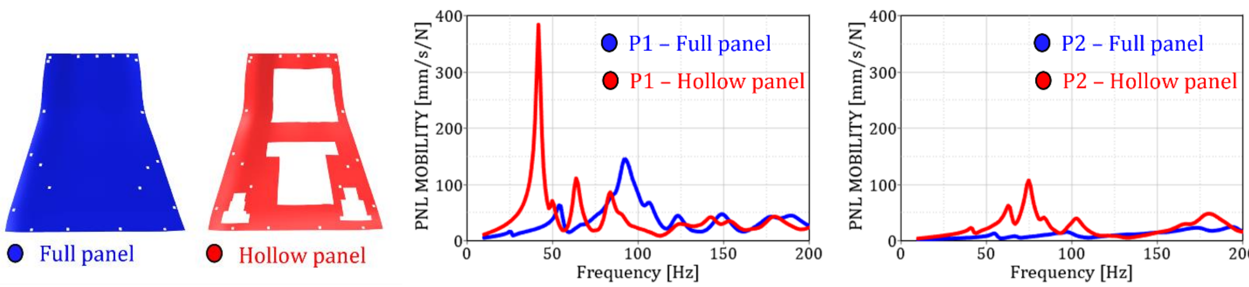

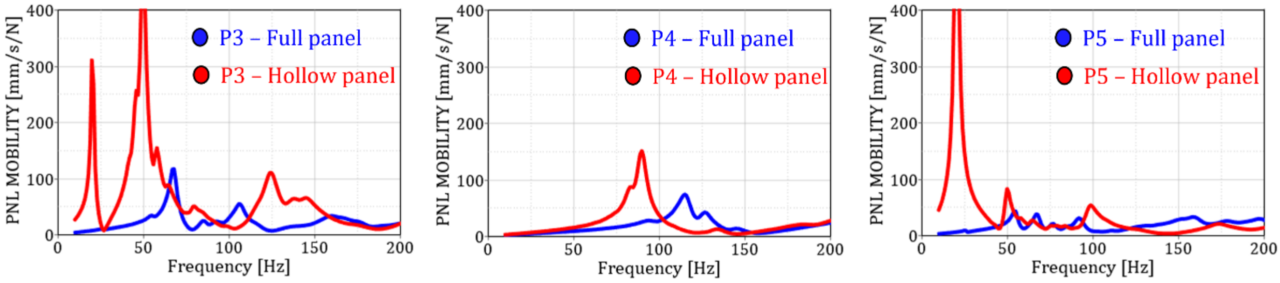

Figure 6.7: Panel mobility results: comparison between the layouts of full panel (blue curve) and hollow panel (red curve).

The results of the panel mobility differ, in particular, at low frequencies (10 - 50Hz). The main discrepancies between the two layouts are highlighted in the nodes called P1, P3 and P5. These nodes are in proximity of the holes in the central zone of the plates, farther to the bolts. These results also apply to the nodes P2 and P4, which are closer to the subframe structure than the other nodes analysed.

If we limit our judgement to the panel mobility to pronounce assumptions regarding the acoustic behaviour of these panel layouts, the full panel configuration seems to be more promising (blue curves). However, the ERP results show a contrasting scenario.

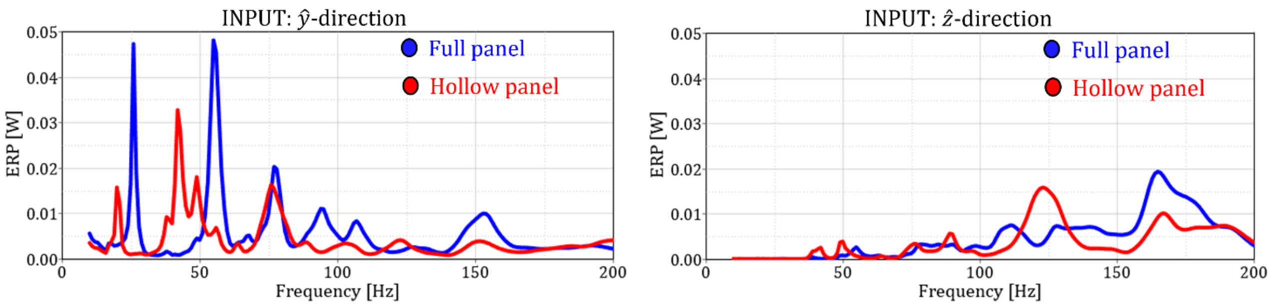

(a) (b)

Figure 6.8: Comparison of ERP behaviour between underbody panels in full (blue curve) and hollow (red curve) layouts.

The ERP results highlight that a plate-shaped panel in full configuration radiates more power than the hollow configuration. This discrepancy is due to the difference in terms of vibrating area.

In general, the mobility panel analyses highlight the local compliance of the node close to the hollow. At equal constraint conditions, the hollow panel perturbs the pressure field of the surrounding air in a lower efficient manner than the full panel. This example shows the utility of the ERP to evaluate NVH performance in BiW configuration.

In this activity research, a methodology is developed that proposes to describe the plate-shaped components of the BiW configuration of a vehicle in terms of Equivalent Radiated Power. The study aims to obtain the approval of a BiW configuration of a vehicle to improve NVH performance and, in particular acoustic performance.

The philosophy of the present methodology is to move the description of the dynamic behaviour of the main structural components in the BiW development stage. The aim is to obtain an improved BiW configuration in terms of NVH performance before the virtual approval of the model. The methodology identifies two significant steps in this design flow:

- Detection of the predominant panels that surround the vehicle cabin
- Improve the dynamic behaviour of the panels satisfying the mass and the manufacturability targets.

The former considers the panel's description in terms of ERP in the frequency domain between 10 to 400 Hz. The discrimination of the predominant panels is extrapolated by the definition of a new participation factor. It considers the relationship between each panel to the total ERP. It is the sum of the radiated power of all the considered panels at a specific frequency. Finally, the improvement of the dynamic behaviour of these panels following, in general, by two different approaches, as summarized in Figure 6.9:

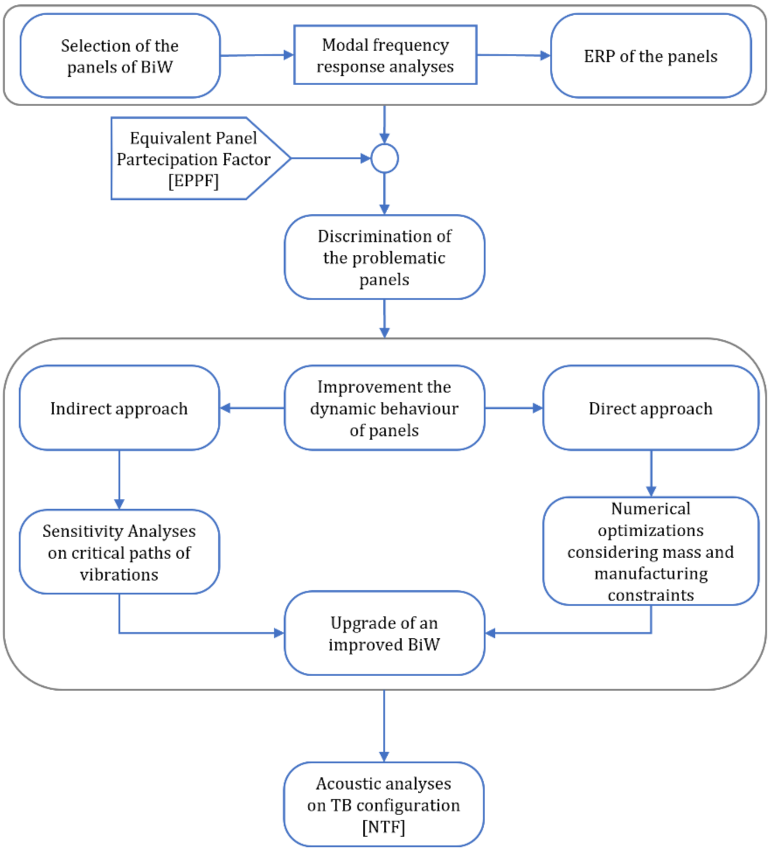

Figure 6.9: Process flow of the methodology.

This second goal of this method aims to reduce the peaks of the total ERP amplitude, modifying the dominant components' dynamics.

The first approach is directly modifying specific components varying their dynamics properties: inertia, stiffness, and damping. The new layout must undergo all the targets of BiW. In particular, the ensemble of the possible layouts is filtered by the targets of weight, manufacturability, safety, costs, ergonomics, and style if the components are visible. Thus, there are different ways to solve the problem in this phase but a limited number of acceptable solutions.

The methodology proposes a numerical optimizations process flow considering the main constraints avoiding the trial-and-error iterative loops. In some scenarios, the direct panel's modifications to reducing total ERP peaks is not the best trade-off. Modifications on its framework can obtain the improvement of the panel behaviour. In this case, it is crucial to identify the source of the vibration's transmission. The transmission path variation could solve the problem without any panel modification. In practice, a direct and indirect mixed approach is applied to minimize the modifications.

The next phase of the methodology concerns the integrations on FE model of the other subsystems to generate the Trimmed-Body configuration. These subsystems could be described in a simplified model to move local internal modes at high frequencies. The final step is to evaluate the acoustic behaviour of the TB by performing the coupled fluid-structure acoustic frequency response analyses.

A test case scenario is presented in the following. The methodology is applied to Ferrari F488 GTB. This high-performance vehicle is characterized by an optimized layout that withstands all the performance targets. The study aims to reduce the interior noise minimizing the weight gain by applying the new methodology proposal.

6.1 - Selection of the influent panels of BiW

The first step of the study concerns the development of the FE model of BiW suitable for extrapolating the ERP of the panels located at the interface to the hypothetical acoustic cavity of the TB configuration. The panels collect the nodes of the discretized components. The considered panels are shown in Figure 6.10 and listed in the following table T 6.1:

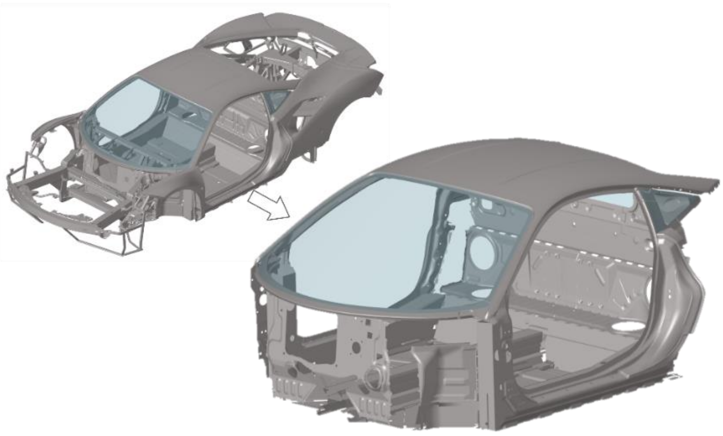

Figure 6.10: BiW panels that surrounds the hypothetical acoustic cavity of the TB configuration.

T 6.1: List of panels identified for the analyses of radiated power. The acronym DS stands for Driver Side and PS for Passenger Side.

PANELS	
SILL DS	B-PILLAR CROSSBAR BOTTOM
SILL PS	B-PILLAR CROSSBAR MID
FRAME DOOR DS	B-PILLAR CROSSBAR TOP
FRAME DOOR PS	WINDSCREEN SIDE REAR DS
COWL	WINDSCREEN SIDE REAR PS
A-PILLAR PS	REAR FIREWALL
A-PILLAR DS	FRONT_FIREWALL
EXTRUSION FLOOR DS	BENCH

EXTRUSION FLOOR PS	TYRE HOUSING DS
FLOOR REINFORCEMENT DS	TYRE HOUSING PS
FLOOR REINFORCEMENT PS	ROOF CROSSBAR REAR
FLOOR DS	ROOF CROSSBAR FRONT
FLOOR PS	ROOF
SEAT REINFORCEMENT DS	WINDSHIELD
SEAT REINFORCEMENT PS	SEAT ATTCHMENTS DS
TUNNEL	SEAT ATTCHMENTS PS

The frequency response analyses include 69 load-cases concerning unit-loads that excite one by one in the three directions the suspension systems, ICE, and gearbox attachments respectively. All the external harmonic loads excite the system in the range of frequency from 10 to 400 Hz. This range is a conventional range in which the interior-borne-noise is manly originated by the structural vibrational phenomena. Thus, it is crucial to obtain accurate results using the modal method when a higher cut-off frequency is defined. In this manner, it is possible saving time of the simulation. The good rule-of-thumb provides to define the cut-off frequency equal at least two times the maximum frequency of the external load. A sensitivity analysis has been conducted to evaluate an acceptable trad-off between simulation time and accuracy of the solution, see table T 6.2.

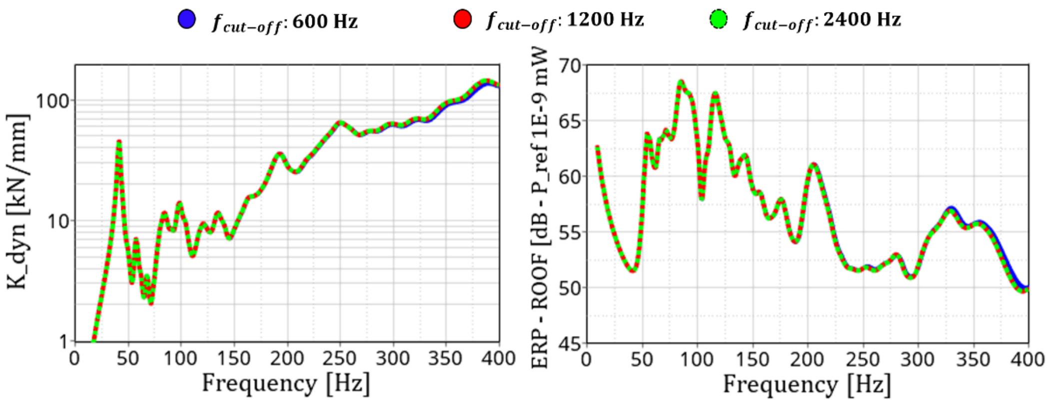

(a) (b)

Figure 6.11: BiW loaded by harmonic unit-load [10-400] Hz, at front suspension in $\hat{z}$-direction. Results comparison between three different cut-off frequencies. (a) Dynamic stiffness. (b) ERP of roof.

Figure 6.11 shows two different results extrapolated from the frequency response analyses of BiW under the unit-load in $\hat{z}$-direction at the front shock-tower of the driver side. In Figure 6.11 the dynamic stiffness (Figure 6.11 (a)) and the ERP of the roof (Figure 6.11 (b)) are presented. Three different cut-off frequencies are compared to identify the discrepancies of the results; the cut-off frequency thresholds are 1.5, 3.0 and 6.0 times the maximum frequency of the load, respectively.

The differences are mainly located at frequencies over 325 Hz for each reported result. The only visible difference is between the lowest cut-off frequency of 600 Hz (solid blue curve) and the other. Thus, the cut-off frequency of 1200 Hz (solid red curve) is great enough to represent the amplitude of the response until 400 Hz adequately, so the case that considers the cut-off frequency of 2400 Hz (green dotted curve) is not an efficient choice.

T 6.2: Summary of the number of modes of the modal basis of each scenario of cut-off frequency and simulation time.

Cut-off frequency	600 Hz	1200 Hz	2400 Hz
Number of modes	963	2891	8781
Simulation Time [hh:mm:ss]	00:33:10	00:53:30	02:27:24

The cut-off frequency of 1200 Hz, which corresponds to 3 times the maximum frequency of the excitation, represents the best parameter in terms of accuracy and reasonable simulation time. On the other hand, the first case is selected for the analyses, that is the cut-off frequency of 600 Hz (1.5 the maximum of the excitation) and the discrepancy of the results at high frequencies is considered acceptable. The BiW model considers more than 2 millions of elements and 1.8 millions of nodes, for a total of 10631511 degrees of freedom. Moreover, the FE model of TB includes more structural subsystems and the acoustic cavity, so the simulation time increase dramatically.

6.2 – EPPF: Equivalent Panel Participation Factor

The results of ERP behaviour of the panels consider 33 curves for each load-cases. The curves represent the amplitude of the radiated power of each panel and the Total ERP. In the following, Fig. 6.12 shows the BiW response due to the excitation of shock absorber anchor points at front shock tower of driver side in $\hat{z}$-direction.

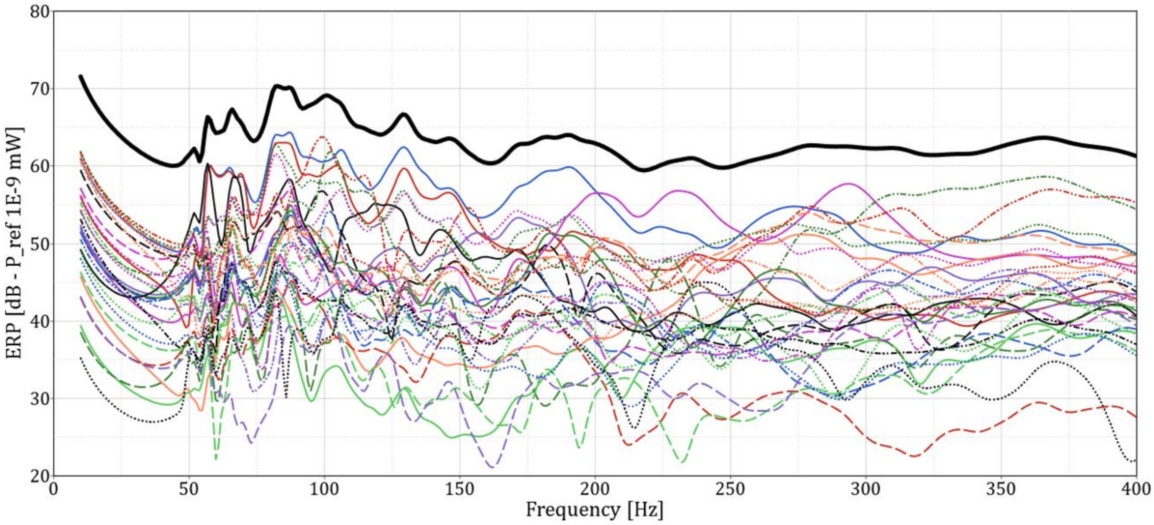

Figure 6.12: Panels ERP compared to Total ERP (solid black curve).

The Total ERP (solid black curve) varies between 60 to 70 dB, and it is higher than the other contributions. The representation of the results considers too many curves to be analysed and compared, but two observations are extrapolated.

The first concerns the trend of the Total ERP, in which the peaks of radiated power correspond to the panels' peaks with a higher level of radiated power. The second concerns the behaviour at low frequencies ranging from 10 to 40 Hz. The ERP of BiW panels in this range is a monotonically decreasing function. This behaviour does not agree with the typical behaviour of the Noise Transfer Function. This misleading deals with the hypothesis in which the ERP is defined. The first is the postulation of inviscid fluid that is only valid for low frequencies until the first natural is reached, as reported in [55]. The second is the hypothesis of constant plane waves in all frequencies. Under this assumption, the radiation factor is unitary. This hypothesis is valid generally in far-field conditions or if the dimension of the radiating structural panel is much bigger than the wavelength. Thus, this hypothesis introduces higher approximations than in low-frequency range.

Luegmair M [55] defines an Advanced ERP formulation that considers the effect of a variable coefficient of radiation which depends on the Helmholtz number, the dimension of the radiating components, and this is described by the Bessel function (J_1). The Helmholtz Number (He) is expressed by Eq. 6.1:

$$He = kR, \qquad 6.1$$

where k is the wavenumber and R is the dimensional characteristic of the vibrating panel. Luegmair M, [87] derives the formulation of radiation factor (σ), also called ERP Loss Factor for a rigid piston:

$$\sigma = \frac{J_1(2He)}{He} \qquad 6.2$$

The behaviour of the Loss Factor (σ) is shown in Figure 6.13:

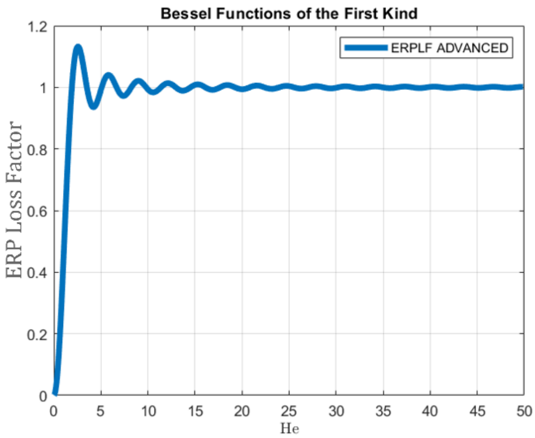

Figure 6.13: Radiation factor over Helmotz number.

Luegmair M [55] defines the Advanced ERP as:

$$ERP_{adv} = (1 - \sigma) \cdot \rho_F c_F \int_A \left|\hat{v}_{S,n}\right|^2 dA. \qquad 6.3$$

The correction on the ERP formulation has been tested for the same load analysis shown in Figure 6.14, focusing the attention on the cowl, and comparing the behaviour of ERP, Advanced ERP, and the NTF of the corresponding TB model evaluated at the right ear of the driver.

The Advanced ERP depends on the characteristic dimension of the radiating component. The cowl is an extruded component, or it could be manufactured by welding bent plates. In any case, its length is the dominant dimension used for the analysis of the ERP Loss Factor. The results show how the advanced description of the ERP could seize with more accuracy the actual behaviour of the sound pressure level at low frequencies than the classic ERP formulation.

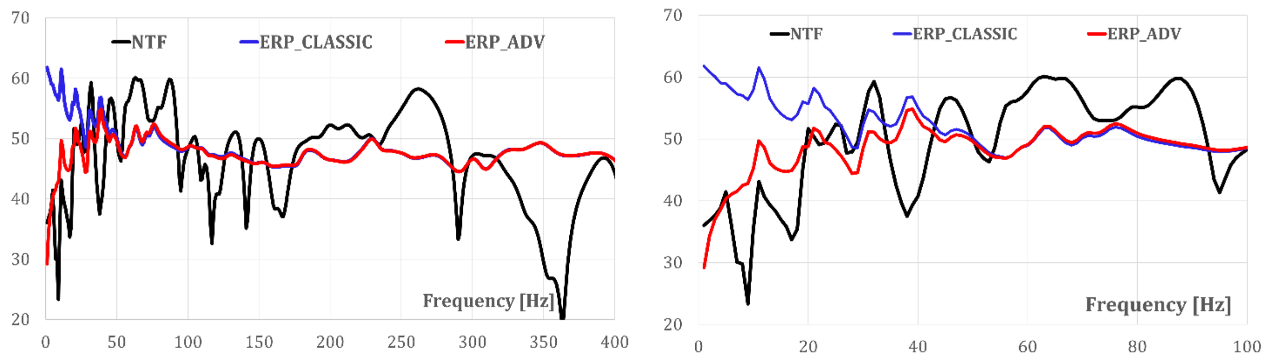

(a) (b)

Figure 6.14: Comparison between Classic ERP (blue curve), Advanced ERP (red curve) and NTF (black curve) in the range of 0-400 Hz (a) and 0-100 Hz (b).

The results highlight the strong approximations on the dynamic of the fluids and the pressure field inside the vehicle cabin. The Advanced ERP could reduce the lack of classic ERP, but it is strongly sensitive to the characteristic dimension of the component under investigation.

The analyses conducted in this research activity refer to the classical formulation of the ERP considering the peak of vibration and avoiding consideration about the amplitude of the radiated power in the frequencies until 40 Hz.

The methodology aims to save time to achieve the virtual approval for the Trimmed Body configuration. Thus, the analyses of each panel's ERP for each load-cases need to be simplified to obtain the aim. For this reason, only load-cases that identify the worst cases are considered for the development of the improved layout of the BiW. These load-cases occurs when the external excitation loads in $\hat{z}$-direction the shock absorbers attachments to the shock towers of driver side front (node 119) and rear (node 319) respectively. Figure 6.15 shows the behaviour of the Total ERP in the frequencies range of interest and the peaks of radiated power analysed:

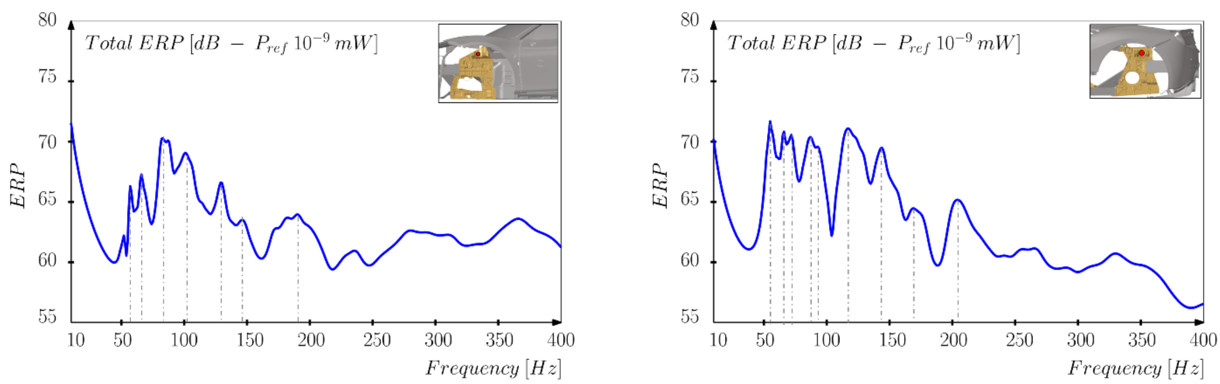

(a) (b)

Figure 6.15: (a) Total ERP of node 119; (b) Total ERP of node 319.

In analogy with the modal participation factor that identifies the modes that contribute to a specific peak of the response amplitude, a new participation factor is defined in terms of equivalent radiated power. This new coefficient is called Equivalent Panel Participation Factor (EPPF), and it calculates the percentage of participation of each panel to the Total ERP at a specific frequency. This approach is similar to the acoustic participation factor of panels to the sound pressure level in the fluid-structural frequency response analyses.

In BiW configuration, this parameter is inapplicable; thus, it is suitable to refer to the total radiated power in place of the sound pressure level at the driver's ear. This approach aims to discriminate the more influential panels to the total radiated power and assume that these panels could also influence the interior noise in the vehicle cabin. EPPF is the product of two factors, as shown in Eq. 6.4:

$$EPPF = \frac{ERP_i}{ERP_{tot}} \cdot R_{Lin,ave} \qquad 6.4$$

The first term is the ratio between the radiated power of the i-th panel to the Total ERP evaluated at a specific frequency. The Total ERP is the sum of the ERP of all the panels, as shown in the following equation:

$$ERP_{TOT} = \sum_{i=1}^{N=\#\,panels} ERP_i \qquad 6.5$$

The other factor is an average linear correlation index between two linear correlation indexes that consider left and right around intervals of frequencies to the specific frequency under investigation:

$$R_{Lin,ave} = \frac{1}{2}\left|\frac{cov(ERP_i, ERP_{tot})_{lh}}{\sqrt{D(ERP_i)_{lh}} \cdot \sqrt{D(ERP_{tot})_{lh}}} + \frac{cov(ERP_i, ERP_{tot})_{rh}}{\sqrt{D(ERP_i)_{rh}} \cdot \sqrt{D(ERP_{tot})_{rh}}}\right| \qquad 6.6$$

The linear correlation index formulation considers the ratio between the covariance of the ERP of the *i*-th panel related to the Total ERP in the interval of frequencies and the product of the root mean square of the two ERP considered (Eq. 6.7-6.8-6.9).

$$cov(ERP_i, ERP_{tot}) = \sum_{lx=i\pm eps=1}^{lx=eps=15} (ERPi_{lx} - \overline{ERPi_{lx}}) \cdot (ERP_{tot} - \overline{ERP_{tot,\ lx}}) \qquad 6.7$$

$$D(ERP_i) = \sum_{lx=i\pm\varepsilon=1}^{lx=\varepsilon=15} (ERPi_{lx} - \overline{ERPi_{lx}})^2 \qquad 6.8$$

$$D(ERP_{tot}) = \sum_{lx=i\pm\varepsilon=1}^{lx=\varepsilon=15} (ERP_{tot,\ lx} - \overline{ERP_{tot,lx}})^2 \qquad 6.9$$

For the sake of simplicity in Figure 6.16, an example of the comparison between the Total ERP and the ERP of the roof is reported. The peak of Total ERP at 82 Hz has been studied, and an around interval ε = 15 Hz is considered.

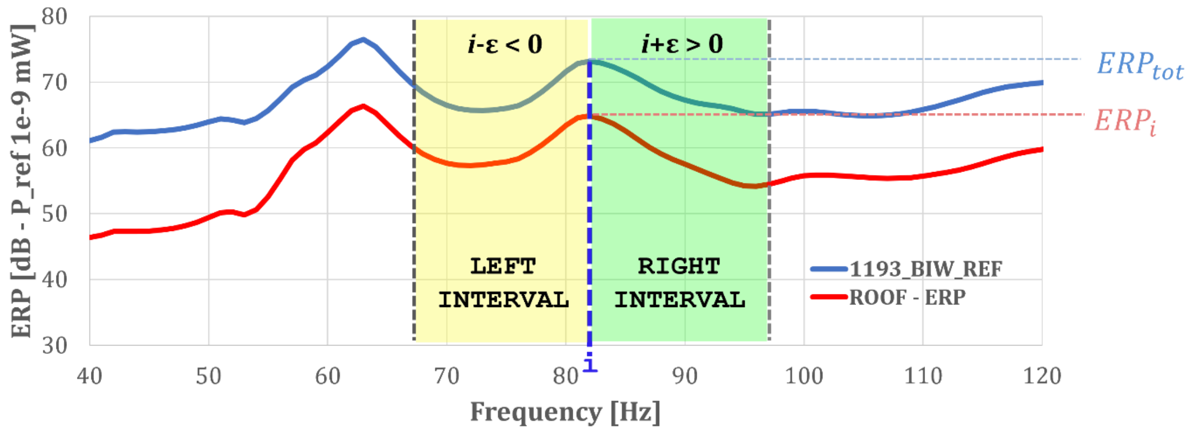

Figure 6.16: Comparison between the ERP of the roof to the Total ERP.

The linear correlation index gives information about how the i-th panels (red curve) influence the shapes of the Total ERP (blue curve) in the around interval considered. This coefficient describes the relationship of the two curves on the hypothesis of linearity. The two different short intervals of frequency around the peak under investigation could better approximate the linearity condition. Each peak of the selected load-cases has been analysed, and their contributions are listed in the following tables:

Table 6.3: Panel contribution results for the peaks of Total ERP referring to Figure 6.15 (a).

	EPPF - Load-case node 119 z-direction						
PANELS	**57 Hz**	**67 Hz**	**84 Hz**	**103 Hz**	**132 Hz**	**146 Hz**	**193 Hz**
ROOF	18.2	16.3	18.4	12.2	27.6	13.9	44.4
ROOF CROSSBAR FRONT	16.4	15.1	15.2	11.3	16.7	12.9	6.0
ROOF CROSSBAR REAR	0.6	0.1	0.8	0.5	0.1	0.6	6.3
FRONT_FIREWALL	0.5	0.4	0.5	0.1	0.1	0.7	1.4
TYRE_HOUSING_DS	0.0	0.3	0.2	0.1	0.1	0.1	0.2
TYRE_HOUSING_PS	0.1	0.3	0.1	0.0	0.0	0.0	0.2
BENCH	1.0	0.6	1.1	0.1	0.3	0.8	0.2
REAR FIREWALL	23.6	7.0	2.8	0.2	0.9	2.4	0.1
B-PILLAR CROSSBAR MID	0.5	0.5	0.9	0.2	0.1	0.2	0.1
B-PILLAR CROSSBAR TOP	0.2	0.1	0.1	0.1	0.0	0.0	0.0
WINDSCREEN SIDE REAR DS	0.0	0.1	0.3	0.0	0.3	0.5	0.0
B-PILLAR CROSSBAR BOTTOM	1.8	0.3	2.6	0.6	0.0	0.3	0.3
TUNNEL	1.0	1.0	0.6	1.5	0.2	0.8	0.0
SEAT ATTCHMENTS DS	0.0	0.1	0.1	0.1	0.0	0.0	0.0
SEAT ATTCHMENTS PS	0.1	0.0	0.0	0.1	0.0	0.0	0.1
SEAT REINFORCEMENT DS	0.2	2.7	0.7	2.2	0.0	0.4	0.3
SEAT REINFORCEMENT PS	1.6	0.6	0.3	2.5	0.1	0.4	0.8
FLOOR DS	0.1	5.9	0.7	10.4	0.3	1.5	1.4
FLOOR PS	2.4	1.5	0.3	14.0	0.3	1.9	2.2
FLOOR REINFORCEMENT PS	0.3	0.5	0.2	0.5	0.4	0.3	0.0

FLOOR REINFORCEMENT DS	0.0	1.4	0.0	0.2	1.0	1.1	0.4
EXTRUSION FLOOR DS	0.1	0.5	0.1	0.5	0.0	0.2	0.1
EXTRUSION FLOOR PS	0.3	0.0	0.0	0.6	0.0	0.1	0.0
A-PILLAR DS	0.1	0.9	0.4	0.2	0.3	0.2	0.6
A-PILLAR_PS	0.2	0.7	0.3	0.2	0.2	0.1	0.2
COWL	0.5	2.2	0.9	1.0	0.7	1.4	3.1
FRAME DOOR DS	4.5	6.3	12.2	7.1	7.0	3.7	9.0
FRAME DOOR PS	4.0	7.2	9.0	4.8	8.0	5.9	4.8
SILL DS	0.0	3.3	1.6	0.1	0.2	0.3	0.2
SILL PS	1.0	1.9	0.7	0.1	0.6	0.2	0.5
WINDSCREEN SIDE REAR PS	0.1	0.1	0.0	0.0	0.0	0.1	0.0
WINDSHIELD	20.7	22.0	28.7	28.6	34.4	48.7	17.1

Table 6.4: Panel contribution results for the peaks of Total ERP referring to Figure 6.15 (b).

	EPPF - Load-case node 319 z-direction								
PANELS	**56 Hz**	**67 Hz**	**73 Hz**	**88 Hz**	**94 Hz**	**119 Hz**	**145 Hz**	**169 Hz**	**206 Hz**
ROOF	21.2	9.6	26.1	56.4	64.5	41.7	16.4	11.3	44.7
ROOF CROSSBAR FRONT	15.9	17.9	11.9	9.7	9.6	0.7	1.8	5.2	1.3
ROOF CROSSBAR REAR	0.5	0.0	1.6	2.9	4.2	3.1	0.4	0.3	2.9
FRONT_FIREWALL	0.4	1.0	0.8	0.1	0.0	0.0	0.1	0.0	0.2
TYRE_HOUSING_DS	0.0	0.3	0.3	0.0	0.0	0.0	0.0	0.1	0.2
TYRE_HOUSING_PS	0.1	0.2	0.3	0.0	0.0	0.0	0.0	0.0	0.1
BENCH	0.7	0.3	1.1	2.3	2.1	1.8	3.4	0.7	6.9
REAR FIREWALL	20.2	13.2	5.2	4.2	1.9	18.4	30.4	5.2	1.8
B-PILLAR CROSSBAR MID	0.4	0.0	0.9	2.0	1.6	0.9	0.7	0.1	0.1
B-PILLAR CROSSBAR TOP	0.2	0.0	0.3	0.4	0.6	0.3	0.0	0.1	0.1
WINDSCREEN SIDE REAR DS	0.1	0.3	0.5	0.0	0.1	2.2	3.0	0.7	0.1
B-PILLAR CROSSBAR BOTTOM	1.7	0.0	0.2	2.6	2.5	1.7	2.2	0.8	3.0
TUNNEL	1.2	0.6	0.6	1.0	0.6	0.8	0.9	1.2	2.4
SEAT ATTCHMENTS DS	0.1	0.0	0.1	0.0	0.0	0.1	0.2	0.2	0.0
SEAT ATTCHMENTS PS	0.1	0.0	0.0	0.0	0.0	0.0	0.0	0.1	0.1
SEAT REINFORCEMENT DS	1.0	1.3	1.5	0.3	0.0	0.7	4.2	4.8	1.6
SEAT REINFORCEMENT PS	1.2	1.3	0.2	0.5	0.6	0.1	0.6	0.8	2.1
FLOOR DS	1.4	2.2	3.7	0.3	0.4	7.2	9.0	9.0	6.5
FLOOR PS	1.8	3.2	0.5	0.7	1.4	3.0	1.4	3.0	4.6
FLOOR REINFORCEMENT PS	0.3	0.7	0.2	0.7	0.7	0.3	0.1	0.0	0.6
FLOOR REINFORCEMENT DS	0.2	0.7	1.1	0.3	0.0	0.2	0.2	0.3	0.0
EXTRUSION FLOOR DS	0.2	0.2	0.2	0.1	0.0	0.2	0.7	0.5	0.1
EXTRUSION FLOOR PS	0.2	0.2	0.0	0.2	0.2	0.1	0.1	0.1	0.5
A-PILLAR DS	0.2	0.7	1.0	0.1	0.0	0.1	0.1	0.2	0.2

A-PILLAR_PS	0.4	0.8	0.5	0.1	0.1	0.2	0.1	0.1	0.1
COWL	0.8	1.4	1.9	0.5	0.1	0.5	0.2	0.3	0.1
FRAME DOOR DS	4.1	8.5	10.6	3.1	0.2	7.7	6.2	11.8	7.2
FRAME DOOR PS	5.7	7.1	2.8	2.4	1.7	6.2	4.8	4.8	9.3
SILL DS	0.7	1.5	1.5	0.4	0.0	0.5	1.1	0.7	0.2
SILL PS	1.0	1.8	0.3	0.4	0.5	0.6	0.7	0.3	0.2
WINDSCREEN SIDE REAR PS	0.1	0.3	0.5	0.3	0.0	0.7	0.1	1.5	0.1
WINDSHIELD	18.0	24.8	23.7	8.1	6.3	0.1	10.9	35.7	2.8

The previous table highlights the panels having a EPPF contribution over 5% in yellow and over 10% in red. The extrapolation of the dominant panels has been obtained considering the average of the all the peaks of the load-cases. The methodology consents either to focus the attention only on the higher peaks or to obtain a reduction of radiated power over all the frequency range. It is more productive try working considering few load-cases representing the worst cases. The dominant panels extrapolated are reported in the following histogram:

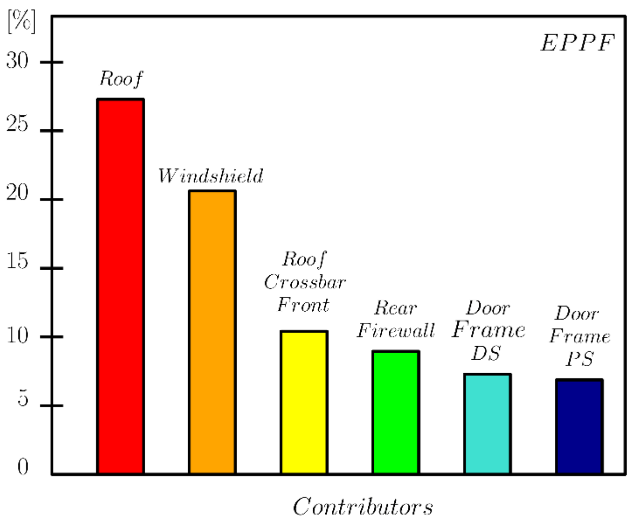

Figure 6.16: Panels that mainly contribute to generating the peaks of Total ERP for the considered load-cases.

This result agrees with the results obtained by the frequency response analyses. In Figure 6.16, the selected panels are isolated and compared to the Total ERP for the load-cases concerning the excitation of the rear shock tower.

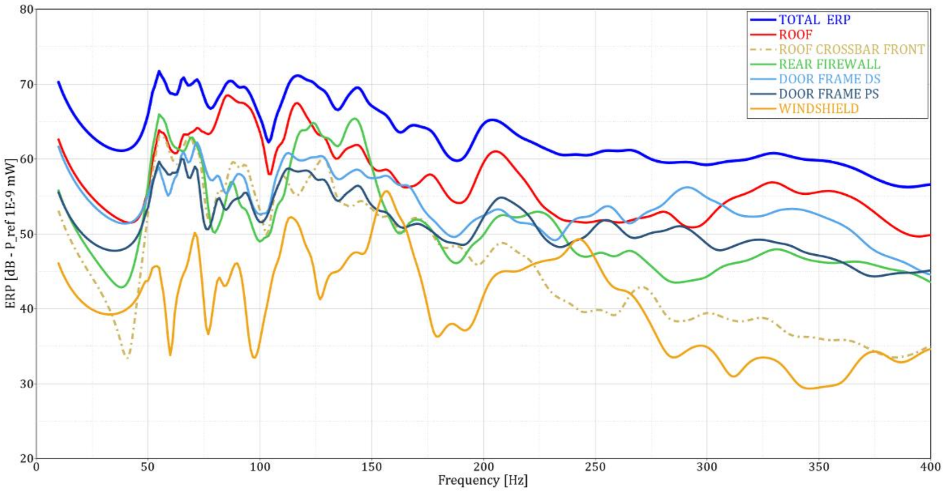

Figure 6.17: Panels that mainly contribute to generating the peaks of Total ERP considered the results for the external unit-load at node 319.

Figure 6.17 shows the radiated power behaviour of the selected panels for the load cases of unit load in $\hat{z}$-direction to node 319. In particular, it is noticed that for the frequency range from 85 Hz to 95 Hz, and at 206 Hz, the level of radiated power of the roof (red curve) is close to the levels of Total ERP (blue curve). On the other hand, the windshield (yellow solid curve) remains at the lower amplitude of ERP along with all the frequencies, but it has a significant influence at low frequencies [88]–[90]. The EPPF seizes the contribution of the windshield thanks to the high values of the linear correlation index.

6.3 - The improvement the dynamic behaviour of the panels

The third step of the methodology deals with the modifications of the selected panels, following the direct or indirect approaches. The results highlighted the need to focus the attention on the upper part of the spaceframe. The mode of vibrations of the widest panels (i.e. the windshield and the roof) transmits the major quantity of energy in the vehicle cabin. The roof is a thin-walled structure component 1mm thick made in aluminium. The design of the roof provides targets of stiffness for the global modes of bending and torsion of the BiW configuration [91], safety (e.g. roof crush resistance in case of rollover event [92]), ergonomics and aesthetics. The latter constraints prohibit any outer variation of the shapes to improve the bending modulus of the structure. The degrees of freedom to reduce the radiated power allow the thickness to be increased with a layer of damping material. The selection's criterion considers the peculiar's material property. In particular, the density, structural damping and layer thickness are the crucial parameters [30]. The typical materials are:

- LA – Layered Asphaltic (0.1 mm layer of aluminium foil);
- Asphalt or bitumen;
- Polymers (e.g. rubber, PUR foam).

The reference model of BiW configuration considers an asphalt damping material, characterized by the following material properties:

T 6.5: Asphaltic material properties

Properties	Value	Units
Young Modulus	2000	MPa
Density	2150	kg/m^3
Poisson coefficient	0.4	/
Damping ratio	0.25	/
Thickness of the layer	3	mm

These are means values referred to the operational conditions for simplicity [16]. In general, these materials are sensitive to temperature and strain rates. The density of the damping material is comparable to the aluminium. Thus, the distribution of the damping material layered needs to be minimized considering the weight target of the project.

The indirect approach suggests improving the framework of the roof. If the components that support the roof are stiffer, the roof will reduce the power radiated into the vehicle cabin. The same approach could also be applied to the windshield framework [93]–[96]. Moreover, the components that constitute the roof's and the windshield's supports present fewer constraints in shape variations (e.g. there are not strictly aesthetic requirements).

From these observations, the approach to improving the BiW considers a numerical optimization loop to improve the components that support the roof by minimizing their weight. Structural optimization is an established instrument to reduce weight in the automotive [97], [98]. Weight reduction is important, as it leads the overall fuel consumption of the car. The literature is rich in contributions aiming to the optimization of structural components, like automotive pistons [99], [100], doors, steering column supports [101], [102], or brake pedals [103].

The weight gain could be redistributed to increase the stiffness of the windshield's framework and increase the roof's thickness.

The next paragraphs treat the structural optimizations of the bench, the rear firewall and the damping material distribution on the roof.

6.3.1 - Structural optimization analyses of the bench

The bench is not one of the main subsystems having significant contributions to radiated power peaks in the load-cases under investigation. On the other hand, the bench in the reference model has a complex shape; in fact, there is a high density of ribs to maximise the flexural out-of-plane momentum of inertia and a wide layer of damping material that almost covers the entire surface.

This configuration offers the possibility to optimise the bench layout reducing the damping material saving mass without affecting the performance. Figure 6.19 shows a portion of the F142M, in which it is possible to analyse the bench subsystem.

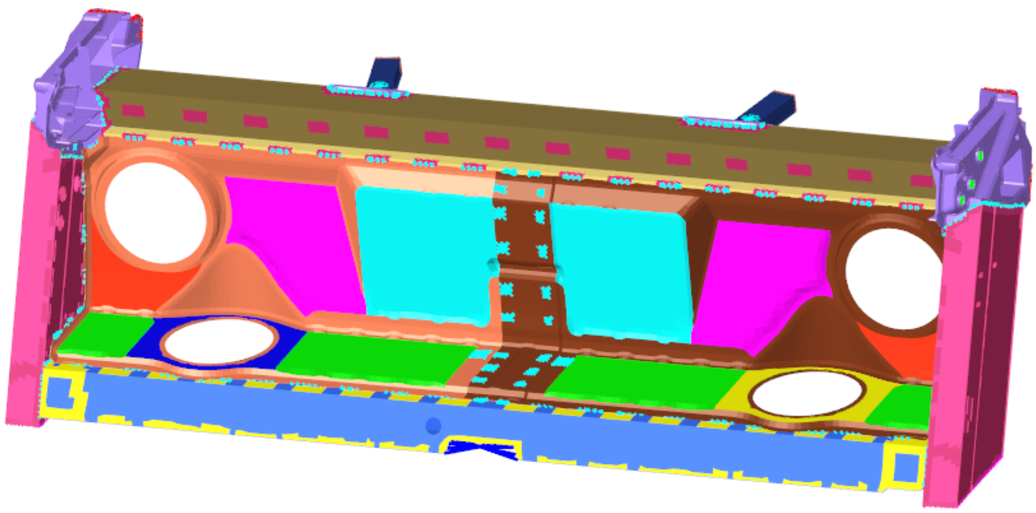

Figure 6.19: Reference bench of F142M: two welded bent plates (brown and orange).

Welding seams and rivets connect the bench to the B-pillars and two rigid crossbars. The numerical optimisation process needs several iterations to achieve convergence. Different approaches have been tested to derive the best trade-off between the accuracy of the solution and simulation time. The basic idea is to minimise the degrees of freedom of the FE element model used for the optimisation loops. On the other hand, it is crucial to consider the dynamic behaviour of the component closer to the design optimisation space; in this way, it is possible to determine the paths of loads and of vibrations properly. In the case under study, the bench is rigidly connected to higher stiffness components. For simplicity, the optimisation problem is performed on a reduced local model, fixed in the connection zones to the rest of BiW. The optimisation process is subdivided into two steps:

- Topography optimization of bench plates
- Free-Size optimization of damping material patches

The former concerns a shape optimisation of different zones of the bench. These zones define the design space of the first step of optimisation. The objective is to move at higher frequencies the first mode of the system by the variation of the plate's shape [104]–[106]. During each iteration, the optimisation algorithm moves the nodes of the design space in the normal direction to the shell. In this way, it is possible to create ribs along the surface of the design space with both free and constraint geometry. The advantage of this peculiar optimisation technique is obtaining stiff plate-shaped structures avoiding increasing the thickness and mass. The constraint on the rib's geometry deals with the manufacturability of the component, so two manufacturing constraints have been imposed on the optimisation problem:

- Linear ribs on green design space (shown in Figure 6.19)
- Symmetric solution to longitudinal vehicle plane ($\hat{y} = 0$)

Moreover, the design space is defined only in local zones not to alter the interface's surface between the bench and the other components. Finally, the ribs are defined by the following parameters:

- Minimum width: 10.0 mm,
- Draw Angle: 45.0°
- Draw Height: 12.0 mm

These parameters are the geometrical bounds of the ribs, and in particular, the height of the ribs is defined as the maximum distance in the normal direction that a node could achieve to the reference plane. As shown in the previous chapters, the first mode shape of a fixed plate is characterised by an out-of-plane displacement field. Thus, maximising the draw height is fundamental to achieving the design objective.

On the other hand, the packaging of a high-performance vehicle minimises the free space between the components. In particular, the vertical part of the bench has the function of a firewall and needs to isolate the passenger compartment from the rear ICE. Furthermore, the height of the ribs is limited in the vehicle compartment direction for ergonomics issues. Thus, a further constraint is established, which imposes the optimisation algorithm to obtain the maximum ribs height, moving the nodes equally of half-height in both directions. The first step of the optimisation of the bench achieved a feasible design moving the first mode of vibration from 140.3 Hz to 209.8 Hz after 11 iterations. The optimized configuration is shown in the following figure:

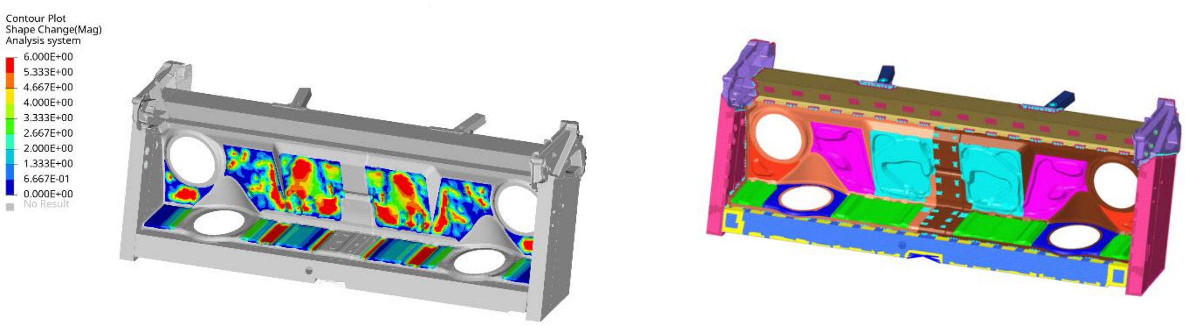

(a) (b)

Figure 6.20: (a) Topography Optimisation results; (b) FE model of first step of optimization process.

The second step of the optimisation process concerns the reduction of ERP peaks by distributing a layer of asphaltic material on the surface of the plate. The optimum distribution of the added material is crucial from a lightweight point of view and for performance. If the material is not properly calibrated, it could have an adverse effect on reducing the system's natural frequencies. The principal limitation of this simplified model concerns the lack of information about the paths of the external loads, caused by the high number of components attached to the bench and its position in the vehicle's layout, far from the excitation zone. For this reason, it needs to evaluate the optimisation process results on the BiW model.

The Free-Size optimisation considers the thickness variations of each design space element. Two new design spaces were defined for the second step. The bench is virtually divided into two panels, named and respectively. The first domain includes all the elements having normal in n_z-direction, while the second one concerns the elements in the vertical plane characterised by the normal to n_x-direction. Figure 6.21 shows the two domains and the fixed constraints located in A, B, C, D, E, F, G and H.

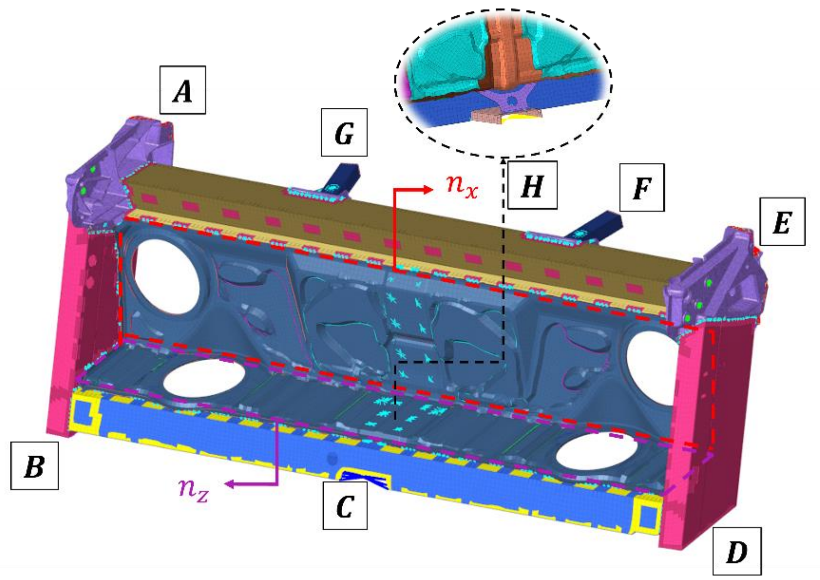

Figure 6.21*: Simplified model of bench of Free Size (FS) optimization analysis.*

The optimisation analysis considers the linear combination of six load-cases. The analysis assumes that the vibrations coming from the road are mainly transmitted by the stiffer components attached to the portion of BiW considered in the simplified model, which are the sills and the rear shock towers. Thus, three load-cases considers the B-Pillar at the driver side (D) and the other the B-Pillar at the passenger side (B). The load-cases excite the structure by applying a unit-load in three directions (after the removal of the corresponding fixed constraint).

The optimisation objective is the minimization of the volume fraction of the two design spaces, considering a damping layer 3 mm thick. This value is a typical thickness of the damping layers. The minimization problem is regulated by specific design constraints concerning the added mass and the average ERP along the frequency of interest. Table T 6.6 reports the design constraints of the optimisation problem. The constraints impose a reduction of 33% of the mass of the damping material and a reduction of the 65% of the average ERP of each panel (n_z, n_x) in the frequency range from 190 Hz to 390 Hz with respect to the FE model which consider a damping layer of 3mm of thickness that covers all the surface of the bench (Figure 6.21).

T 6.6*: Design constraints of Free-Size optimization – Bench Optimisation – Step 2*

	Design Constraint	**Value**	**Units**
1	Mass of damping material	1.52	kg
3	ave-ERP F_x (B) - n_x panel	0.64	mW
2	ave-ERP F_y (B) - n_x panel	7.81	mW
4	ave-ERP F_z (B) - n_x panel	1.93	mW
5	ave-ERP F_x (B) - n_z panel	12.5	mW
6	ave-ERP F_y (B) - n_z panel	0.69	mW
7	ave-ERP F_z (B) - n_z panel	2.78	mW
8	ave-ERP F_x (D) - n_x panel	7.71	mW
9	ave-ERP F_y (D) - n_x panel	0.58	mW

10	ave-ERP F_z (D) - n_x panel	1.62	mW
11	ave-ERP F_x (D) - n_z panel	11.67	mW
12	ave-ERP F_y (D) - n_z panel	0.54	mW
13	ave-ERP F_z (D) - n_z panel	2.78	mW

The optimization considers the symmetry to the longitudinal plane even if the behaviour of the simplified system is not symmetric. This is due to the approximations made during the extrapolation of the simplified model from the BiW and for the local non-symmetric features of the components. The solution of the optimisation has been achieved after twelve iterations and the results are shown in Figures 6.22 and 6.23.

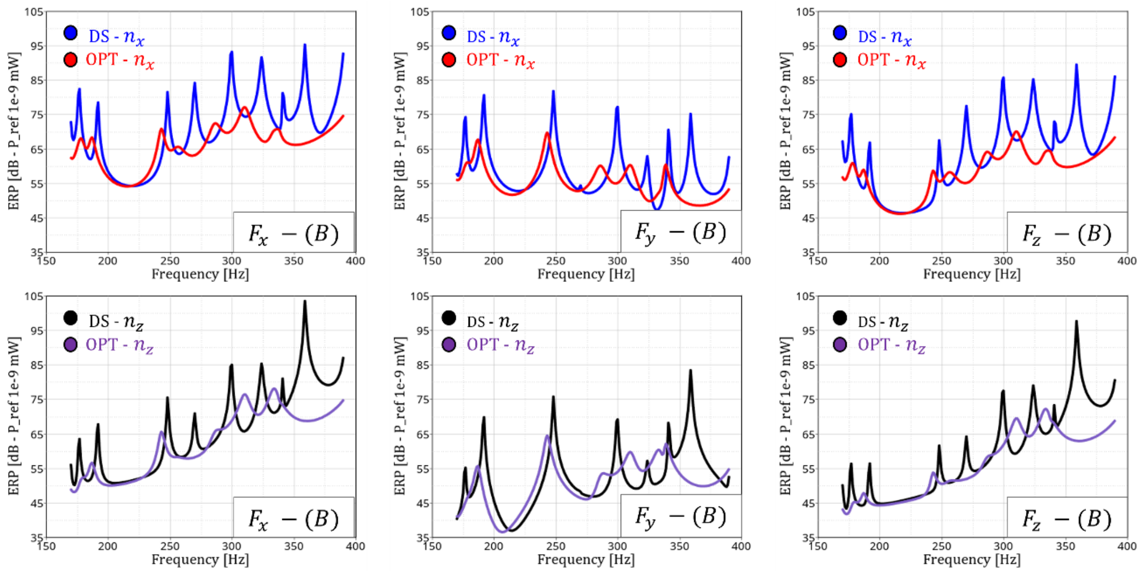

Figure 6.22: Optimization results: Comparison between design space model (DS) and optimised configuration.

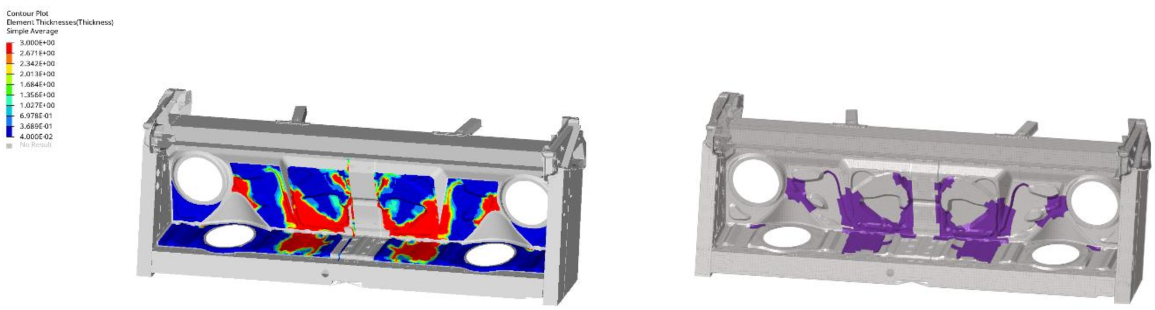

(a) (b)

Figure 6.23: (a) Free Size optimisation results; (b) Optimized layout of the bench for the new concept of BiW.

The results show the reduction of ERP of the bench plates facing an added mass of 1.52 kg. Figure 6.22 reports only the results of the three loads applied at the bottom of the B-Pillar at the passenger side (B). The corresponding results of the driver-side load-cases remain coherently in good agreement. This is due to the macro-symmetry of the simplified model and of the loading system, and of the symmetric constraints imposed during the optimisation simulation. The results show that the reduction in natural frequencies levels of the first vibration modes originated from the effect of the added mass.

On the other hand, the damping material can significantly reduce the amplitude of the peak of ERP. The distribution of the damping material shown in Figure 6.23 (a) is concentrated to the zone that remained flat after the first step of optimisation. Moreover, the material is mainly added in at the middle of the bench, which is the less stiff zone of the fixed plates. The optimised layout of the bench weights 3.87 kg, which corresponds to an increased weight of 1.6% than the BiW reference layout. The validation of the optimisation analysis has been tested off the BiW model, particularly for the load-case of unit-load in $\hat{z}$-direction applied to the rear shock tower at the shock absorbers hardpoint (node 319). The bench has significant contribution to the Total ERP in these load-cases at 206 Hz. Figure 6.24 shows the comparison between the ERP of the bench of the reference model (blue curve) and the new layout of the BiW (red curve), respectively.

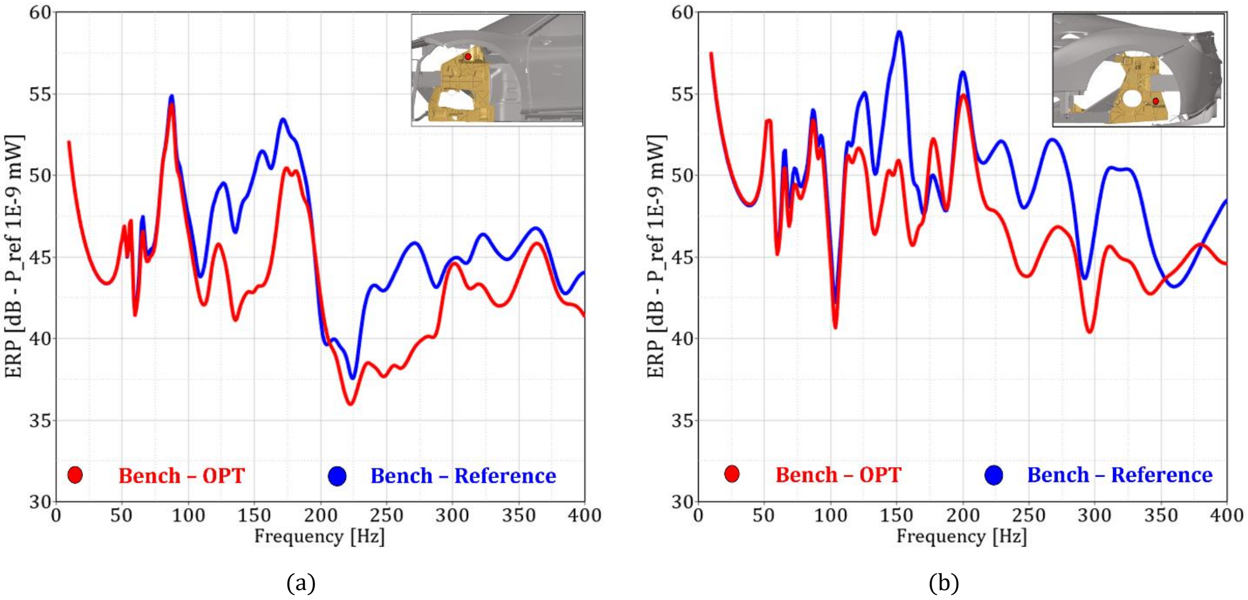

Figure 6.24: (a) Bench ERP of load in z-direction at 119 (b) Bench ERP of load in z-direction at 319

6.3.2 - Structural optimization analyses of the roof

The roof is one of the vehicle's widest panels, and its framework is not stiff as the bench's framework.

For this reason, the optimisation of the roof has been performed using the entire BiW models considering the formulation of the solid element at the first order. The best practice usually discretises the 3D structures by solid elements of the second order. This simplification reduces the degrees of freedom of the system, saving the simulation time for each iteration of the optimisation loop, but it introduces a numerical discrepancy between the stiffness of the actual solid 3D structures and their numerical description. A structure modelled by a first-order solid element is generally stiffer than the second-order elements formulation considering the same mesh size. This behaviour is due to the higher numerical approximation of the displacements field solution in the solid element at the first order. The second-order formulation considers more nodes in which the solution is evaluated, and for this reason, the interpolation function results more accurate. Thus, the numerical model has been adequately tuned to reobtain a good agreement to the actual dynamic behaviour of the BiW configurations by degrading the modulus of elasticity of these components of the 20%, as shown in Figure 6.25:

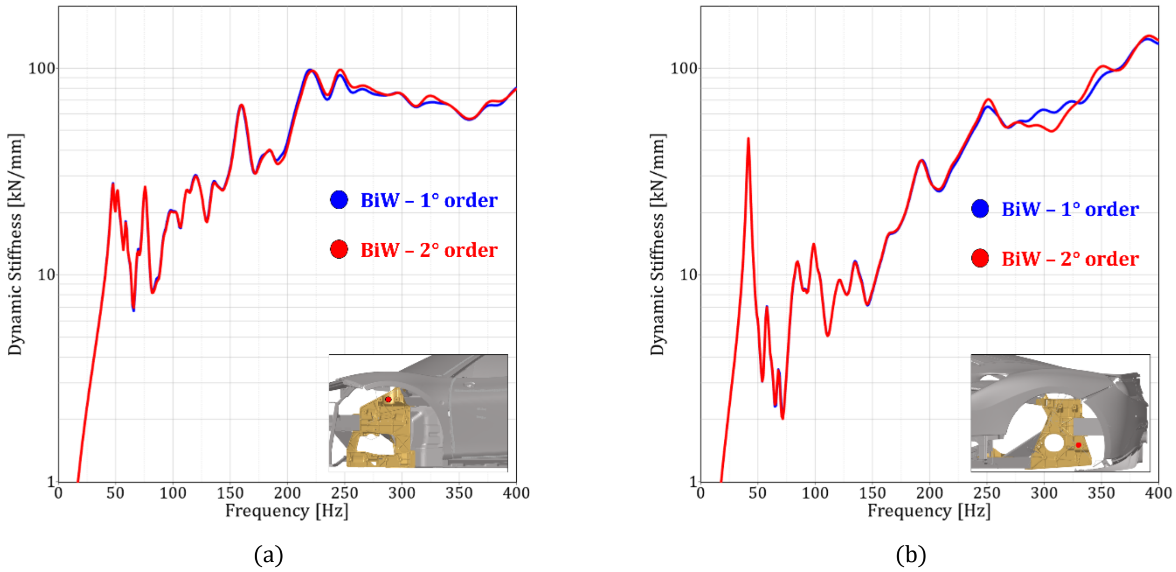

Figure 6.25: (a) Dynamic stiffness of 119; (b) Dynamic stiffness of 319.

The simplified FE model is in good agreement with the dynamic stiffnesses of the load-cases under investigation evaluated with the detailed FE model of BiW. The discrepancies of the FE models, which considers first-order solid elements and the corresponding material degraded, is considered acceptable for the optimisation analyses if they are compared with the simulation time, see Table T 6.7:

T 6.7: Comparison of simulation time and modes of vibration included in the modal basis of detailed and simplified FE models respectively.

F142M - BiW	**Number of modes [0 - 600] Hz**	**Simulation time [hh:mm:ss]**
Detailed description of solid elements [2nd order]	963	00:33:10
Simplified description of solid elements [1st order + 0.8·$E_{Young\ Mod.}$]	959	00:16:33

The approach employed is analogous to the second step of the bench's Free Size (FS) optimisation. A design space was defined considering a 3 mm damping asphalt layer covering the roof surface. The optimisation algorithm intents damping material volume fraction to be minimised, which is varying the thickness of each element of the design space. Two design constraints drive the optimisation loop to an optimum solution imposing an average reduction of ERP of the roof panel in the frequency range of interest from 50 to 400 Hz of 40% and accepting an increase in weight of 25% concerning the reference model, in which the mass of the damping pads is 1.0 kg.

The convergence to a feasible design solution has been achieved after 18 iterations and more than 5 hours. The distribution of damping material is shown in the following figure:

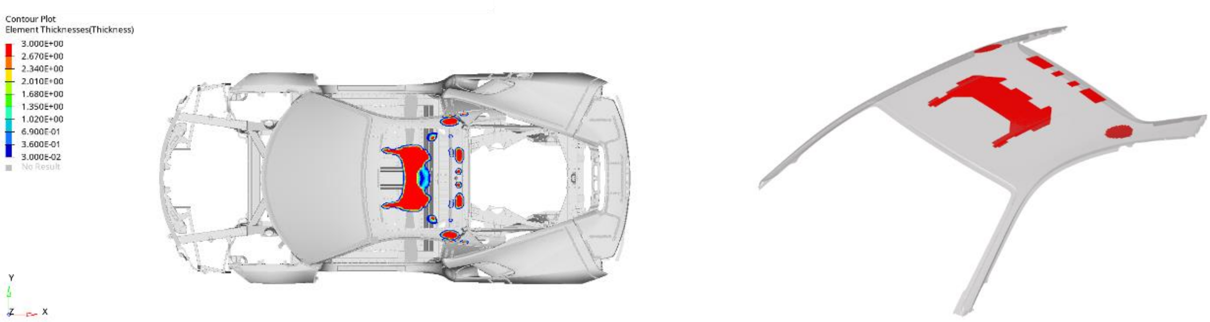

(a) (b)

Figure 6.26: (a) Free Size optimisation results; (b) Optimized layout of the roof for the new concept of BiW.

The new layout of the damping material is concentrated in the central zone of the roof, the same as the bench case. Other patches have been applied moving in the rear zone of the roof upon the rear crossbar that sustains the roof. This configuration suggests improving the stiffness of the roof framework in that zone, particularly the crossbar and the upper part of the rear firewall. Figure 6.27 compares the ERP of the roof between the reference BiW model (blue curve) and the optimised layout (red curve).

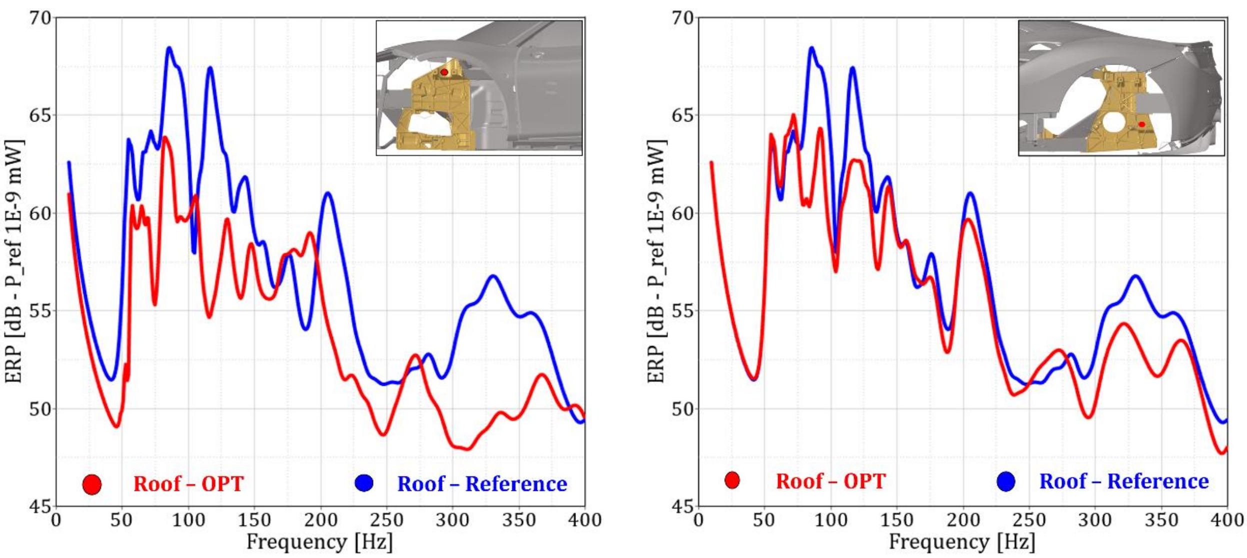

(a) (b)

Figure 6.27: (a) Roof ERP of load in z-direction at node 119 (b) Roof ERP of load in z-direction at node 319.

6.3.3 - Structural optimization analyses of the rear firewall

The rear firewall is the fourth panel mainly influent following the analyses of the EPPF. This panel is located above the bench, and it is connected to the B-Pillar crossbar in the bottom edge, to the B-Pillars at the sides, and rigidly supports the rear windscreen, as shown in Figure 6.28. The rear windscreen is included in the BiW models for its not negligible contribution to the torsional stiffness of the spaceframe. On the other hand, it weighs 3.14 kg and, with its significant inertia, excites the rear firewall's vibration modes. Improving this panel's stiffness could reduce the total radiated power at the peaks frequencies and indirectly stiffen the roof framework.

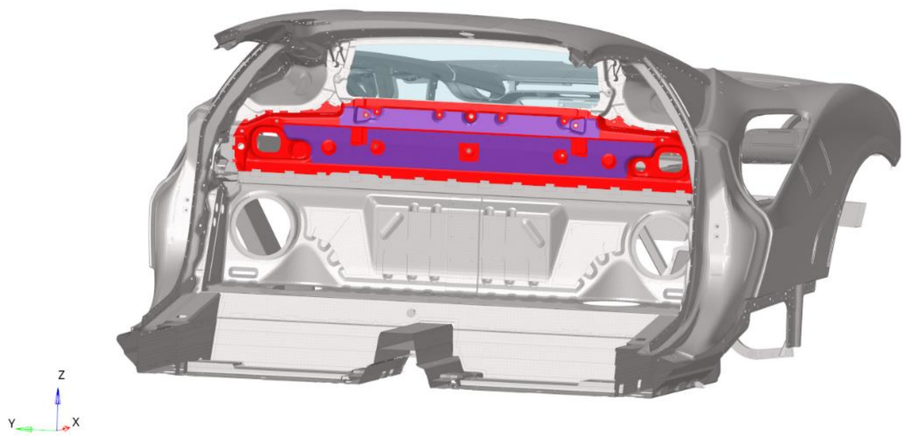

Figure 6.28: Reference rear firewall of F142M: Aluminium plate (red) and Damping layer (purple).

The rigid framework around the firewall permits, also, in this case, to isolate the panel to minimise the optimisation time. A different approach is implemented to improve the out-of-plane flexural stiffness of the aluminium plate (the red component in Figure 6.28). The aim is to connect the optimum combination of the geometrical parameters of linear ribs to the optimum ribs' distribution. In general, a considerable number of possible combinations of rib parameters could comply with the design limits, but the number of analyses to perform usually result utopian from a practice point of view.

In recent decades, algorithms were developed to minimise the number of tests to extrapolate the optimum configuration of the solutions of specific problems close to the best solution. In particular, the Genetic Algorithm (GA) could dramatically reduce the number of simulations than the Full Factorial (FF) method [98]. GA is based on human genetics to build new samples to analyse based on previous results considering random effects. This approach consents to study a design space of a population of samples and to test a few portions of these, orienting the calculations to the best samples' selection.

The optimisation process of the rear firewall considers the GA to evaluate the optimum combination of possible rib's geometrical parameter to consent to the topography optimisation to obtain the best reduction of ERP. Therefore, a topography optimisation is performed at each individual selected by the GA. A simplified FE model of the rear firewall is developed for this test case considering a minimum number of elements. The FE model does not consider the damping layer material in this phase, and it is fixed at the connection nodes to the other components, as shown in Figure 6.29.

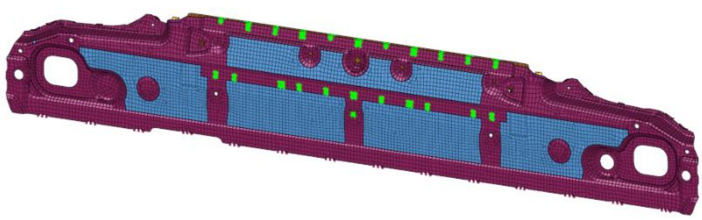

Figure 6.29: Reference rear firewall of F142M: Aluminium plate (red) and Damping layer (purple).

Figure 6.29 shows the design space (the blue navy component) defined for each optimisation loop, in which includes only the zone that does not compromise the surfaces' interface and the fitting with the other components. The firewall is subjected to an external unit-load in normal direction located in the geometrical centre. The objective function of the topography optimisation is to minimise the average ERP considering the design constraint of reduce the amplitude of ERP peaks below 5 W, which corresponds to a reduction of 85%. The optimisation problem considers also a linearity constraint of the ribs aligned to the vertical axis (i.e. $\hat{z}$-direction). This direction results more efficient from an out-of-plane flexural stiffness because the ribs could improve direct the path of loads from the rigid attachments points which are more densify along $\hat{z}$-direction than $\hat{y}$-direction.

The GA combines the geometrical parameters of the ribs' section, which are the minimum width (W), the inclination angle (α) and the draw height(H), represented in Figure 6.30:

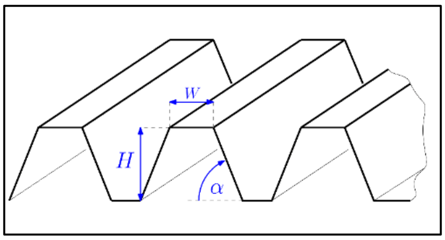

Figure 6.30: Geometrical parameters of linear rib's cross section. W indicates the minimum width, α the inclination angle and H the maximum height.

The GA, self-build and defines an individual of a population considering its phenotype, a vector containing a specific combination of the geometrical parameters. The phenotype is the practical, "external" translation of the genotype, which considers the ensemble of the alleles. The alleles are defined by a binary code related to the specific geometric parameter value. The chromosome includes the sequence of alleles specific for each individual and could be subjected to random mutation or crossover to another chromosome to generate a new generation of individuals to test. The design space considers four parameters' levels that determine 64 possible samples to test. Table T 6.8 reports the parameters and the corresponding values.

T 6.8: Design Space for the optimisation of rib's section properties.

LEVELS	**PARAMETERS**		
	W [mm]	**α [°]**	**H [mm]**
L1	5	45	15
L2	10	50	20
L3	15	55	25
L4	20	60	30

The GA implemented in this study considers a population of six individuals for four generations each. The first generation is randomly selected in the design space. The link between the genotype and the phenotype is expressed by a translation code that associates a binary number to a specific level of each parameter. The dimension of the binary number representing an allele of a chromosome is equal to the power of two exponents. Thus, the possible alleles are 00, 01, 10, 11. Figure 6.31 shows an example of the translation between genotype to phenotype.

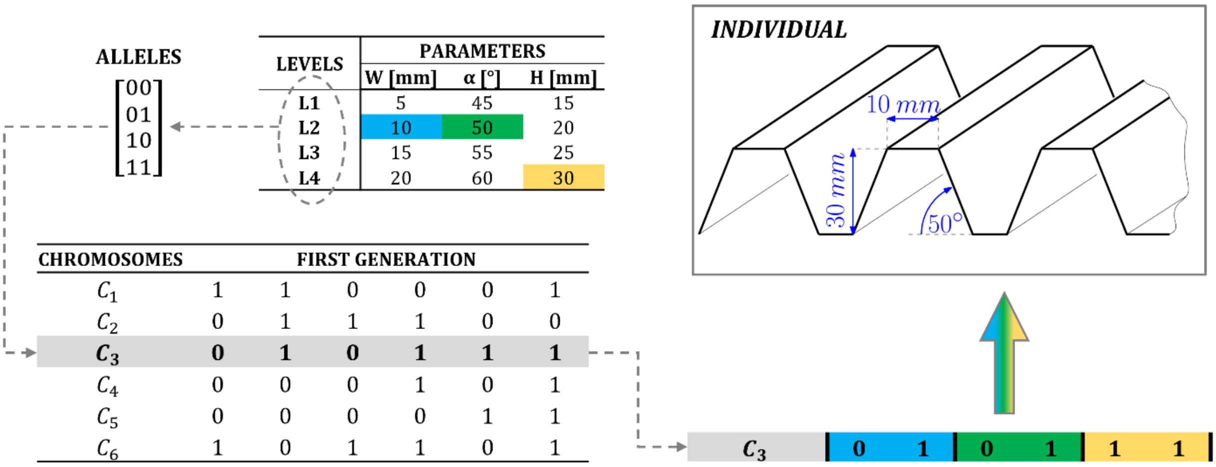

Figure 6.31: Example of translation between genotype to phenotype of the 3rd chromosome belonging to the first generation.

The GA algorithm is implemented on Matlab script that generates the first six FE models with specific rib section properties. The results of the six topography optimisations are analysed by the fitness function of the GA that neglects the unfeasible solutions and selects the two best results by evaluating the minimum average ERP. These results are the parents of the second generation of individuals. Two different mechanisms are defined to generate the new chromosomes in analogy with human genetics: the crossing-over and the mutation, as shown in Figure 6.32.

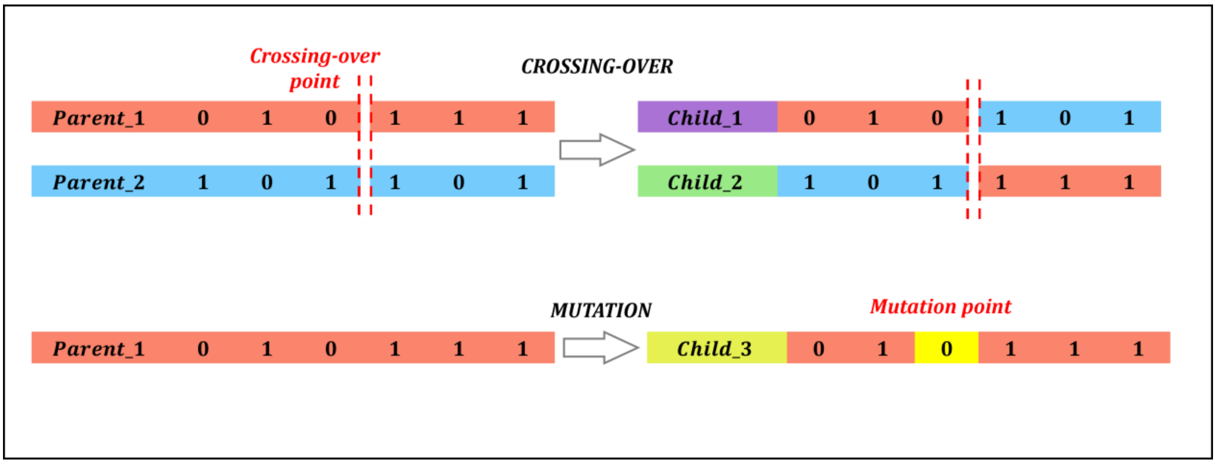

Figure 6.32: Mechanisms for the creation of a new generation.

The crossing-over and the mutation points are randomly defined avoiding the risk of influencing the converge to obvious combinations. Moreover, the best results of each loop are compared to the previous generation to avoid losing better solutions. The Matlab ® developed is reported in Appendix A.2.

The optimisation process evaluates all the 24 topography optimisation and finds the optimal result solution in the Parent_1 of the third generation corresponding to the 17-th topography optimisation.

This individual considers a rib section of 5 mm of minimum width, 60° of inclination angle and 15 mm of draw height. The optimisation process has been compared with the results of the Full Factorial method, which had been simulated by means of 64 topography optimisation analyses. Figure 6.33 shows the comparison between the methods considering a three-dimensional plot:

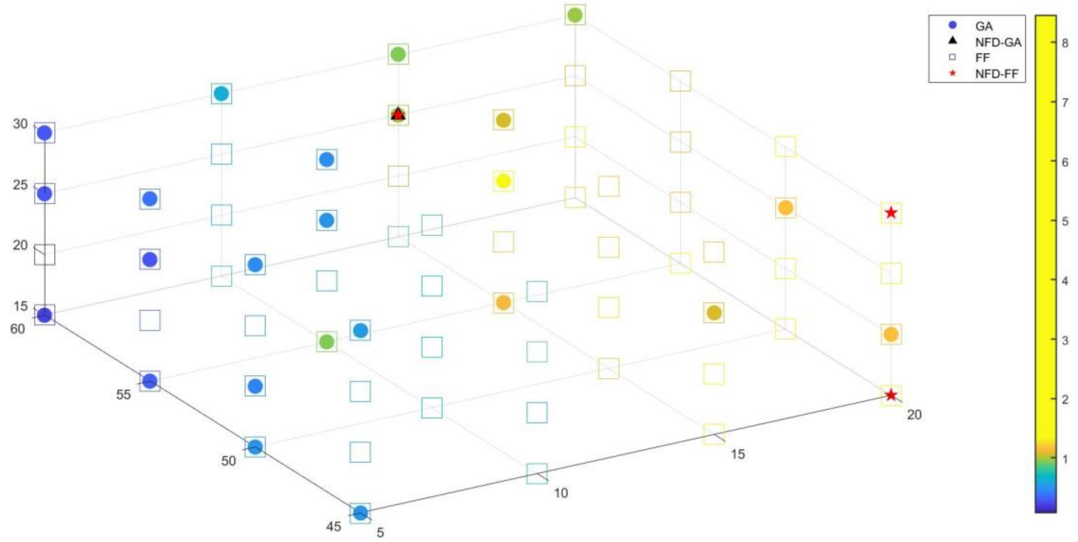

Figure 6.33: Comparison between the FF and GA algorithm. The tags NFD in the plot's legend stand for not-feasible-design, and it considers the unacceptable solutions.

The plot shows the circles' concentration, which represents the GA iterations, around the best solution (dark blue solid circle) at the coordinates (5, 60, 15).

The Full Factorial finds a better solution, but it represents the unique combinations of the geometrical parameters able to produce a more efficient topography optimisation. On the other hand, the GA algorithm saves 45% of the overall simulation time. The result of the corresponding topography optimisation is reported in the following figure.

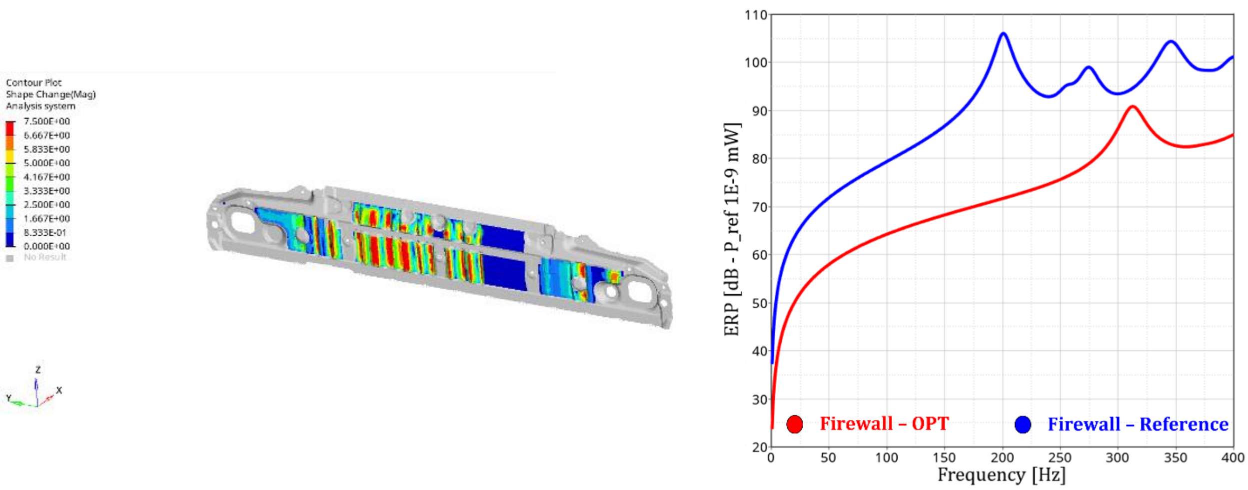

(a) (b)

Figure 6.34: (a) Optimised layout of the rear firewall (b) Comparison of the results of the simplified models between the reference firewall (blue curve) and new concept (red curve).

The comparison of the new morphology of the rear firewall results stiffer than the reference model. In fact, the first peak of resonance is higher 100 Hz more than the first peak of the reference. Thus, the optimisation method offers an interesting possibility in developing new plate-shaped components. The result obtained from the simplified model must have been tested in the BiW FE model to properly evaluate its actual performance, as shown in the following figure.

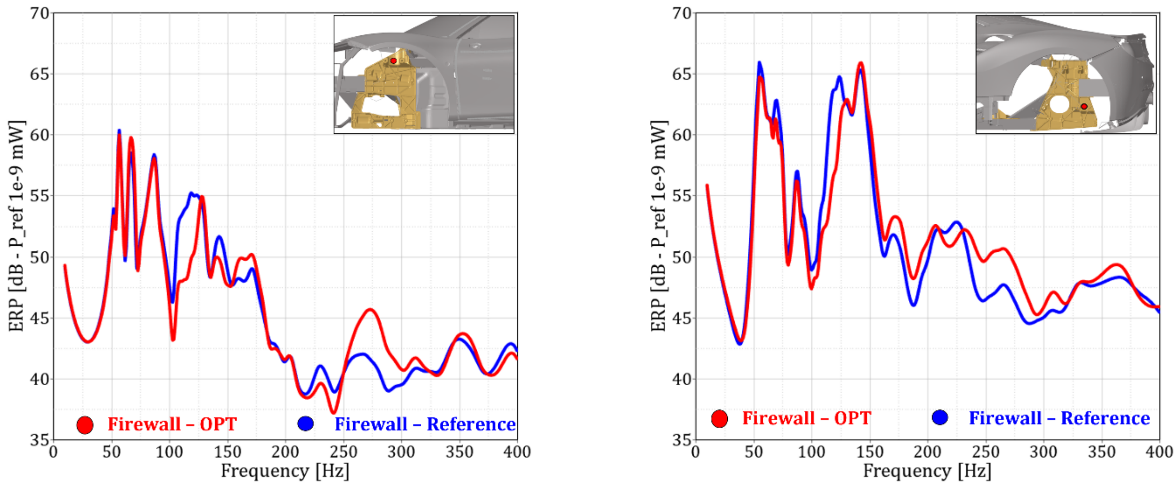

(a) (b)

Figure 6.35: (a) Roof ERP of load in z-direction at 119 (b) Roof ERP of load in z-direction at 319.

The ERP by the rear firewall in the analyses of the BiW model show limited improvements compared to the analogues analyses to the previous components. This phenomenon is due to the significant simplification of the actual dynamic behaviour of the firewall in the sub-model used in the optimisation analysis. Significant reduction of the radiated power is observed around 120 Hz for the both load-cases and in the resonance peaks ranging from 50 Hz to 100 Hz. The enhanced out-of-plane flexural stiffness of the firewall is the principal cause of these improvements and the higher peaks of ERP over 250 Hz. The new layout of the aluminium plate of the rear firewall will be included in the new concept of BiW for its improved behaviour at low frequencies, which are mainly contribute to the peaks of total ERP.

6.4 - Definition of new BiW configuration

The new configuration of BiW needs other modifications to reduce the total ERP. The results of the EPPF highlight the necessity to vary the dynamic behaviour of the windshield and door frames. The windshield presents requirements strictly and is generally out from the modifications' perimeter. Thus, it is more suitable to adopt an indirect approach by modifying its framework. The windshield is generally constrained to the BiW by a sealing glue characterised by poor rigidity. Loureiro A. L. et al. [107] studies the mechanical properties of adhesive bonding also employed for automotive applications. In their works, the authors show that the typical sealing used for connecting the windshield to its metallic frame is, in general, polyurethane polymers characterised by high elongation at break, and they are classified in detail terms of shear modulus. Despite the sealing glue, the windshield has a significant influence on the global stiffness performance of the BiW, and it is one of the heaviest panels. It is a composite sandwich material made from the outer skins of glass and a PVB core in the middle. The core has the function of dampening the vibration of the outer skins. In the literature, several studies were performed to analyse the properties of the windscreen for its significant influence on the dynamic behaviour of the automotive chassis and its description in FE models. In terms of NVH performance, the main effect of the gluing connection is isolating the vibrations of the windscreen from the vehicles. The significant weight of the windscreen establishes the first modes of vibrations at low frequencies. Thus, it is crucial to decouple these vibrations close to the vehicle cabin from the panels of the BiW.

The reduction of peaks of radiated power by the windshield could be obtained by modifying its frame, enhancing the inertia moduli of the following components:

- Cowl
- Door frame at both sides
- Front and rear crossbar of the roof
- Roof

The roof also plays a crucial role in the windshield dynamic; therefore, enhancing its thickness could imply a double advantage: reducing the ERP of the two most contributors of the total ERP.

Figure 6.36 shows the components under investigation:

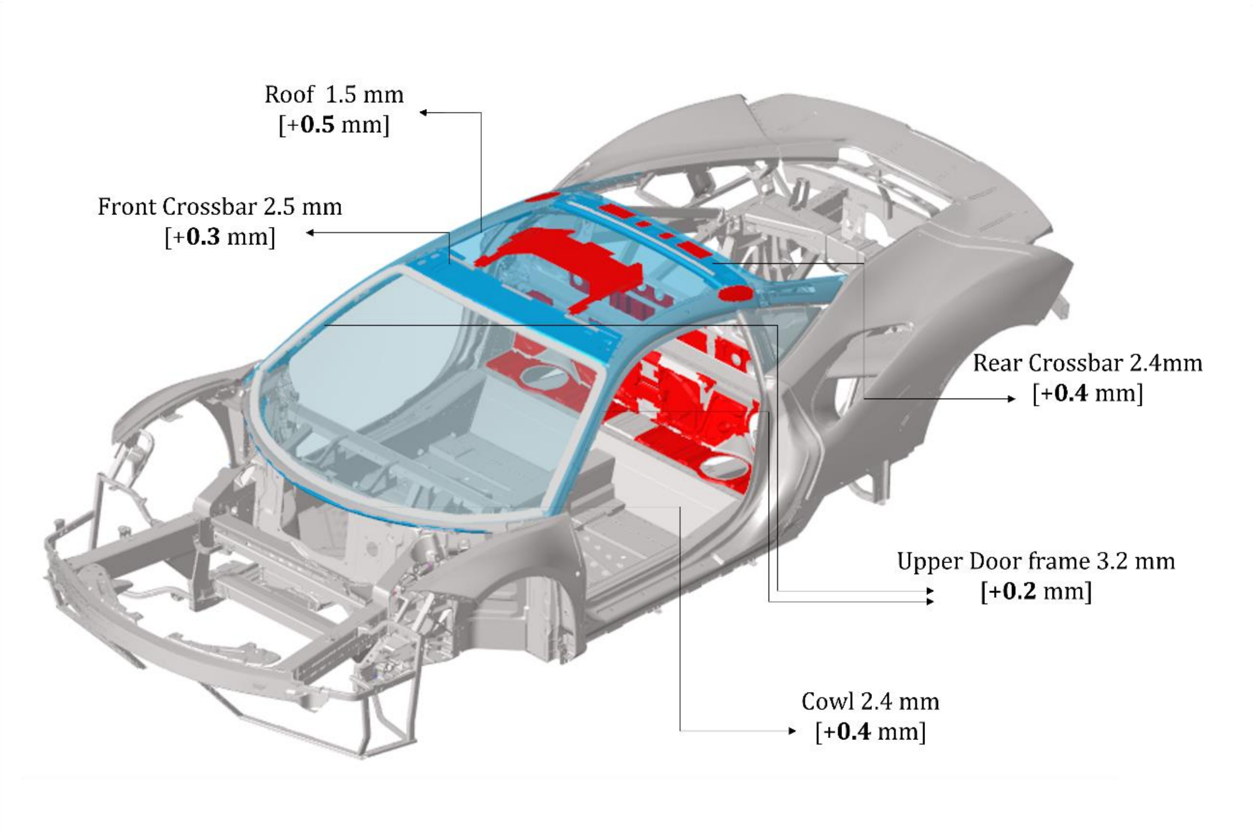

Figure 6.36: New configuration of BiW: optimised components in red and in light blue the components with augmented thickness.

Finally, Table T 6.9 summaries the modifications apply to the BiW configurations in terms of mass. The new thickness of the components had been defined considering the weight target to avoid an increase of over 1.5% of the BiW weight. In particular, the main increase in thickness had concerned the roof (+0.5 mm), which is the panel that mainly radiated power in the frequencies investigated.

T 6.9: Summary of the modification applied to the new BiW configuration

COMPONENTS	REFERENCE [kg]	NEW CONFIGURATION [kg]
ROOF	5.04	7.18
ROOF DAMPING LAYER	0.99	1.29
BENCH	3.81	3.87
REAR FIREWALL	1.87	1.90
FRONT ROOF CROSSBAR	2.17	2.44
COWL	1.98	2.34
REAR ROOF CROSSBAR	2.02	2.39
UPPER DOOR FRAMES	3.39	3.60
TOTAL	**21.26**	**25.01**

The new configuration of BiW adds 3.75 kg to the overall BiW configuration. The results of BiW and TB analyses will be discussed in the next chapter.

7 - Results

This chapter will present and discuss the results of the methodology tested on Ferrari F488 GTB. The first analyses compare the reference BiW configuration, and the new concept developed by implementing the proposed methodology. Figure 7.1 shows the results in terms of total ERP for the load-cases considered in the previous chapter.

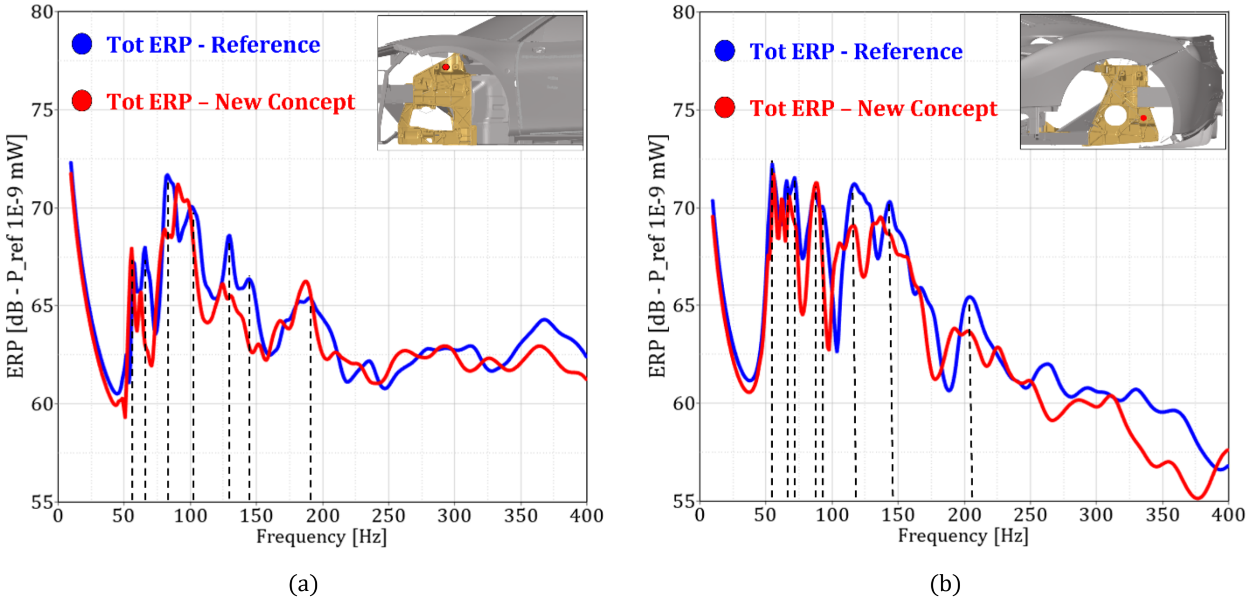

Figure 7.1: Total ERP comparison: (a) load in z-direction at 119; (b) load in z-direction at 319.

The new concept results are more efficient than the reference BiW configuration. Despite the minimum increase in weight of 3.75 kg, representing 1.4% of the total weight of 265.7 kg, the total ERP is significantly reduced at most of the analysed peaks of radiated power. Table T 7.1 and 7.2 collect the EPPF evaluated in the early phase of the methodology on the selected panels to simplify the evaluation of the results.

T 7.1: Panel contribution results for the peaks of Total ERP referring to Figure 7.1(a).

	EPPF - Load-case 119 z-direction						
PANELS	**57 Hz**	**67 Hz**	**84 Hz**	**103 Hz**	**132 Hz**	**146 Hz**	**193 Hz**
ROOF	18.2	16.3	18.4	12.2	27.6	13.9	44.4
ROOF CROSSBAR FRONT	16.4	15.1	15.2	11.3	16.7	12.9	6.0
ROOF CROSSBAR REAR	0.6	0.1	0.8	0.5	0.1	0.6	6.3
REAR FIREWALL	23.6	7.0	2.8	0.2	0.9	2.4	0.1
FRAME DOOR DS	4.5	6.3	12.2	7.1	7.0	3.7	9.0
FRAME DOOR PS	4.0	7.2	9.0	4.8	8.0	5.9	4.8
WINDSHIELD	20.7	22.0	28.7	28.6	34.4	48.7	17.1

The frequency range from 50 Hz to 100 Hz highlights the effect of the windshield panel, in particular at 67 Hz and 84 Hz.

The first peak studied does not change the amplitude. A possible explanation is that the panels surrounding the vehicle cabin are not the actual sources of vibrations, but the high radiated power is the consequence of a global mode of the BiW. The modifications applied are not sufficient to move the frequency of the global modes far enough from that frequency. A different situation happens to the peak of resonance at 103 Hz. In this case, the coupling of close modes enhances the amplitude of the radiated power. In the frequency range from 100 Hz to 150 Hz, a significant reduction of total ERP gained 5 dB at each peak. Globally, the stiffening of the windshield seems to have mainly a positive effect on the Total ERP. The principal negative effect occurs at 193 Hz, in which the stiffer roof moves its modes of vibration at higher frequencies and around the pre-existent peak of resonance. A coupled-mode slightly enhances the amplitude of the radiated power.

T 7.2: Panel contribution results for the peaks of Total ERP referring to Figure 7.1(b).

	EPPF - Load-case 319 z-direction								
PANELS	**56 Hz**	**67 Hz**	**73 Hz**	**88 Hz**	**94 Hz**	**119 Hz**	**145 Hz**	**169 Hz**	**206 Hz**
ROOF	21.2	9.6	26.1	56.4	64.5	41.7	16.4	11.3	44.7
ROOF CROSSBAR FRONT	15.9	17.9	11.9	9.7	9.6	0.7	1.8	5.2	1.3
BENCH	0.7	0.3	1.1	2.3	2.1	1.8	3.4	0.7	6.9
REAR FIREWALL	20.2	13.2	5.2	4.2	1.9	18.4	30.4	5.2	1.8
FRAME DOOR DS	4.1	8.5	10.6	3.1	0.2	7.7	6.2	11.8	7.2
FRAME DOOR PS	5.7	7.1	2.8	2.4	1.7	6.2	4.8	4.8	9.3
WINDSHIELD	18.0	24.8	23.7	8.1	6.3	0.1	10.9	35.7	2.8

Table T 7.2 reports the main contributions of EPPF for the case of Figure 7.1(b), in which a slight reduction of the Total ERP is visible at the first three peaks at low frequency. This small reduction of Total ERP underlines a good behaviour of the optimised rear firewall and the stiffer windshield framework. The peaks at these frequencies are close to the global modes of the BiW configuration and do not simply reduce the panels' vibrations without significantly increasing the mass. A constant reduction of the ERP is noticeable over 100 Hz.

The results suggest that the EPPF could be a helpful tool to guide the designer to develop a BiW with an improved dynamic performance of the panels facing a minimum weight increase.

In the next section of the chapter, the results of acoustic frequency response analyses are presented of the TB configurations, showing the comparison of the TB models obtained by including the reference BiW and the new concept, respectively. The analyses aim to simulate the actual acoustic behaviour of the TB configuration under unit-loads to obtain the noise transfer functions suitable to reconstruct the interior noise by combinations methods such as the Transfer Path Analysis (TPA). These NTF simulates the interior noise originated by the contact between the roughness of the road profile and the tyres, which is called rolling noise. Thus, the results are referred to the suspensions hardpoints of the driver side for simplicity. The nomenclature of the loaded nodes is shown in Figure 7.2:

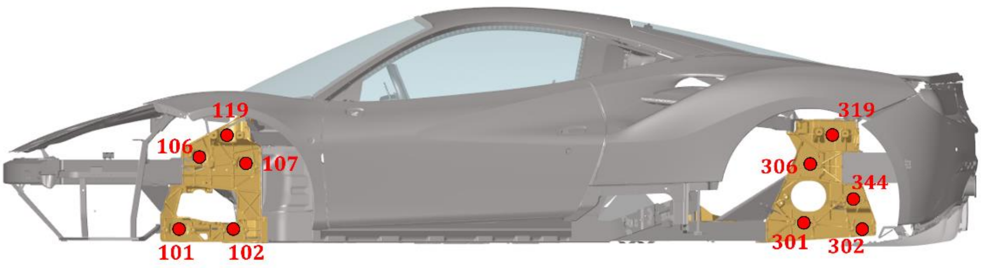

Figure 7.2: Attachments nodes at front and rear shock towers.

The acoustic target for the NTF is defined at 55 dB over 50 Hz. Figure 7.3 and 7.4 shows the sound pressure levels at the driver's right ear.

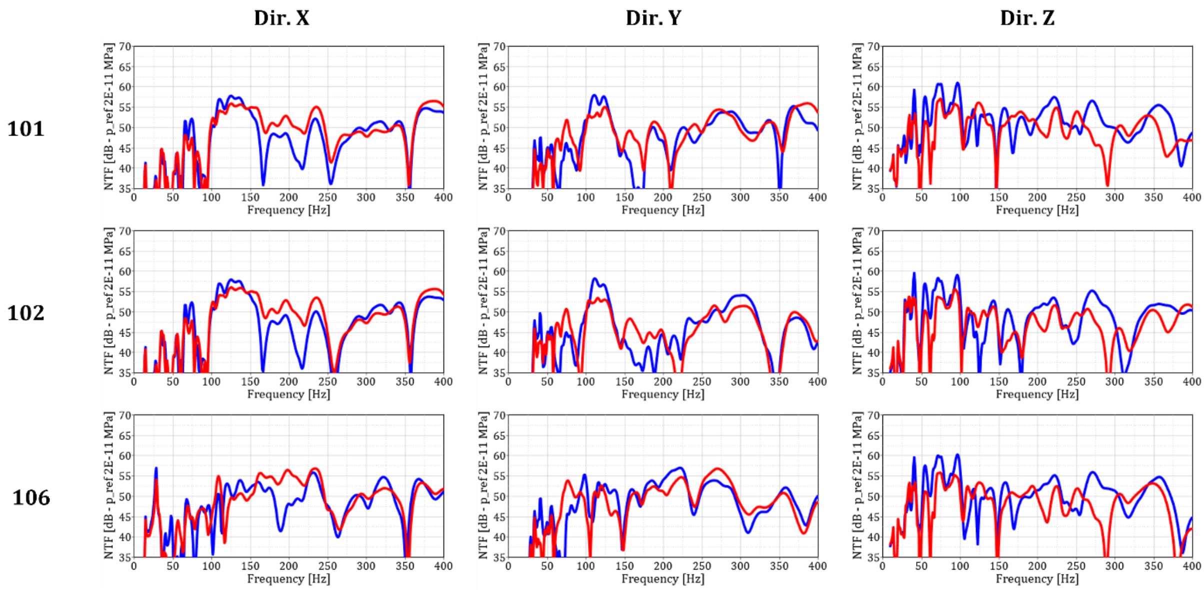

Figure 7.3: Noise Transfer Function of front shock towers

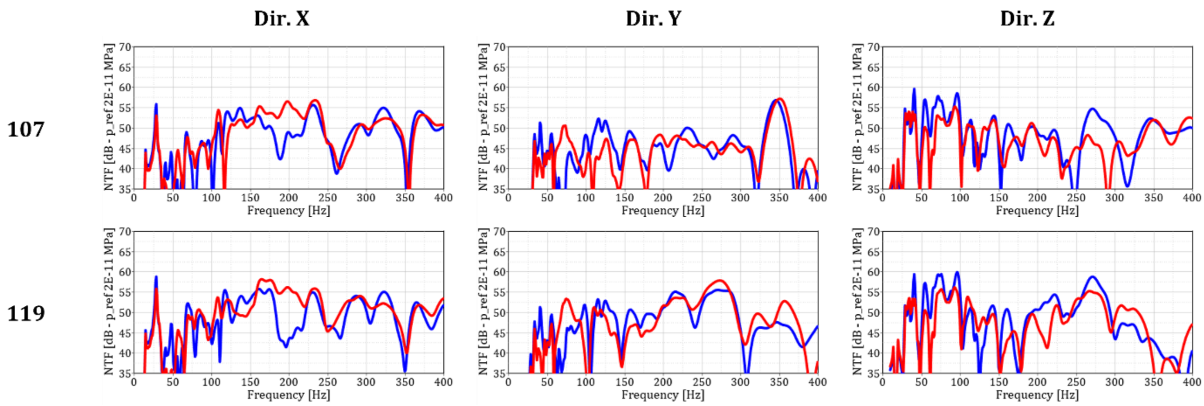

Figure 7.4: Noise Transfer Function of front shock towers

The noise from the front suspension is characterized by similar macroscopic behaviour considering the different directions respectively. The results in x-direction highlight a coherent behaviour of the new TB configuration to the reference model. Two main trends could be observed from these curves. The former ranges from 10 Hz to 100 Hz, in which the new configuration is globally at lower levels of sound pressure than the reference. This behaviour is coherent to the observations extrapolated from the study of the Total ERP of the BiW configuration. The latter is the range between 150 Hz and 250 Hz that shows the opposite trends, but the overall level of the pressure is close to the acoustic target. The behaviour of the acoustic response by loads from y-direction and z-direction is better than the reference model. The highest peaks of the pressure of the reference model are reduced, moving the performance at the target levels. There is no evidence to associate the reduction to a target level to the quantity to the total equivalent radiated power of the BiW configurations. The methodology offers a helpful tool to the designer to orient the design closer to the acoustic targets without considering all the necessary subsystems that characterise the TB dynamics and define the acoustic cavity.

Finally, Figure 7.5 and 7.6 report the Noise Transfer Functions concerning the loads transmitted by the rear shock tower.

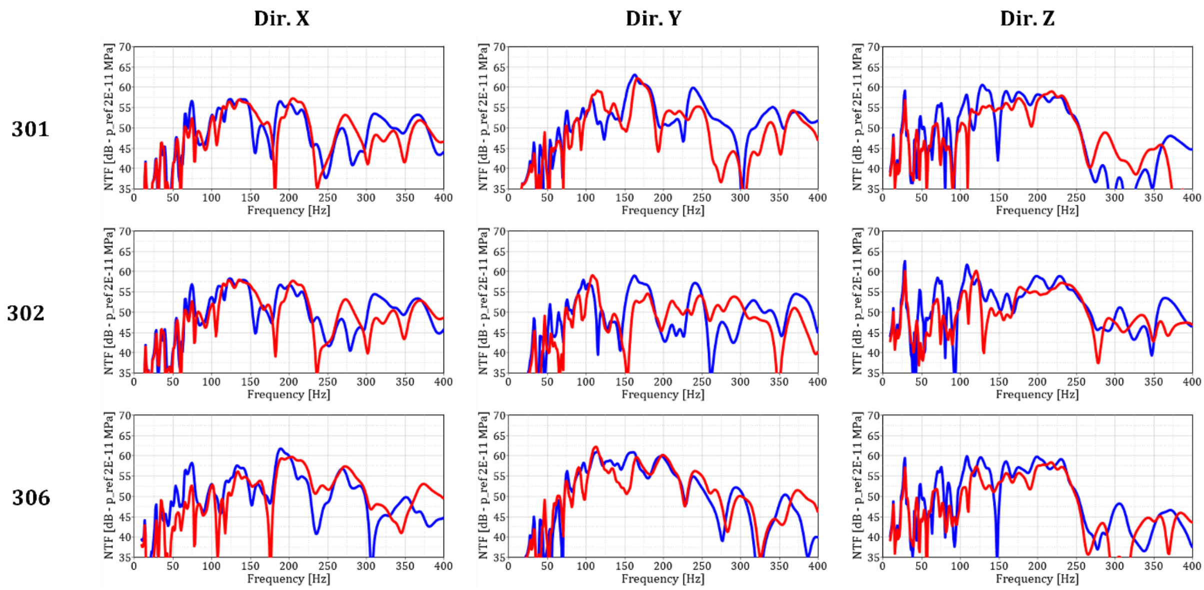

Figure 7.5: Noise Transfer Function of rear shock towers. . The blue curves represent the reference TB model acoustical behaviour. The red curves are referred to the new configuration of the TB model.

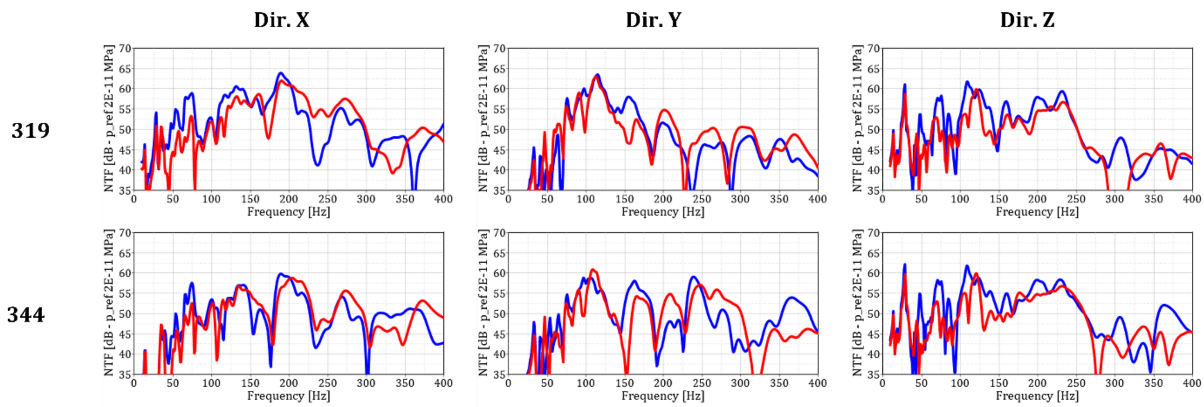

Figure 7.6: Noise Transfer Function of rear shock towers. . The blue curves represent the reference TB model acoustical behaviour. The red curves are referred to the new configuration of the TB model.

The sound pressure levels felt by the driver's ear is globally reduced. All the peaks have been attenuated at the low-frequency range. This result is coherent with the previous observations for the front shock towers. The combined effect of the stiffer windshield frame and the optimised distribution of the damping material have significantly improved the acoustic performance of the TB configuration.

8 – Conclusions and Future Works

This activity research proposes a methodology oriented to defining NVH targets during the design of the BiW configuration. The study has investigated the typical loads' conditions of the virtual and experimental approval of the TB configuration migrating these peculiar analyses in the early development phase of a new vehicle. A new participation factor based on the evaluation of the ERP has been employed to give information to the design of the panels that mainly could influence the peaks of sound pressure levels in the acoustic cavity of the TB configuration. The acoustic frequency response analyses have been performed to evaluate the coherence of the forecasts applied in the BiW configuration. The results have confirmed the effectiveness of the proposed methodology.

Several studies could be developed on the methodology and applications of a broad spectrum of vehicles to define coherent targets of ERP for each panel that surrounds the acoustic cavity.

The methodology proposed could be deeply analysed and strengthened, focusing attention on several open points. First of all, it could be helpful to investigate the simplification in sub-models of the specific panels under investigation. In particular, the influence of the boundary conditions is crucial in evaluating the dynamic stiffness of the system. The fixed boundary condition applied typically on the panel's perimeter could determine misleading information about the actual dynamic behaviour of the panels. This approach could become a real advantage in terms of the efficiency of the design resources when a repeatable and specific system of boundary conditions and external loads is established for each possible scenario. Thus, the results of the optimisation loops defined in the direct approach of the methodology could be more effective in the BiW model. The optimisation loop proposed and tested on the bench could develop also considering the optimisation of the connections of the panels to its frame. This optimisation phase could precede and guide the topography optimisation step. The topology optimisation (TO) could be suitable for extrapolating an optimised distribution of the welding seam along the perimeter of the bench. In recent years, it has been common practice in automotive application models the welding same by solid hexahedral elements connected to the components by a system of 1D elements [108]. An example of this possible future work is presented in the following Figure 8.1.

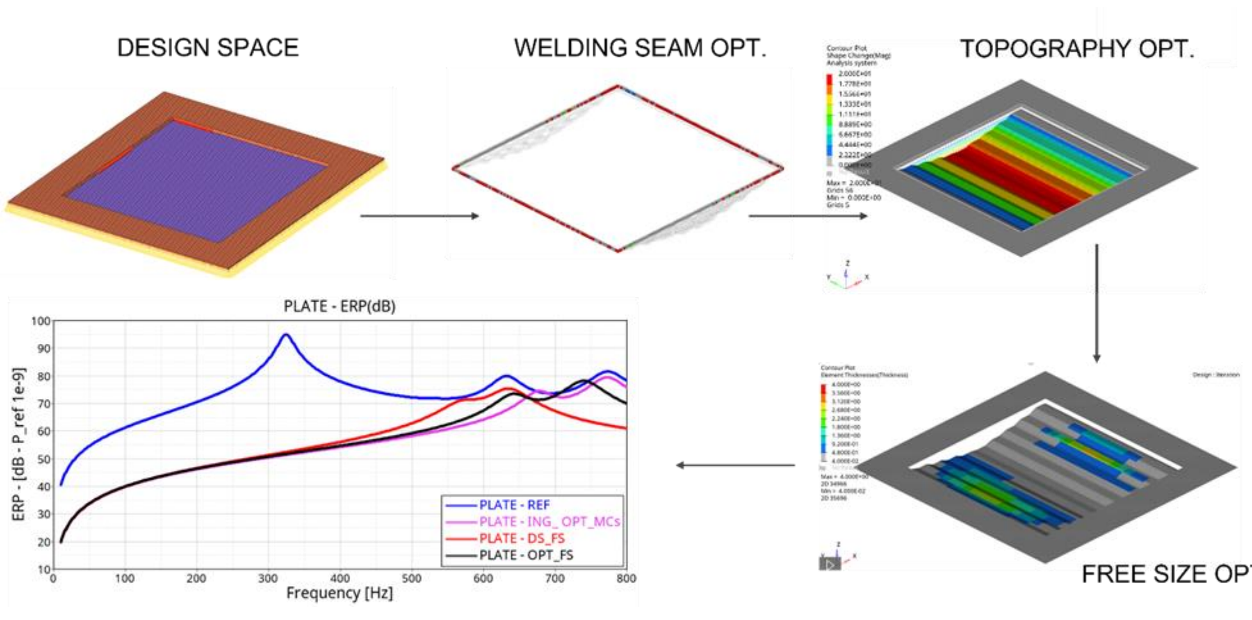

Figure 8.1: Improved optimization loop of a fixed square plate loaded in the CoG in the out-of-plane direction.

Another topic to be investigated more deeply is the application of the GA algorithm used to optimise the cross-section properties of the ribs of the firewall. The algorithm generated is at an "embryonic" state, but the results were satisfying for what concerns the aim of the study. Finally, the optimisation loops presented in this methodology have to be applied to all the influent components to minimise the increase in the weight and save time from the trial-&-error approach.

The applicability of the methodology in practice could be obtained after a large scale of other test-case vehicles. In this way could be possible to define the ERP target for each panels vehicle belonging to the same market segment or performance and guide the designer to achieve the NVH performance easily.

Bibliography

[1] E. Bonisoli, C. Delprete, and C. Rosso, "Comparison between Dynamic Condensation Techniques in Automotive Application".

[2] G. Gomes Carvalho Luis Guilherme Mariano Viana Martins, G. Gomes Carvalho, and L. Guilherme Mariano Viana Martins, "Application of CAE (Computer Aided Engineering) Superelement Technique for NVH (Noise, Vibration and Harshness) attributes on a Trimmed-Body Vehicle Structure in order to assist Supplier commodity development based also on NVH Requirements," 2017.

[3] G. C. Everstine, "Structural analogies for scalar field problems," *International Journal for Numerical Methods in Engineering*, vol. 17, no. 3, pp. 471–476, 1981.

[4] A. Craggs, "THE TRANSIENT RESPONSE OF A COUPLED PLATE-ACOUSTIC SYSTEM USING PLATE AND ACOUSTIC FINITE ELEMENTSt," 1971.

[5] V. Adams and A. Askenazi, "Building Better Products with Finite Element Analysis, 1999." OnWord Press.

[6] R. D. Cook, D. S. Malkus, M. E. Plesha, and R. J. Witt, "Concepts and Applications of Finite Element Analysis, Wiley," 2002.

[7] D. J. Gorman, "Accurate analytical type solutions for the free in-plane vibration of clamped and simply supported rectangular plates," *Journal of Sound and Vibration*, vol. 276, no. 1–2, pp. 311–333, Sep. 2004, doi: 10.1016/j.jsv.2003.07.037.

[8] A. W. Leissat, "THE FREE VIBRATION OF RECTANGULAR PLATES," 1973.

[9] S. Sung, S. Chao, H. Lingala, and L. Mundy, "Structural-acoustic analysis of vehicle body panel participation to interior acoustic boom noise," SAE Technical Paper, 2011.

[10] Z. Li, X. Su, J. Tan, H. Wang, and W. W. Wu, "Multi-objective optimization of the layout of damping material for reducing the structure-borne noise of thin-walled structures," *Thin-Walled Structures*, vol. 140, no. March, pp. 331–341, 2019, doi: 10.1016/j.tws.2019.03.046.

[11] W. L. Li, "Vibration analysis of rectangular plates with general elastic boundary supports," *Journal of Sound and Vibration*, vol. 273, no. 3, pp. 619–635, Jun. 2004, doi: 10.1016/S0022-460X(03)00562-5.

[12] J. H. Kang and A. W. Leissa, "Three-dimensional vibration analysis of thick hyperboloidal shells of revolution," *Journal of Sound and Vibration*, vol. 282, no. 1–2, pp. 277–296, Apr. 2005, doi: 10.1016/j.jsv.2004.02.031.

[13] C. M. Wang and S. Kitipornchai, "Relationship Between Vibration Kirchhoff Polygonal Plates With Simply Supported Edges," 2000. [Online]. Available: http://vibrationacoustics.asmedigitalcollection.asme.org/

[14] Y. Xing and B. Liu, "New exact solutions for free vibrations of rectangular thin plates by symplectic dual method," *Acta Mechanica Sinica/Lixue Xuebao*, vol. 25, no. 2, pp. 265–270, Apr. 2009, doi: 10.1007/s10409-008-0208-4.

[15] A. D. Pierce, *Acoustics: an introduction to its physical principles and applications*. Springer, 2019.

[16] L. Morello, L. R. Rossini, G. Pia, and A. Tonoli, *The Automotive Body: Volume I: Components Design*. Springer, 2011.

[17] L. Morello, L. R. Rossini, G. Pia, and A. Tonoli, *The Automotive Body: Volume II: System Design*. Springer, 2011.

[18] V. Rotondella, “Metodologie NVH per applicazioni automotive: valutazione delle prestazioni vibroacustiche attraverso l’analisi agli elementi finiti,” 2017.

[19] G. Salvina, “Impiego di tecniche multibody per la predizione della radiazione acustica e del comfort interno di veicoli per l’autotrazione,” 2012.

[20] J. Lu, “Noise reduction and sound quality improvement with acoustic windshield,” SAE Technical Paper, 2008.

[21] T. Lenkutis, A. Čerškus, N. Šešok, A. Dzedzickis, and V. Bučinskas, “Road Surface Profile Synthesis: Assessment of Suitability for Simulation,” *Symmetry (Basel)*, vol. 13, no. 1, p. 68, 2020.

[22] J. Feng, X. Zhang, K. Guo, F. Ma, and H. R. Karimi, “A frequency compensation algorithm of four-wheel coherence random road,” *Mathematical Problems in Engineering*, vol. 2013, 2013.

[23] W. Schiehlen, “White noise excitation of road vehicle structures,” *Sadhana*, vol. 31, no. 4, pp. 487–503, 2006.

[24] R. S. Barbosa, “Vehicle dynamic response due to pavement roughness,” *Journal of the Brazilian Society of Mechanical Sciences and Engineering*, vol. 33, no. 3, pp. 302–307, 2011.

[25] C. R. Hua, Y. Zhao, Z. W. Lu, and H. Ouyang, “Random vibration of vehicle with hysteretic nonlinear suspension under road roughness excitation,” *Advances in Mechanical Engineering*, vol. 10, no. 1, p. 1687814017751222, 2018.

[26] C. J. Dodds and J. D. Robson, “The description of road surface roughness,” *J Sound Vib*, vol. 31, no. 2, pp. 175–183, 1973.

[27] S. Donders *et al.*, “A reduced beam and joint concept modeling approach to optimize global vehicle body dynamics,” *Finite Elements in Analysis and Design*, vol. 45, no. 6–7, pp. 439–455, 2009.

[28] E. Yuksel, G. Kamci, and I. Basdogan, “Vibro-acoustic design optimization study to improve the sound pressure level inside the passenger cabin,” *Journal of Vibration and Acoustics*, vol. 134, no. 6, 2012.

[29] S. Marburg, “Developments in structural-acoustic optimization for passive noise control,” *Archives of computational methods in engineering*, vol. 9, no. 4, pp. 291–370, 2002.

[30] L. Splendi, “Finite Element Structural Optimization: Automotive Applications for NVH Purposes,” 2014.

[31] A. Takezawa, M. Daifuku, Y. Nakano, K. Nakagawa, T. Yamamoto, and M. Kitamura, “Topology optimization of damping material for reducing resonance response based on complex dynamic compliance,” *Journal of Sound and Vibration*, vol. 365, pp. 230–243, 2016.

[32] J. M. Dickens, J. M. Nakagawa, and M. J. Wittbrodt, “A critique of mode acceleration and modal truncation augmentation methods for modal response analysis,” *Comput Struct*, vol. 62, no. 6, pp. 985–998, 1997.

[33] T. Rose, “Using residual vectors in MSC/NASTRAN dynamic analysis to improve accuracy,” in *MSC World Users’ Conference*, 1991, pp. 1–18.

[34] J. Dickens and A. Stroeve, “Modal truncation vectors for reduced dynamic substructure models,” in *41st Structures, Structural Dynamics, and Materials Conference and Exhibit*, 2000, p. 1578.

[35] J. M. Dickens and K. v Pool, “Modal truncation vectors and periodic time domain analysis applied to a cyclic symmetry structure,” *Comput Struct*, vol. 45, no. 4, pp. 685–696, 1992.

[36] A. J. Salmonte, “Considerations on the residual contribution in modal analysis,” *Earthquake Engineering & Structural Dynamics*, vol. 10, no. 2, pp. 295–304, 1982.

[37] N. Roy and A. Girard, “Impact of residual modes in structural dynamics,” in *Spacecraft Structures, Materials and Mechanical Testing 2005*, 2005, vol. 581.

[38] J. H. Foxwell and R. E. Franklin, “The Vibrations of a Thin-Walled Stiffened Cylinder in an Acoustic Field,” *Aeronautical Quarterly*, vol. 10, no. 1, pp. 47–64, Feb. 1959, doi: 10.1017/s0001925900001426.

[39] G. B. Warburton, “Vibration of a Cylindrical Shell in an Acoustic Medium,” *Journal of Mechanical Engineering Science*, vol. 3, no. 1, pp. 69–79, 1961, doi: 10.1243/JMES_JOUR_1961_003_011_02.

[40] A. J. Pretlove, “Free vibrations of a rectangular panel backed by a closed rectangular cavity by a closed rectangular cavity,” *Journal of Sound and Vibration*, vol. 2, no. 3, pp. 197–209, 1965, doi: 10.1016/0022-460X(65)90108-2.

[41] G. M. L. Gladwell and G. Zimmermann, “On energy and complementary energy formulations of acoustic and structural vibration problems,” *Journal of Sound and Vibration*, vol. 3, no. 3, pp. 233–241, 1966, doi: 10.1016/0022-460X(66)90092-7.

[42] G. M. L. Gladwell, “A variational formulation of damped acousto structural vibration problems,” *Journal of Sound and Vibration*, vol. 4, no. 2, pp. 172–186, 1966, doi: 10.1016/0022-460X(66)90120-9.

[43] V. Mason, “Rectangular finite elements for analysis of plate vibrations,” *Journal of Sound and Vibration*, vol. 7, no. 3, pp. 437–448, 1968, doi: 10.1016/0022-460X(68)90141-7.

[44] C. Q. Howard and B. S. Cazzolato, *Acoustic analyses using MATLAB and ANSYS*.

[45] G. C. Everstine, “Finite element formulatons of structural acoustics problems,” *Computers & Structures*, vol. 65, no. 3, pp. 307–321, 1997.

[46] N. Atalla and F. Sgard, *Finite element and boundary methods in structural acoustics and vibration*. CRC Press, 2015.

[47] O. C. Zienkiewicz and Y. K. Cheung, “Finite elements in the solution of field problems,” *The Engineer*, vol. 220, no. 5722, pp. 507–510, 1965.

[48] C. Zienkiewicz, “FLUID-STRUCTURE DYNAMIC INTERACTION AND WAVE FORCES. AN INTRODUCTION TO NUMERICAL TREATMENT,” 1978.

[49] Perrone. N, “Component Mode Synthesis (CMS) definition applied to Automotive components for Noise, Vibration and Harshness (NVH) analyses: state of the art and proposal of a new best practice,” 2018.

[50] J. Du, Z. Liu, W. L. Li, X. Zhang, and W. Li, “Free in-plane vibration analysis of rectangular plates with elastically point-supported edges,” *Journal of Vibration and Acoustics, Transactions of the ASME*, vol. 132, no. 3, pp. 0310021–03100211, Jun. 2010, doi: 10.1115/1.4000777.

[51] A. W. Leissa, “The historical bases of the Rayleigh and Ritz methods,” *Journal of Sound and Vibration*, vol. 287, no. 4–5, pp. 961–978, Nov. 2005, doi: 10.1016/j.jsv.2004.12.021.

[52] Y. Xing and B. Liu, “Closed form solutions for free vibrations of rectangular Mindlin plates,” *Acta Mechanica Sinica/Lixue Xuebao*, vol. 25, no. 5, pp. 689–698, Oct. 2009, doi: 10.1007/s10409-009-0253-7.

[53] D. Lennstrom, R. Johnsson, A. Nykanen, and A. Agren, “Determination of Radiated Sound Power from an Electric Rear Axle Drive In-Situ and its Contribution to Interior Noise,” *SAE International Journal of Passenger Cars - Mechanical Systems*, vol. 6, no. 3, pp. 1554–1563, Nov. 2013, doi: 10.4271/2013-01-9120.

[54] D. Fritze, S. Marburg, and H. J. Hardtke, “Estimation of radiated sound power: A case study on common approximation methods,” *Acta Acustica united with Acustica*, vol. 95, no. 5, pp. 833–842, Sep. 2009, doi: 10.3813/AAA.918214.

[55] M. Luegmair, “Advanced Equivalent Radiated Power (ERP) Calculation for Early Vibro-acoustic Product Optimization.” [Online]. Available: https://www.researchgate.net/publication/315799640

[56] M. Klaerner, S. Marburg, and ; Lothar Kroll, “FE based measures for structure borne sound radiation.”

[57] C. Y. Wang and C. M. Wang, “Exact Solutions for Strings, Membranes, Beams, and Plates STRUCTURAL VIBRATION,” 2014.

[58] F. Fahy and P. Gardonio, “Sound and Structural Vibration Radiation, Transmission and Response,” 2007.

[59] M. Pirnat, G. Čepon, and M. Boltežar, “Structural-acoustic model of a rectangular plate-cavity system with an attached distributed mass and internal sound source: Theory and experiment,” *Journal of Sound and Vibration*, vol. 333, no. 7, pp. 2003–2018, Mar. 2014, doi: 10.1016/j.jsv.2013.11.044.

[60] D. Kong, G. Wang, W. Li, and J. Ni, “Sound radiation from the plate backed by the rectangular cavity,” *International Journal of Mechanical Sciences*, vol. 191, Feb. 2021, doi: 10.1016/j.ijmecsci.2020.106072.

[61] X. Qin, Y. Wang, C. Lu, S. Huang, H. Zheng, and C. Shen, “Structural acoustics analysis and optimization of an enclosed box-damped structure based on response surface methodology,” *Materials and Design*, vol. 103, pp. 236–243, Aug. 2016, doi: 10.1016/j.matdes.2016.04.063.

[62] J. Park and P. Gu, “A new experimental methodology to estimate chassis force transmissibility and applications to road NVH improvement,” *SAE transactions*, pp. 2238–2249, 2003.

[63] R. Rengarajan, S. Noll, and R. Singh, “Explanation for Variability in Lower Frequency Structure-Borne Noise and Vibration: Roles of Rear Subframe Dynamics and Right-Left Spindle Phasing,” *SAE International Journal of Vehicle Dynamics, Stability, and NVH*, vol. 2, no. 1, 2018.

[64] M. Klaerner, S. Marburg, and L. Kroll, “FE based measures for structure borne sound radiation,” in *INTER-NOISE and NOISE-CON Congress and Conference Proceedings*, 2014, vol. 249, no. 6, pp. 1563–1569.

[65] A. Kulshreshtha, S. Yadav, B. N. Singh, and V. Ranjan, “Sound radiation of simply supported rectangular plate using finite element method,” *Vibroengineering Procedia*, vol. 29, pp. 195–200, 2019.

[66] Y. Wang, C. Lu, X. Qin, S. Huang, G. Fu, and X. Ni, “Analysis and control of structure-borne noise for a trimmed body by using panel acoustic participation method,” *Thin-Walled Structures*, vol. 119, pp. 828–838, 2017.

[67] X. Han, Y.-J. Guo, H.-D. Yu, and P. Zhu, “Interior sound field refinement of a passenger car using modified panel acoustic contribution analysis,” *International Journal of Automotive Technology*, vol. 10, no. 1, pp. 79–85, 2009.

[68] T. C. Lim, “Automotive panel noise contribution modeling based on finite element and measured structural-acoustic spectra,” *Applied acoustics*, vol. 60, no. 4, pp. 505–519, 2000.

[69] Y. Yu, G. Zhao, and B. Wang, “Midfrequency structural/acoustic optimization with a complex variable sensitivity analysis method,” *AIAA Journal*, vol. 57, no. 12, pp. 5447–5461, 2019, doi: 10.2514/1.J058235.

[70] T. C. Lim, “Automotive panel noise contribution modeling based on ®nite element and measured structural-acoustic spectra.” [Online]. Available: www.elsevier.com/locate/apacoust

[71] M. A. Panza, “A review of experimental techniques for NVH analysis on a commercial vehicle,” *Energy Procedia*, vol. 82, pp. 1017–1023, 2015.

[72] T. Shin, Y. S. Kim, K. An, and S. K. Lee, “Transfer path analysis of rumbling noise in a passenger car based on in-situ blocked force measurement,” *Applied Acoustics*, vol. 149, pp. 1–14, Jun. 2019, doi: 10.1016/j.apacoust.2019.01.015.

[73] D. Lennström, M. Olsson, F. Wullens, and A. Nykänen, “Validation of the blocked force method for various boundary conditions for automotive source characterization,” *Applied Acoustics*, vol. 102, pp. 108–119, Jan. 2016, doi: 10.1016/j.apacoust.2015.08.019.

[74] C. Pezerat and F. Chevillotte, “Identification of Blocked Forces and Moments of an Oil Pump Fixed on a Test Bench by Using an Inverse Vibration Technique,” in *SAE Technical Papers*, Jun. 2018, vol. 2018-June, no. June. doi: 10.4271/2018-01-1502.

[75] M. v van der Seijs, J. M. Harvie, and D. P. Song, “Road Noise NVH: Embedding Suspension Test Benches in NVH Design using Virtual Points and the TPA Framework,” 2021.

[76] D. de Klerk and D. J. Rixen, “Component transfer path analysis method with compensation for test bench dynamics,” *Mechanical Systems and Signal Processing*, vol. 24, no. 6, pp. 1693–1710, 2010, doi: 10.1016/j.ymssp.2010.01.006.

[77] B. S. Kim, G. J. Kim, and T. K. Lee, “The identification of tyre induced vehicle interior noise,” *Applied Acoustics*, vol. 68, no. 1, pp. 134–156, Jan. 2007, doi: 10.1016/j.apacoust.2006.05.020.

[78] W. Kropp, P. Sabiniarz, H. Brick, and T. Beckenbauer, “On the sound radiation of a rolling tyre,” *Journal of Sound and Vibration*, vol. 331, no. 8, pp. 1789–1805, Apr. 2012, doi: 10.1016/j.jsv.2011.11.031.

[79] M. Bennur, “Vehicle Mid-Frequency Response Using the Superelement Component Dynamic Synthesis Technique,” in *SAE Technical Papers*, Apr. 2015, vol. 2015-April, no. April. doi: 10.4271/2015-01-1320.

[80] J. T. Young, “ON THE CRAIG-BAMPTON METHOD AN INTRODUCTION TO BOUNDARY NODE FUNCTIONS, BASE SHAKE ANALYSES, LOAD TRANSFORMATION MATRICES, MODAL SYNTHESIS AND MUCH MORE,” 2000.

[81] R. CRAIG, JR., “On the use of attachment modes in substructure coupling for dynamic analysis,” Mar. 1977. doi: 10.2514/6.1977-405.

[82] H. van der Auweraer, P. Mas, S. Dom, A. Vecchio, K. Janssens, and P. van de Ponseele, “Transfer path analysis in the critical path of vehicle refinement: the role of fast, hybrid and operational path analysis,” 2007.

[83] M. Kiani, H. Shiozaki, and K. Motoyama, “Simulation-based design optimisation to develop a lightweight body-in-white structure focusing on dynamic and static stiffness,” *International Journal of Vehicle Design*, vol. 67, no. 3, pp. 219–236, 2015.

[84] M. Kiani and A. R. Yildiz, “A comparative study of non-traditional methods for vehicle crashworthiness and NVH optimization,” *Archives of Computational Methods in Engineering*, vol. 23, no. 4, pp. 723–734, 2016.

[85] M. Abbasi, M. Fard, and A. Khalkhali, “Dynamic Stiffness Investigation of an Automotive Body-in-White by Utilizing Response Surface Methodology,” RMIT University, 2018.

[86] D. Wang and K. Cai, "Optimizing the static–dynamic performance of the body-in-white using a modified non-dominated sorting genetic algorithm coupled with grey relational analysis," *Engineering Optimization*, vol. 50, no. 4, pp. 615–633, 2018.

[87] M. Luegmair and H. Münch, "Verbesserte Equivalent Radiated Power (ERP)-Berechnung."

[88] J. Lu, "Lightweight Acoustic-Grade PVB Windshield to Reduce Vehicle Interior Noise," in *SAE 2009 Noise and Vibration Conference and Exhibition*, 2009, no. 2009-01–2138.

[89] J. Lu, "Noise reduction and sound quality improvement with acoustic windshield," SAE Technical Paper, 2008.

[90] K. Vasudeva, M. Philip, and O. Reis, "Method Development and Analysis of Tensile Stresses in Windscreens A Study on the dynamic stresses on windscreens subjected to random vibrations," 2018.

[91] B. T. Chandru and P. M. Suresh, "Finite element and experimental modal analysis of car roof with and without damper," *Materials Today: Proceedings*, vol. 4, no. 10, pp. 11237–11244, 2017.

[92] A. Vettorello and G. A. Campo, "Material model development of sandwich composite: Numerical-experimental investigation of head dummy impacting at vehicle interior components," in *Key Engineering Materials*, 2020, vol. 827 KEM, pp. 55–60. doi: 10.4028/www.scientific.net/KEM.827.55.

[93] R. Scigliano, M. Scionti, and P. Lardeur, "Verification, validation and variability for the vibration study of a car windscreen modeled by finite elements," *Finite Elements in Analysis and Design*, vol. 47, no. 1, pp. 17–29, 2011.

[94] L. Hinke, L. Pichler, H. J. Pradlwarter, B. R. Mace, and T. P. Waters, "Modelling of spatial variations in vibration analysis with application to an automotive windshield," *Finite Elements in Analysis and Design*, vol. 47, no. 1, pp. 55–62, 2011.

[95] Z. M. Hafizi, A. M. Aizzuddin, N. I. A. Halim, and M. F. Jamaludin, "Modal properties investigation of car body-in-white with attached windscreen and rear screen," in *IOP Conference Series: Materials Science and Engineering*, 2017, vol. 257, no. 1, p. 012038.

[96] J. Lu, J. Pyper, R. Weber, and J. Fisk, "Windshields with new PVB interlayer for vehicle interior noise reduction and sound quality improvement," *SAE transactions*, pp. 1909–1919, 2003.

[97] M. Cavazzuti, A. Baldini, E. Bertocchi, D. Costi, E. Torricelli, and P. Moruzzi, "High performance automotive chassis design: A topology optimization based approach," *Structural and Multidisciplinary Optimization*, vol. 44, no. 1, pp. 45–56, Jul. 2011, doi: 10.1007/s00158-010-0578-7.

[98] M. Cavazzuti, *Optimization methods: From theory to design scientific and technological aspects in mechanics*. Springer Berlin Heidelberg, 2013. doi: 10.1007/978-3-642-31187-1.

[99] F. R. Du and Z. Tao, "Study on lightweight of the engine piston based on topology optimization," in *Advanced Materials Research*, 2011, vol. 201–203, pp. 1308–1311. doi: 10.4028/www.scientific.net/AMR.201-203.1308.

[100] S. G. Barbieri, M. Giacopini, V. Mangeruga, and S. Mantovani, "A Design Strategy Based on Topology Optimization Techniques for an Additive Manufactured High Performance Engine Piston," *Procedia Manufacturing*, vol. 11, pp. 641–649, 2017, doi: 10.1016/j.promfg.2017.07.162.

[101] S. Mantovani, G. A. Campo, and M. Giacalone, "Steering column support topology optimization including lattice structure for metal additive manufacturing," *Proceedings of the Institution of*

Mechanical Engineers, Part C: Journal of Mechanical Engineering Science, 2020, doi: 10.1177/0954406220947121.

[102] G. A. Campo, A. Vettorello, and M. Giacalone, "Optimization methodology for continuous heterogeneous structures: A preliminary design of an engine mounting bracket," in *Key Engineering Materials*, 2020, vol. 827 KEM, pp. 116–121. doi: 10.4028/www.scientific.net/KEM.827.116.

[103] M. Abdi, I. Ashcroft, and R. D. Wildman, "Design optimisation for an additively manufactured automotive component," 2018. [Online]. Available: http://creativecommons.org/licenses/by/4.0/

[104] G. Allaire and G. Michailidis, "Modal basis approaches in shape and topology optimization of frequency response problems," *International Journal for Numerical Methods in Engineering*, vol. 113, no. 8, pp. 1258–1299, 2018.

[105] R. Picelli, W. M. Vicente, R. Pavanello, and Y. M. Xie, "Evolutionary topology optimization for natural frequency maximization problems considering acoustic–structure interaction," *Finite Elements in Analysis and Design*, vol. 106, pp. 56–64, 2015.

[106] A. Guellec, M. Cabrol, J. Jacqmot, and B. van den Nieuwenhof, "Optimization of trim component and reduction of the road noise transmission based on finite element methods," 2018.

[107] A. L. Loureiro, L. F. M. da Silva, C. Sato, and M. A. V. Figueiredo, "Comparison of the mechanical behaviour between stiff and flexible adhesive joints for the automotive industry," *Journal of Adhesion*, vol. 86, no. 7, pp. 765–787, Jul. 2010, doi: 10.1080/00218464.2010.482440.

[108] V. Rotondella, A. Merulla, A. Baldini, and S. Mantovani, "Dynamic modal correlation of an automotive rear subframe, with particular reference to the modelling of welded joints," *Advances in Acoustics and Vibration*, vol. 2017, pp. 1–10, 2017, doi: 10.1155/2017/8572674.

Appendix – A.1

In this section is reported the Matlab ® for the evaluation of the ERP of a simply supported plate.

The first script concerns the analytical analysis, and the second one the post-processing based on the FE results of the velocity in the $\hat{z}$-direction of the plate grids.

```
% ----------------------------------------------------%
%     Input section                                   %
% ----------------------------------------------------%

% Element centroid grid definition
length_x =1000;
length_y =500;
height_z= 1;
el_size=10;
n_x= length_x/el_size;
n_y= length_y/el_size;
n_elements=n_x*n_y;
el_IDs=zeros(n_x*n_y,4);
k=1;
for j = 1:n_x
   for i = 1:n_y
      el_IDs(k,1)=k;
      el_IDs(k,2)=j*el_size-el_size/2;
      el_IDs(k,3)=i*el_size-el_size/2;
      el_IDs(k,4)=height_z;
      k=k+1;
   end
end
% mechanical properties of the plate

E = 71000;  % [MPa]
rho = 2.71e-9;   %  [ton/mm^3]
nu = 0.33;
h = 1;  % plate thickness [mm]
% --------------------------------------------------------------------- %
% simply-supported plate natural frequencies computation  %
% --------------------------------------------------------------------- %

D = E*h^3/(12*(1-nu^2));
n_max = 20;
dim_modal_base = (n_max)^2;
%
mode_index=[];
for i=1:n_max
   for j = 1:n_max
      mode_index = [ mode_index ; i j ];
   end
end
%
```

```matlab
freq_n =  1./(2.*pi).*sqrt(D/rho/h).*((mode_index(:,1).*pi./length_x).^2
+(mode_index(:,2).*pi./length_y).^2);
n_modes = 350;


% natural frequencies sorting
temp=sortrows([freq_n mode_index],1);
freq_n = temp(:,1);
mode_index = temp(:,2:3);

% use only the first n_modes
plate_n_freq = freq_n(1:n_modes);
plate_mode_index = mode_index(1:n_modes,:);

% modal mass computation
delta_m = rho*h*length_x*length_y/4*ones(1,n_modes);

% ---------------------------------------------------------------------- %
% frequency response analysis computation with unit load
% ---------------------------------------------------------------------- %

F0 = 1; % force amplitude [N]
x_F0 = 500;
y_F0 = 250;
FREQi = [1:1:400];

% Calculating the external load vector in terms of modal participation
F_m =
F0.*sin(plate_mode_index(:,1).*pi.*x_F0./length_x).*sin(plate_mode_index(:,2).*pi.*y_F0./length_y);
% mode shapes computation
z_disp_mode = zeros(n_modes,size(el_IDs,1));
for g = 1:n_modes
   for p = 1:n_x*n_y
      z_disp_mode(g,p) = z_disp_mode(g,p) +
sin(plate_mode_index(g,1)*pi*el_IDs(p,2)/length_x).*sin(plate_mode_index(g,2)*pi*el_IDs(p,3)/length
_y);
   end
end
%
%
%
omega = zeros(1,size(FREQi,2));
for t=1:length(FREQi)
   omega(:,t) = 2*pi*FREQi(t);
   A = diag((plate_n_freq.*2*pi).^2.*delta_m.')-diag(delta_m.')*(omega(:,t)^2);
   PFMODE(:,t) = inv(A)*F_m;
end
struct_q=PFMODE(1:n_modes,:);
z_disp = (z_disp_mode.'*struct_q).';


% k_dyn
k_dyn_modes = zeros(n_modes,1);
for g = 1:n_modes
   k_dyn_modes(g,:) = k_dyn_modes(g,:) +
sin(plate_mode_index(g,1)*pi*500/length_x).*sin(plate_mode_index(g,2)*pi*250/length_y);
```

```
end
k_dyn = (k_dyn_modes.'*struct_q).';

% velocity of loaded node
vel_load_grid = zeros(size(FREQi,2,1));
for s = 1:size(FREQi,2)
   vel_load_grid(s,1) =vel_load_grid(s,1) + omega(:,s)*k_dyn(s,1);
end

% ------------------------------------------------------------------------ %
%          ERP computation
% ------------------------------------------------------------------------ %

rho_f = 1.2e-12;  % fluid density [ton/mm^3]
B = 0.13872;     % Bulk Modulus [MPa]
c0 = sqrt(B/rho_f); % speed of sound in air [mm/s]
quad_vel_ave =zeros(1,size(FREQi,2));
A = (z_disp).^2;
for k = 1:size(FREQi,2)
   quad_vel_ave(1,k)= quad_vel_ave(1,k)+ length_x*length_y*omega(1,k)^2*sum(A(k,:));
end
%
ERP=zeros(1,size(FREQi,2));
for t = 1:size(FREQi,2)
   ERP(1,t) = 0.5*rho_f*c0*quad_vel_ave(1,t);
end
%
ERP_REFdB = 1e-10;                   %reference power [Nmm/s]
ERP_dB =10*log10(ERP/ERP_REFdB).';       % [dB]
```

```
% ------------------------------------------------------------------------ %
% Comparison with FE analysis resuts
% ------------------------------------------------------------------------ %


% number of subcases in each file PCH
nodes_num=4851;
% FREQi (FREQ1) Data
F1=0;
DF=1;
NDF=400;
nodi = nan(1,1);
j=0; % subcase index

% ------------------------------------------------------------------------ %
%          PCH file reading
% ------------------------------------------------------------------------ %


%          Importing mesh data

% Mesh data have been exported in a text file A
txt = textscan(fopen(A),'%s','delimiter','\n');
```

```
% A has two sections, named NODES and ELEMENTS.
% Find the starting and ending points of each sections

nstart = 2 ;
nend = find(strcmp(txt{1}, 'END NODES'), 1, 'first') - 1;
estart = nend + 3;
eend = find(strcmp(txt{1}, 'END'), 1, 'last') - 1;

% Detecting the import options to read the text as a table

opts = detectImportOptions(A);
opts.DataLines = [1,Inf];
opts.VariableOptions(1,5) = opts.VariableOptions(1,4);
tbl = readtable(A,opts);

fclose('all');

%exporting nodal coordinates and connectivity matrices
coord = tbl {nstart:nend,2:4};
conn  = tbl {estart:eend,2:5};

% Results importing initialization

% results of the FE simulation are stored in the following file:
char_file='piastra_disp_new.pch'

% number of subcases in each file PCH
nodes_num=5151;
% FREQi (FREQ1) Data
F1=0;
DF=1;
NDF=400;
nodi = nan(1,1);
j=0; % subcase index

%         PCH file reading

fid=fopen(char_file);
line=fgetl(fid);
while ~feof(fid);
 line=fgetl(fid);
 if strfind(line,"$FREQUENCY");
  j=j+1
  disp(line);
  nodi(j)=str2num(line(13:28));
  line=fgetl(fid);
  for k = 1:nodes_num
      disp_x(k,j) = str2num(line(25:37));
      disp_y(k,j) = str2num(line(43:55));
      disp_z(k,j) = str2num(line(59:72));
      fgetl(fid);
      fgetl(fid);
      fgetl(fid);
      line=fgetl(fid);
```

```
  end
 end
end


% ------------------------------------------------------------------------ %
% Normal velocity computation
% ------------------------------------------------------------------------ %

% How the computation works:

%  nodal velocities from PCh file          -->
% -->    deformations                      -->
% -->    normal to each element            -->
% -->    normal to each node               -->
% -->    velocity normal to each node      -->
% -->    ERP


FREQi = [1:1:400];
% initializing the displacement cell array
disp = cell(1,length(FREQi));
for k = 1:length(FREQi)
   disp{1,k}{:,:} = zeros(size(coord));
end
def = disp;
% defining the displacements in disp
for k = 1:length(FREQi)
   disp{1,k}{:,:} = [disp_x(:,k),disp_y(:,k),disp_z(:,k)];
end
% defining the strain cell array
coord(:,3)=0;
for n = 1:length(FREQi)
   def{1,n}{:,:} = [disp_x(:,n)+coord(:,1),disp_y(:,n)+coord(:,2),disp_z(:,n)+coord(:,3)];
end
%  element normal cell array initialization
el_norm = disp;
mean_norm = disp;
norma = disp;
% element normal definition
for k = 1:length(FREQi)
   for i = 1:size(conn,1)
% node 2 - node 1
      a_1 = def{1,k}{1,1}(conn(i,2),:)- def{1,k}{1,1}(conn(i,1),:);
% node 4 - node 1
      a_2 = def{1,k}{1,1}(conn(i,4),:)- def{1,k}{1,1}(conn(i,1),:);
% node 2 - node 3
      b_3 = def{1,k}{1,1}(conn(i,2),:)- def{1,k}{1,1}(conn(i,3),:);
% node 4 - node 3
      b_4 = def{1,k}{1,1}(conn(i,4),:)- def{1,k}{1,1}(conn(i,3),:);
% averaging the normals to the planes defined by the two semi-elements
      mean_norm{1,k}{1,1}(i,:) = 0.5*(cross(a_2 , a_1) + cross(b_3 , b_4));
% normalizing the normal vectors
      norma{1,k}{1,1}(i,1) = sqrt(sum(mean_norm{1,k}{1,1}(i,:).^2));
```

```matlab
        el_norm{1,k}{1,1}(i,:)=mean_norm{1,k}{1,1}(i,:)./norma{1,k}{1,1}(i,1);
    end
end

grid_norm = cell(1,length(FREQi));
% The normal vector associated to each node is defined as the average
% of the normals to the elements adjacent to that node.
for f = 1:length(FREQi)
    for g = 1:size(coord,1)
        [row_conn, column_conn] = find(conn == g);
        grid_norm{1,f}{1,1}(g,:) = mean(el_norm{1,f}{1,1}(row_conn,:));
    end
end
% nodal velocity cell array initialization
velocity = cell(1,length(FREQi));
omega = (2*pi*FREQi).';
for k = 1:length(FREQi)
    velocity{1,k}{:,:} = [omega(k,1)*disp_x(:,k),omega(k,1)*disp_y(:,k),omega(k,1)*disp_z(:,k)];
end
% dot product between the overall nodal velocity and the normal relative to
% that node
vel_norm = zeros(size(disp_x));
for k = 1:length(FREQi)
    for   n = 1:size(coord,1)
        vel_norm(n,k) = dot(velocity{1,k}{1,1}(n,:),grid_norm{1,k}{1,1}(n,:));
    end
end
% ERP computation
FREQi = [1:1:400];
length_x = 1000;
length_y = 500;
rho_f = 1.2e-12;                % fluid density [ton/mm^3]
B = 0.13872;                    % Bulk Modulus [MPa]
c0 = sqrt(B/rho_f);             % speed of sound through air [mm/s]
quad_vel_ave =zeros(1,size(FREQi,2));
el_size = 10;                   % mesh size
delta_area = zeros(size(coord,1),1);
    for g = 1:size(coord,1)
        [row_conn, column_conn] = find(conn == g);
        delta_area(g,1) = 0.25*el_size^2*(size(row_conn,1));
    end
A = delta_area.*(vel_norm).^2;
    for k = 1:size(FREQi,2)
        quad_vel_ave(1,k)= quad_vel_ave(1,k)+sum(A(:,k));
    end
%
ERP=zeros(1,size(FREQi,2));
for t = 1:size(FREQi,2)
    ERP(1,t) = 0.5*rho_f*c0*quad_vel_ave(1,t);
end
%
ERP_REFdB = 1e-9;               %Reference power [Nmm/s]
ERP_dB =10*log10(ERP/ERP_REFdB).';      % [dB]
```

Appendix A.2

In this section is reported the Matlab ® used for the structural optimisation of the rear firewall.

```
clear
clc

%Parameter number
n_param=5;

%Parameter space domain
%Matrix that summaries the parameters domain: dimINTERVALS=n_param X 2

INTERVALS=[ 5,20;     % Variation interval of the first parameter
   45,60;             %                       ...
   15,30;             %                       ...
   10,30;             %                       ...
   7,70];             % Variation interval of the last parameter


%Definition of the exponents which are equal to the discretization level of each interval 2^exp
EXP=[1,3,2,3,3];

%Input parameter matrix
INPUT=zeros(n_param,2^max(EXP));
for i=1:n_param
   lb=INTERVALS(i,1);
   ub=INTERVALS(i,2);
   aus=lb:(ub-lb)/(2^EXP(i)-1):ub;
   size_aus=length(aus);

   for j=1:size_aus
      INPUT(i,j)=aus(j);
   end

end


%Number of simulations for each generation, that is the number of the “individuals” generated for
%each generation.
sim_for_gen=6;

%Number of generation
num_gen=4;


%Inizialization of the first generation
for i=1:sim_for_gen

   P_genotype(i,:)=rand(1,sum(EXP));
```

```
  for j=1:sum(EXP)
    if P_genotype(i,j)<0.5
      P_genotype(i,j)=0;
    else
      P_genotype(i,j)=1;
    end
  end

%Cycle to exclude the repetitions
  while sum(ismember(P_genotype,P_genotype(i,:),'row'))>1
    P_genotype(i,:)=mutation(P_genotype(i,:));
  end

end


%Translation phase: Genotype to Phenotype
for i=1:sim_for_gen

  for j=1:n_param
    comp_unit_allele_j=0;
    bin_vect_j=[];

    for gg=1:j
      comp_unit_allele_j= comp_unit_allele_j +EXP(gg);
    end

    esp=EXP(j);
    for y=1:exp
      bin_vect_j(y)=P_genotype(i,comp_unit_allele_j-exp+y);
    end

    ind_in=bin2dec(num2str(bin_vect_j))+1;
    P_phenotype(i,j)=INPUT(j,ind_in);

  end
end


%Simulation number

sim=0;                  %Simulation number index
gen_jump=0;

for g=1:num_gen         %Main cycle for the selection of the best individuals for the next generation

  for f=1:sim_for_gen   %Fitness function evaluation of the g-th generation

    sim=sim+1;          %Simulation number


      a=P_phenotype(f,:);
```

```
%Fitness Evaluation

    % Input File: FE model ( *.fem)
    femREAD=fopen('topog_rear_firwall.fem');
    name=['TOPOGRAPHY_N' num2str(sim)];            %new folder name
    mkdir(name)                                    %create new folder
    %
    cd (sprintf('TOPOGRAPHY_N%i', sim))            %change directory
    %                                              %New FE model (balnk file *.fem)
    femWRITE=fopen(sprintf('TOPOGRAPHY_N%i.fem', sim), 'w'); %'w' (= writing)
    count_line = 1;
    while ~feof(femREAD)
      riga=fgetl(femREAD);
      fprintf(femWRITE, [riga, ' \n']);
      count_line = count_line + 1;
      if length(strfind(riga,'DTPG'))~=0
        fprintf(femWRITE,'+       %i.0', a(1));
        fprintf(femWRITE,'     %i.0    YES     ', a(2));
        fprintf(femWRITE,'%i.0    NORM                SPC\n', a(3));
        count_line = count_line +1;
        riga=fgetl(femREAD);
        %copy the final part
        while ~feof(femREAD)
          riga=fgetl(femREAD);
          fprintf(femWRITE, [riga, ' \n']);
          count_line =count_line + 1;
        end
      end
    end
    % Run the FE topography optimisation in a specific directory
    fclose(femREAD);
    op_path=sprintf('"C:/Program Files/Altair/2021/hwsolvers/scripts/optistruct.bat"
TOPOGRAPHY_N%i.fem', sim);
    system(char(op_path));

    % Post-Processing section: find the key-information from the output file of the FEA, in particular:
               % identification number of the simulation
               % feasible (=1) / unfeasible design (=0)
               % average ERP of the last iteration.
    OUTPUT_OPT(f,1) = f;
    outREAD=fopen(sprintf('TOPOGRAPHY_N%i.out',sim));
    iter = 1;
    while ~feof(outREAD)
      out_line=fgetl(outREAD);
      if length(strfind(out_line,'Objective Function (Minimize FRERP) =  '))~=0
        disp(out_line)
        ERPmedio_iter(iter,1) = str2num(out_line(40:50));
        out_line=fgetl(outREAD);
        OUTPUT_OPT(f,2)= ERPmedio_iter(iter,1);
        iter = iter+1;
      elseif length(strfind(out_line,'Solver FAILED'))~=0
        OUTPUT_OPT(f,2)=1000;                   %Penalty factor for unfeasible solutions
      end

      if  length(strfind(out_line,' FEASIBLE DESIGN'))~=0
```

```
        OUTPUT_OPT(f,3) = 1;

      end
    end
    fclose(outREAD);

    cd ..

    %fitness: f-th individual belonging to the g-th generation
    fit(f,1)=f;
    if OUTPUT_OPT(f,3)==1
      fit(f,2)=0.5*OUTPUT_OPT(f,2);   %Penalty factor of fitness function for feasible design
    else
      fit(f,2)=2.0*OUTPUT_OPT(f,2);   % Penalty factor of fitness function for unfeasible design
    end


    %Place the fitness values in a hystory vector
    fit_rec(sim,1)=sim;
    fit_rec(sim,2)=OUTPUT_OPT(f,2);             %place ERP value
    fit_rec(sim,3)=OUTPUT_OPT(f,3);             %F/NF design
    fit_rec(sim,4)=fit(f,2);                    %Fitness value

    sequence_var (sim,:) =P_phenotype(f,:);
    sequence_individuals(sim,:) =P_genotype(f,:);
  end

  if g < num_gen %If the actual generation is not the last -> initialization of the new generation

    %The fitness function is used to extrapolate the best individuals (minimum values of the fitness)
    [~,x1]=sort(fit(:,2));

    %Index of the two best individuals
    par1_indx=x1(1);
    par2_indx=x1(2);

    % The two best individuals become the two parents of the new generation
    par1=P_genotype(par1_indx,:);
    par2=P_genotype(par2_indx,:);

    %Storing of the best individual of g-th generation and its fitness value
    BEST(g,:)=par1;
    best_fit(g)=fit(par1_indx,2);

    if g>1                         %Condition valid only from the 2nd generation
      if best_fit(g-1)<best_fit(g)   %This condition consider the scenario in which the best
                                     %individual of the (g-1)-th generation has a lower fitness value
                                     %than the best one of the g-th generation.
        gen_jump = gen_jump +1;
        best_fit(g)=best_fit(g-1);
        BEST(g,:)=BEST(g-1,:);
        par2=par1;                   %The best individual of the g-th generation become the second
                                     %parent of the actual generation.
        par1=BEST(g,:);              %The best one of the (g-1)-th generation is the first parent of
                                     %the actual generation
```

```
    end
  end

  %Evaluation of the new generation
  for c=1:sim_for_gen

    if c==1

      P_genotype(c,:)=mutation(par1);       %The first individual of the new generation is a
                                            %mutation of the first parent.

      %No repetition condition
      while sum(ismember(sequence_individuals,P_genotype(c,:),'row'))>0 ||
sum(ismember(P_genotype,P_genotype(c,:),'row'))>1
        P_genotype(c,:)=mutation(P_genotype(c,:));
      end



    elseif c==2
      P_genotype(c,:)=mutation(par2);       %The second individual of the new generation is a
                                            %mutation of the second parent.
      %No repetition condition
      while sum(ismember(sequence_individuals,P_genotype(c,:),'row'))>0 ||
sum(ismember(P_genotype,P_genotype(c,:),'row'))>1
        P_genotype(c,:)=mutation(P_genotype(c,:));
      end


    else

      if floor(c/2)*2~=c %if "c" è odd
        [child1,child2]=crossover(par1,par2);
        P_genotype(c,:)=child1;
      %No repetition condition
        while sum(ismember(sequence_individuals,P_genotype(c,:),'row'))>0 ||
sum(ismember(P_genotype,P_genotype(c,:),'row'))>1
          P_genotype(c,:)=mutation(P_genotype(c,:));
        end
      else
        P_genotype(c,:)=child2;
       %No repetition condition
        while sum(ismember(sequence_individuals,P_genotype(c,:),'row'))>0 ||
sum(ismember(P_genotype,P_genotype(c,:),'row'))>1
          P_genotype(c,:)=mutation(P_genotype(c,:));
        end
      end

    end

  end
```

```
%Translation phase: Genotype to Phenotype
    for i=1:sim_for_gen

      for j=1:n_param
        comp_unit_allele_j=0;
        bin_vect_j=[];

        for gg=1:j
          comp_unit_allele_j= comp_unit_allele_j +EXP(gg);
        end

        esp=EXP(j);

        for y=1:exp
          bin_vect_j(y)=P_genotype(i,comp_unit_allele_j-exp+y);
        end

        ind_in=bin2dec(num2str(bin_vect_j))+1;
        P_phenotype(i,j)=INPUT(j,ind_in);

      end

    end


  end

end


plot3(sequence_var(:,1), sequence_var (:,2), sequence_var (:,3),'-.')

%Visualization of the generation sequences
text(sequence_var(1:sim_for_gen*num_gen,1),sequence_var(1:sim_for_gen*num_gen,2),sequence_var(
1:sim_for_gen*num_gen,3),cellstr( num2str(fit_rec(1:sim_for_gen*num_gen,1)) ))

[not,index_best]=min(fit_rec(:,2));
comb_best=sequence_var (fit_rec(index_best,1),:);


%Crossover e mutation functions

function [cr1,cr2]=crossover(d,m)
f=length(d);
cr_point1=round((f-2)*rand+1);
%one point crossover
for i=1:f(2)

  if i<=cr_point1
    cr1(i)=d(i);
  else
    cr1(i)=m(i);
  end

  if i<=cr_point1
```

```
      cr2(i)=m(i);
   else
      cr2(i)=d(i);
   end

end

end

function m=mutation(v)
f=length(v);
m=v;

mut_inx=round((f-1)*rand+0.5);

if m(mut_inx)==0
   m(mut_inx)=1;
else
   m(mut_inx)=0;


end

end
```
